$5

QEX

INCLUDING: COMMUNICATIONS QUARTERLY

Forum for Communications Experimenters

March/April 2002

OK1DNZ's VHF/UHF Diplexer

ARRL The national association for AMATEUR RADIO
225 Main Street
Newington, CT USA 06111-1494

Enjoy the Best Design Ideas and Technical Features from Applied MICROWAVE & WIRELESS

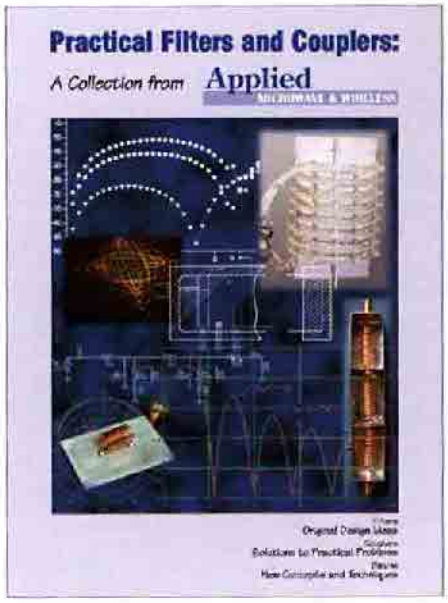

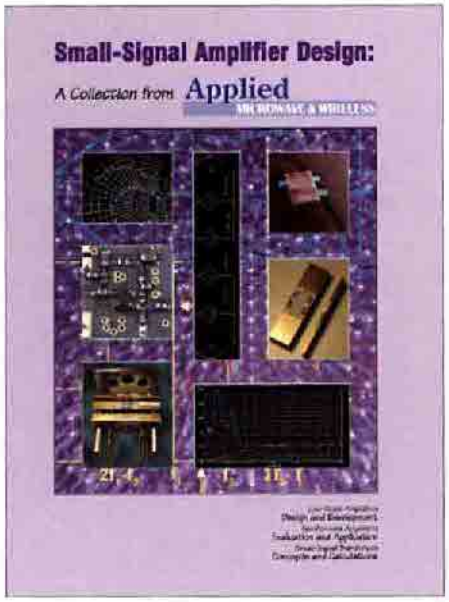

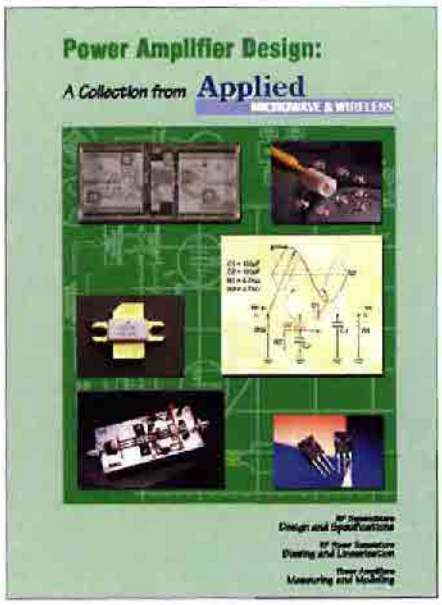

Practical Filters and Couplers

Offers 13 articles on classic as well as current design and testing filters, couplers and baluns. Provides quick access to:

Crucial Concepts
- Matching Double-Tuned LC Filters
- Microwave Filter Design
- Balun Design for Wireless

Practical Solutions
- Filters without PC Boards
- HF Diplexers with Helical Resonators
- Bridging Coupling

Original Designs
- Computer-Aided Active Filter Synthesis
- Design of Active Equalizers with Controlled Gain Slope
- Electronic Directional Couplers

80 pages, large format softcover, ISBN 1-884932-21-5
NP-43 ..... $24.95

Small-Signal Amplifier Design

Concentrates on four aspects of small-signal amplifier design:

Small-Signal Amplifier Design
- RF/Microwave Amplifier Design
- Available Gain Amplifier Design
- Avoiding RF Oscillation

LNA Design
- LNA Design for Simultaneous Low-Input VSWR and Low-Noise
- Exact Simulation of LANS Reduces Design Cycle Time
- Design and Development of Special Low-Noise Amplifiers for GPS Application

Distortion Prediction and Reduction
- Intermodulation: Concepts and Calculations
- Wideband Gain Block Amplifier Design Techniques
- Second Order Effects in Feedforward Amplifiers

Computer Simulation and Device Modeling
- Evaluation of Parasitic Parameters for Packaged Microwave Transistors
- Develop SPICEHigh-Frequency Small-Signal Tranistor Models from Data Sheets
- Linear and EM Simulation Cuts Design Time of a 3.8 GHz Amplifier

104 pages, large format softcover, ISBN 1-884932-24-X
NP-44 ..... $29.95

Power Amplifier Design*

Over twenty experts put everything you need to know about power amplifier linearization, measuring, modeling and distortion at your fingertips. (Re)discover how to:

Improve Amplifiers and Amplifier Applications
- Digitally Controlled Potentiometers Improve Cost and Reliability
- The Magnetron: A Low-Noise, Long-Life Amplifier
- Efficient RF Power Amplifiers for Digital Communications

Model and Suppress Amplifier Distortion
- Envelope Distortion Models with Memory
- Using Digital Modulation to Measure and Model RF Amplifier Distortion
- Suppress Spectral Sidelobe Regrowth with Data Signal Predistortion

Specify Amplifier Linearity
- Specifying Power Amplifier Linearity via Intermodulation Distortion
- Amplifier Linearization Using Adaptive RF Predistortion
- Biasing LDMOS FETs for Linear Operation

112 pages, large format softcover, ISBN 1-884932-26-6
NP-45 ..... $29.95

*Available March 2002

For more information, or to place your order on-line, point your browser to **www.noblepub.com**

NOBLE PUBLISHING

Noble Publishing Corporation
630 Pinnacle Court, Norcross, GA 30071
Tel: 770-449-6774 • Fax: 770-448-2839 • www.noblepub.com

QEX

INCLUDING: COMMUNICATIONS QUARTERLY

QEX (ISSN: 0886-8093) is published bimonthly in January, March, May, July, September, and November by the American Radio Relay League, 225 Main Street, Newington CT 06111-1494. Yearly subscription rate to ARRL members is $24; nonmembers $36. Other rates are listed below. Periodicals postage paid at Hartford, CT and at additional mailing offices.

POSTMASTER: Send address changes to: QEX, 225 Main St, Newington, CT 06111-1494
Issue No 211

Mark J. Wilson, K1RO
Publisher

Doug Smith, KF6DX
Editor

Robert Schetgen, KU7G
Managing Editor

Lori Weinberg
Assistant Editor

Peter Bertini, K1ZJH
Zack Lau, W1VT
Ray Mack, WD5IFS
Contributing Editors

Production Department

Steve Ford, WB8IMY
Publications Manager

Michelle Bloom, WB1ENT
Production Supervisor

Sue Fagan
Graphic Design Supervisor

David Pingree, N1NAS
Technical Illustrator

Joe Shea
Production Assistant

Advertising Information Contact:

John Bee, N1GNV, *Advertising Manager*
860-594-0207 direct
860-594-0200 ARRL
860-594-4285 fax

Circulation Department

Debra Jahnke, *Manager*
Kathy Capodicasa, N1GZO, *Deputy Manager*
Cathy Stepina, *QEX Circulation*

Offices

225 Main St, Newington, CT 06111-1494 USA
Telephone: 860-594-0200
Telex: 650215-5052 MCI
Fax: 860-594-0259 (24 hour direct line)
e-mail: qex@arrl.org

Subscription rate for 6 issues:

In the US: ARRL Member $24, nonmember $36;

US by First Class Mail: ARRL member $37, nonmember $49;

Elsewhere by Surface Mail (4-8 week delivery): ARRL member $31, nonmember $43;

Canada by Airmail: ARRL member $40, nonmember $52;

Elsewhere by Airmail: ARRL member $59, nonmember $71.

Members are asked to include their membership control number or a label from their *QST* wrapper when applying.

In order to ensure prompt delivery, we ask that you periodically check the address information on your mailing label. If you find any inaccuracies, please contact the Circulation Department immediately. Thank you for your assistance.

Copyright ©2002 by the American Radio Relay League Inc. For permission to quote or reprint material from *QEX* or any ARRL publication, send a written request including the issue date (or book title), article, page numbers and a description of where you intend to use the reprinted material. Send the request to the office of the Publications Manager (permission@arrl.org)

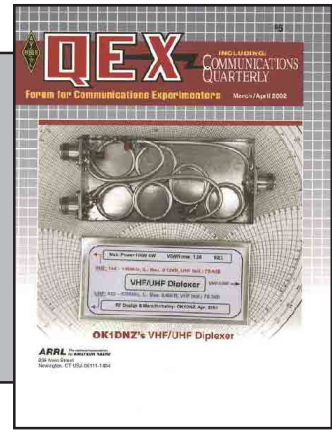

About the Cover

Transmission lines and coils inside the VHF/UHF Diplexer (see Zanek, page 47).

Features

3 **Build a 250-MHz Network Analyzer**
By Steve Hageman

11 **A 455-kHz IF Signal Processor for SSB/CW**
By William E. Sabin, W0IYH

17 **About Monopoles and Dipoles**
By Valentin Trainotti, LU1ACM

25 **The Fractal Loop Antenna: Understanding the Significance of Fractal Geometry in Determining Antenna Performance**
By Dr. Steven R. Best, VE9SRB

35 **Some Notes on Turnstile-Antenna Properties**
By L. B. Cebik, W4RNL

47 **A Low-Loss VHF/UHF Diplexer**
By Pavel Zanek, OK1DNZ

52 **A Homebrew Shaft Encoder**
By Doug Smith, KF6DX

Columns

62 **Out of the Box**

55 **RF** *By Zack Lau, W1VT*

60 **Letters to the Editor**

62 **Next Issue in *QEX***

Mar/Apr 2002 *QEX* Advertising Index

Active Electronics: 63
American Radio Relay League: 64, Cov III, Cov IV
Atomic Time, Inc.: 64
Down East Microwave Inc.: 64
Roy Lewallen, W7EL: 64
Nemal Electronics International, Inc.: 64
Noble Publishing; Cov II
Palomar: 63
Teri Software: 51
Tucson Amateur Packet Radio Corp: 34
TX RX Systems Inc.: 16
Universal Radio, Inc.: 46

THE AMERICAN RADIO RELAY LEAGUE

The American Radio Relay League, Inc, is a noncommercial association of radio amateurs, organized for the promotion of interests in Amateur Radio communication and experimentation, for the establishment of networks to provide communications in the event of disasters or other emergencies, for the advancement of radio art and of the public welfare, for the representation of the radio amateur in legislative matters, and for the maintenance of fraternalism and a high standard of conduct.

ARRL is an incorporated association without capital stock chartered under the laws of the state of Connecticut, and is an exempt organization under Section 501(c)(3) of the Internal Revenue Code of 1986. Its affairs are governed by a Board of Directors, whose voting members are elected every two years by the general membership. The officers are elected or appointed by the Directors. The League is noncommercial, and no one who could gain financially from the shaping of its affairs is eligible for membership on its Board.

"Of, by, and for the radio amateur, "ARRL numbers within its ranks the vast majority of active amateurs in the nation and has a proud history of achievement as the standard-bearer in amateur affairs.

A bona fide interest in Amateur Radio is the only essential qualification of membership; an Amateur Radio license is not a prerequisite, although full voting membership is granted only to licensed amateurs in the US.

Membership inquiries and general correspondence should be addressed to the administrative headquarters at 225 Main Street, Newington, CT 06111 USA.

Telephone: 860-594-0200
Telex: 650215-5052 MCI
MCIMAIL (electronic mail system) ID: 215-5052
FAX: 860-594-0259 (24-hour direct line)

Officers

President: JIM D. HAYNIE, W5JBP
3226 Newcastle Dr, Dallas, TX 75220-1640
Executive Vice President: DAVID SUMNER, K1ZZ

The purpose of *QEX* is to:
1) provide a medium for the exchange of ideas and information among Amateur Radio experimenters,
2) document advanced technical work in the Amateur Radio field, and
3) support efforts to advance the state of the Amateur Radio art.

All correspondence concerning *QEX* should be addressed to the American Radio Relay League, 225 Main Street, Newington, CT 06111 USA. Envelopes containing manuscripts and letters for publication in *QEX* should be marked Editor, *QEX*.

Both theoretical and practical technical articles are welcomed. Manuscripts should be submitted on IBM or Mac format 3.5-inch diskette in word-processor format, if possible. We can redraw any figures as long as their content is clear. Photos should be glossy, color or black-and-white prints of at least the size they are to appear in *QEX*. Further information for authors can be found on the Web at **www.arrl.org/qex/** or by e-mail to **qex@arrl.org**.

Any opinions expressed in *QEX* are those of the authors, not necessarily those of the Editor or the League. While we strive to ensure all material is technically correct, authors are expected to defend their own assertions. Products mentioned are included for your information only; no endorsement is implied. Readers are cautioned to verify the availability of products before sending money to vendors.

Empirical Outlook

Investments in Technology

Recently, the ARRL leadership appointed a working group for so-called software-defined radios (SDRs). That group will join the existing Digital Voice Working Group in a major push to advance the state of our art. This action is a significant step within Amateur Radio toward upgrading our capabilities. Much work has already been done on DSP-based radios and it falls to us to build on it for the future.

Michael Marcus, Associate Chief for Technology, Office of Engineering and Technology at the FCC sees the SDR as a way to engender interest in "smart" radio systems that help revive experimentation within Amateur Radio. The premise is that if you give more flexibility and control to radio operators, they will play with those possibilities and perhaps come up with new and better things. Mike is right to encourage Amateur Radio to make the most of what is available to us.

Presenting advanced controls in safe and useful ways is a major challenge, though. It is easy to imagine minor alterations to transmitter software that would produce signals occupying too much bandwidth, resulting in adjacent-channel interference. Manufacturers are rightly concerned about the amount of customer support required after releasing intimate details of their products. They view certain facets of digital transceiver design as proprietary and find little incentive to let them go without recompense. It is therefore likely that open-architecture software-radio design will be left to amateurs for the foreseeable future. US hams and manufacturers have led the way in SDRs. We have been doing it for at least five years now. *QEX* is lining up some more articles on the subject—stay tuned.

High-speed digital networking is achieving great bounds in the commercial world that hams could easily match. An ARRL working group for that is also in the works. Inexpensive equipment is readily available to help us occupy the part of our spectrum that is at risk of being overrun by commercial interests—especially the 23-cm, 13-cm and 5-cm bands. As pressure builds to make the best use of our resources, we must embrace and improve on such technologies. Check our Letters column for additional comments on high-speed networking.

As it turns out, there are excellent tie-ins among digital voice, SDRs and digital networking. Embedded digital audio systems are already in use on the Internet and we have every reason to deploy them over radio links. Development of high-speed modulation schemes may benefit voice, data and video operations. Your comments, please!

In This Issue

Follow Steve Hageman as he describes how he turned his VHF source project into a scalar network analyzer. Discover how eight more ICs and a little effort can add great versatility to your shack. We continue our journey through Bill Sabin, W0IYH's transceiver with a look at his 455-kHz-IF circuit. It provides most of the IF features you'd expect in a high-quality rig, including gain control, speech processing and CW envelope shaping, in an all-analog design.

We have three antenna articles that should provide some food for thought. Valentin Trainotti, LU1ACM, brings us some observations about monopoles and dipoles. Tino relates some history of these antennas and brings valuable insight into what makes them work. Steve Best, VE9SRB, takes a hard look at unconventional loop antennas, including fractal topologies. His analysis leads him to some conclusions about their multiresonant behavior. Augmenting his recent *QST* article, L. B. Cebik, W4RNL, offers a detailed investigation of turnstiles and similar antennas. He has discovered some interesting relationships between feed methods and radiation patterns.

Pavel Zanek, OK1DNZ, returns with another neat project you can build on a budget: a VHF/UHF diplexer. It might be just what you need for your dual-band antenna or transceiver. In *Out of the Box*, Ray Mack, WD5IFS, presents a review piece by Cornell Drentea, KW7CD. The object of review is the Almost All Digital Electronics L/C meter model II B.

Doug Smith, KF6DX, presents information on how you can build a shaft encoder for your rig. Learn how to do it at minimum expense and maximize your enjoyment. In *RF*, Zack Lau, W1VT, completes his discussion of 10-GHz DXing by describing a homebrew offset feed for small satellite-TV dishes. *73, Doug Smith, KF6DX,* **kf6dx@arrl.org**. □□

Build a 250-MHz Network Analyzer

Network analyzers are wonderfully useful in design work, yet commercial models are expensive. Here's an inexpensive homebrew version for your bench.

By Steve Hageman

A network analyzer is used to help circuit designers verify the frequency response of their circuits. With the addition of some simple receiver circuits, the previously published VHF-source project[1] can be turned into a full-featured and calibrated scalar network analyzer. The resulting instrument should prove valuable for all amateur HF and VHF circuit measurements. If you built—or are contemplating building—the VHF source project, then you will be pleased to know that this eight-IC addition expands the RF source into a versatile measuring instrument.

[1]Notes appear on page 10.

9532 Camelot Dr
Windsor, CA 95492
shageman@sonic.net

Analyzer Architecture

This analyzer follows its commercial cousins in design and implementation.[2] As can be seen in the block diagram of Fig 1, the heart of this project is a previously published RF source (See Note 1).

The analyzer uses the typical, three-receiver design (see Note 2). The source's RF output is routed to the RF input of the R and A receiver. These receivers sample the RF via a pair of Mini-Circuits directional couplers. The coupler separates the forward and reflected portions of the RF and directs them to the appropriate R and A detectors. This allows reflection measurements to be made.

The RF is then routed through the device under test (DUT) to the B-term receiver. The terminology used for the receivers (ie, R, A and B terms) follows a long-standing tradition in the test and measurement industry (see Note 2). The R term is aptly named for the reference. The reference is the actual forward power applied to the DUT. This term is used in a ratio for all the DUT measurements. The A term is the reflected power from the DUT. When a reflected-power/reference-power (A/R) measurement is made, the result is the true input match of the DUT versus frequency.

The B term is used to make transmission measurements of the DUT. When a transmission/reference (B/R) measurement is made, the result is the true gain or loss of the network.

Some analyzer designs use a single receiver with either PIN-diode or mechanical switches to switch the receiver among the different channels. This can be cost effective in a micro-

wave analyzer because the cost of a receiver might be very high; however, the heart of the receiver circuit used here is the Analog Devices AD8307 logarithmic detector IC. This very-high-performance IC is lower in cost than the lowest-cost RF relay, so I used one per channel. Another downside of using a switched receiver is the settling time as the receiver is switched between channels.

The architecture described is a scalar analyzer. That is, no phase information is available, as would be the case with a vector network analyzer or VNA. A VNA typically operates with tuned receivers that require an LO-frequency offset from the RF source frequency. While a VNA has higher performance than a scalar analyzer, I judged that the increased circuit complexity required would have made the project too complex to be practical.

Nevertheless, a scalar analyzer can be used for many test and measurement applications around the workshop. After all, scalar information is an infinite improvement over the alternative: simply tuning for the greatest signal strength, a procedure that we all have had to resort to from time to time!

Receiver Circuits

At the heart of the receiver design (Fig 2) is the AD8307. It contains all the circuitry needed to detect a CW RF signal from dc to 500 MHz in an 8-pin package.

The input impedance of the AD8307 is approximately 1.15 kΩ. To match this to 50 Ω requires an equivalent shunt impedance of approximately 52 Ω. Using two 105-Ω, 1%, 1206-size SMT resistors provides an excellent high-frequency match for the B-term receiver. Since the DUT sees the match of the B-term receiver directly, we must use special care when building this portion of the circuit (as will be discussed later). A series 121-Ω resistor, R3, helps to isolate the input capacitance of the log amplifier from the RF path and provides for electrostatic-discharge (ESD) protection.

The output of the AD8307 (U1) is filtered (C6) and amplified by 1.64 (U2) to match the receiver output to the 0-4.096 V input range of the subsequent A/D converter stage. The dynamic range of the B-term receiver is from approximately +17 dBm (1-dB compression) to about –70 dBm. Using the internal VHF source at +15 dBm provides a maximum dynamic range of approximately 85 dB when measuring passive circuits such as filters.

The R, A and B receivers use the same arrangement of detector and post-amplification as the B-term receiver. However, a coupler is used as the interface to the DUT. Three primary specifications of the coupler are important to us:

1. *Coupling factor*—the amount of forward or reflected signal that is sampled from the DUT input. This factor is expressed in decibels. For the Mini-Circuits coupler used in this project, the coupling factor is typically 19 dB. This means that if 0 dBm were applied to the coupler in

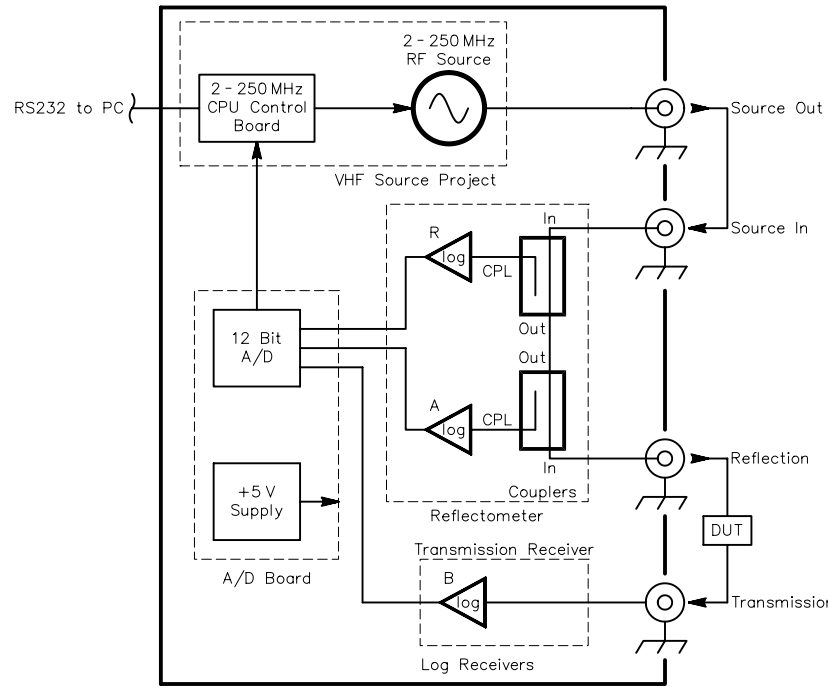

Fig 1—Just eight additional ICs added to the VHF source elevate that project into a full-featured scalar network analyzer.

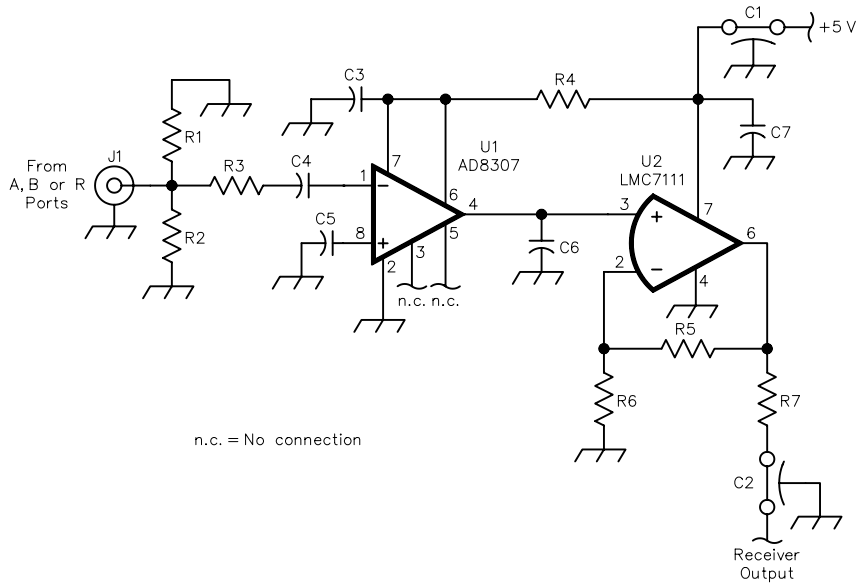

Fig 2—The heart of the analyzer is the Analog Devices AD-8307 (U1). These ICs were developed for power measurement and control in the wireless-communication market. They are used here as wide-dynamic-range CW receivers. The three R, A and B receivers used are identical in design. The only critical portion of the circuit is from the RF input (J1) to pin 1 of U1. See the text for some notes on building the receiver.

the forward direction, –19 dBm would be measured at the forward-coupled port. More coupling "steals" more power from the DUT; less coupling reduces the received and measured signal and this can reduce the dynamic range.

2. *Directivity*—essentially the leakage of the forward power into the reverse-power path (and vice versa). Ideally, this factor would be 0 (or –∞ dB); practically, the couplers chosen have directivities of –50 dB at low frequencies to about –35 dB at the top end of the frequency band.
3. *Through-line loss and through-line port match*—these terms usually go hand in hand. A lower through-line loss usually means a better port match. Port match is very important. When measuring the reflection of a 50-Ω DUT, we need an excellent port match to ensure that our test instrument does not cause unnecessary reflections (ie, we want a SWR of 1:1, ideally).

A/D Converter

The A/D converter (Fig 3) is based on a Maxim MAX186, 12-bit design. This A/D features a built-in precision reference and an eight-channel input multiplexer. For this application, only three channels are used.

The MAX186 is a successive-approximation converter with internal track-and-hold. Most integrated A/D converters eject a current charge from the multiplexer input port when a conversion is being made or the input multiplexer is switched from channel to channel. If the source impedance of the circuit driving the A/D is zero, this charge causes no voltage error at the input. However, connecting a converter like this directly to the output of an op amp (especially a low-bandwidth op amp like the LMC7111) can cause a significant voltage perturbation during conversion. Remember that the output impedance of an op amp is not low at high frequencies. In fact, a plot of the output impedance of an op amp versus frequency looks inductive. Resistors R1-R3 and capacitors C4-C6 dampen the charge ejected from the A/D converter and help to keep the current in a tight loop right at the converter. These components also provide some degree of low-pass filtering that applies video filtering to the receiver outputs.

The resolution of the detector-A/D converter combination is about 0.025 dB per least-significant bit (LSB) of the converter. This is more than adequate resolution to produce aesthetically pleasing, low-apparent-noise displays. The A/D is controlled by a three-wire serial interface and plugs directly into a spare internal serial-bus connector on the source's existing CPU board.

The A/D board is also the logical place for the +5-V regulator that is used to power the receivers and the A/D. This regulator directly connects to the VHF source project's +5-V unregulated power bus.

Construction Details

The network-analyzer addition was built breadboard-style in four sections that correspond to the two schematics (Figs 2 and 3) and the block diagram (Fig 1). The receivers were built to fit into die-cast aluminum enclosures for maximum shielding from themselves, stray RF and nearby radio stations. The only critical portion of the analyzer's circuits is the RF path; the rest of the circuitry is relatively layout-insensitive; nearly any reasonable layout will work.

The receivers should have short RF paths that start from the SMA-to-PC-board connectors (see parts list). The most-critical items here are the two termination resistors. These resistors must be placed directly from the center conductor to the frame of the SMA connector right at the connector to maintain low SWRs for the receivers. Fig 4 shows the basic arrangement of the input circuit. The input circuit is built "three-dimensionally," suspended in air with 1206-size SMT components as shown. The input pin of the AD-8307 detector is soldered directly to the chain of suspended parts as shown.

While this construction method does not maintain the 50-Ω transmission-line environment that we would ideally want, it works well as long as we keep the total length of the circuit shorter than about λ/20 and stray reactance is minimized. I find working with SMT components in this manner is very easy with 1206-sized parts. I use a fine, pointed-tip Weller soldering iron and small amounts of 0.025-inch-diameter solder.

Since the detectors have usable bandwidths of 500 MHz and very large dynamic ranges, take precautions to keep

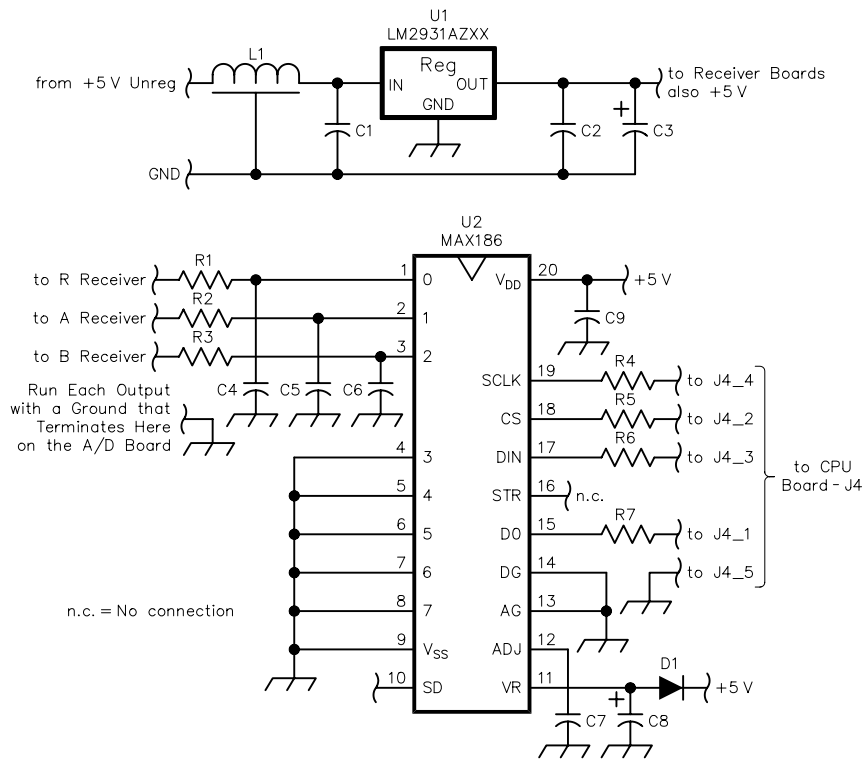

Fig 3—The A/D converter was built on a small piece of copper-clad PC-board material. The interface to the VHF Source CPU is via J4, this connector was laid out on the Source's original CPU board. The Maxim 186 A/D converter is a 12-bit device that gives about 0.025-dB resolution in this project.

all RF from external sources out of the receivers. I accomplished this by housing the receivers in die-cast aluminum enclosures as described. I also used feedthrough capacitors for all the power and signal lines entering the enclosure.[3] Additionally, the B-term receiver should be housed in a separate enclosure from the R receiver. This is because we are trying to preserve a possible 80-dB dynamic range and this kind of isolation is much easier to achieve if both receivers are in separate shielded compartments. Since the R- and A-term receivers' isolation requirements are set by the directivity of the couplers, they can be mounted in the same enclosure as long as all the inputs and outputs (including power and ground) are kept separate.

I mounted the A/D converter board and the receivers on the top cover of the VHF source's cabinet. The RF connections are made with flexible RG-179 coax-to-bulkhead BNC connectors, with the other end terminated in a SMA coax connector attached to the receiver input. You must use good coax connectors for all the RF connections. Simply stripping the coax pigtail style will not work well at these frequencies considering the measurement resolution of this instrument.

I mounted the Mini-Circuits couplers behind the instrument's front panel as shown in Fig 5. This keeps the through-line path short and simple, preserving the port match and minimizing power loss.

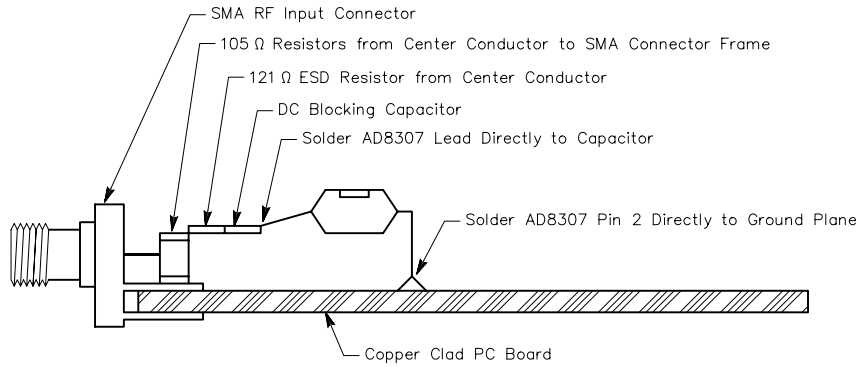

Fig 4—The critical part of each receiver is the input circuit. This is a side view of how I built my receivers on a small piece of copper-clad PC-board material. It is important to keep the total length of the input circuit below about λ/20 (around two inches in free air) to preserve the input match and bandwidth of the receiver circuits.

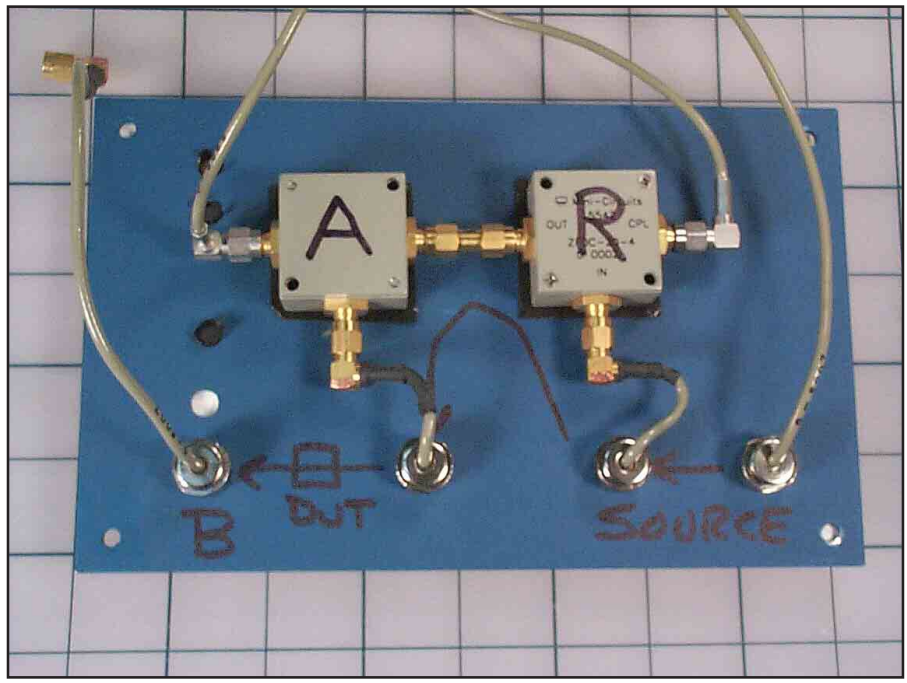

Fig 5—The Mini-Circuits couplers are mounted directly to the back of the analyzer front panel. The RF through-path length is minimized and the couplers are connected together with a SMA coupling connection. Be sure to use the proper coax-to-connector assembly methods; pigtail connections have too much inductance for the analyzer.

Measurement Calibration Routines

Measurement accuracy enhancement is possible using error correction on the raw measurement data to produce a more accurate result. These techniques have been used since the 1970s when computers were first introduced to network analyzers. The basic scheme is shown in Fig 6. Here, the DUT is connected to a perfect measurement coupler through a two-port error adapter. The arrows in the error-adapter block denote signal flow and the error adapter is modeled using signal-flow-graph techniques.

So now we have a system that measures the DUT's actual reflection coefficient, Γ_a, through an error adapter that transforms the DUT's actual reflection coefficient to the measured reflection coefficient, Γ_m. By calibrating the system against some standard, well defined reflection devices, such as a short circuit, open circuit or load and determining the error-adapter coefficients, we can find Γ_a from our measurement of Γ_m.

What happens next is a large amount of matrix math and signal-flow graphic analysis, which has been covered extensively in other publications.[4]

The result is intuitive and the error adapter ends up modeling three major error terms:

1. Directivity of the coupler—this is really the dynamic-range floor of the reflection measurement.
2. Reflection frequency-response tracking—this is how well the R and A terms of the measurement coupler track with frequency.

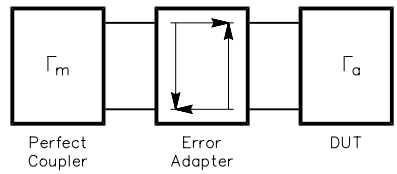

Fig 6—Error correction in a network analyzer is done by inserting an "error adapter" between the DUT and an assumed-perfect coupler. During calibration, a known standard load, open and short-circuit terminations are used in place of the DUT. The characteristics of the error adapter can then be determined and hence we can derive the actual reflection coefficient of the DUT.

3. Effect of a non-perfect source match of the measurement coupler—if the measurement system does not have a perfect match, the signal will be reflected from the measurement port back to the DUT (and vice versa) causing a measurement error.

Directivity itself is easily measured. If we place a good 50-Ω load on the reflection port, then no signal is reflected into the A term and all the signal at the A-term receiver is caused entirely by the directivity of the coupler.

Reflection tracking is the frequency-response error from the R term to the A term with frequency. Offset errors between the receivers are also included. The reflection-tracking term is easily measured. Using a high-quality short or open circuit on the reflection port will cause the entire signal to be reflected back to the receiver and tracking can be easily determined. I used a modified form of reflection tracking here, which has been used in industry for some time with scalar analyzers. I use both a measured short and a measured open, then use both values to get an average reflection-tracking term.

The last error term arises because of the nonideal source match of the measurement port. This causes some of the signal reflected by the DUT to be reflected and measured again by the A-term receiver. Intuitively, this is worse with highly reflective DUTs. If the DUT is a good match to 50 Ω, it won't reflect anything itself and hence the mismatch at the receiver port is inconsequential. A highly reflective DUT, on the other hand, combined with a poor measurement-port match can cause quite a lot of signal reflection and re-reflection, contributing to measurement errors.

The source match is usually measured with the help of good-quality (and precisely modeled) short and open-circuit standards. Short and open circuits are on opposite ends of the Smith chart and are known quantities. When the math is done, it turns out that two equations can be mapped to these two known standards, and the source match can be directly solved.

In this project, source match is adequate (more than 15-dB return loss at all frequencies), and given that the receivers have a worst-case 1-dB peak-to-peak combined nonlinearity, the source-match term can be ignored. Ignoring this term gives a typical apparent measurement error of approximately 0.3 dB when measuring an open or short circuit over the full frequency range. This is well within the achievable accuracy of the instrument overall.

The final error-correction equation used for the reflection port is:

$$\Gamma_a = \frac{\Gamma_m - e_{00}}{e_{10}e_{01}} \qquad \text{(Eq 1)}$$

where Γ_a is the actual reflection coefficient; Γ_m is the measured reflection coefficient; e_{00} is the directivity term and $e_{10}e_{01}$ is the reflection-tracking term. Notice that these values are all expressed as linear ratios, not decibels.

To calibrate the transmission (B/R) receiver path, a simple through-line connection is made from the reflection port to the transmission port. A frequency sweep is then made and a simple offset correction is created between the R- and B-term receivers at every frequency point.

The complete calibration is done in relation to frequency. When a start frequency, stop frequency and the number of frequency points are specified, sufficient conditions are known to perform a calibration at every measurement point.

Error correction is a wonderful concept and it can provide measurements that are much more accurate. However, it can only account for systematic errors. It cannot correct for repeatability errors—such as the repeatability in mating connectors—and it cannot account for random drift or noncorrected drift in the measurement circuits.

Calibration Standards

The measurement-calibration routines mostly remove offsets, frequency tracking and directivity from measurements using known standards. However, these procedures do not correct for gain errors in the receivers. To calibrate the gain of the receivers, two simple calibration devices need to be constructed. The first device is a known-reflection standard. This device is constructed with two 150-Ω, 1% resistors (connected in parallel for 75 Ω total) mounted to a BNC socket. The known-reflection standard is measured with an ohmmeter and the value is stored in a file so the calibration program can use it to determine the actual gain of the A and R receivers. The 75-Ω reflection value produces a 1.5:1 SWR (13.98 dB return loss) against which the R and A receivers are measured.

The other standard is a 20-dB attenuator. The attenuator is constructed using six 121-Ω, 1% resistors. This arrangement (shown in Fig 7) produces an attenuator with a reasonably precise attenuation and minimizes the inductance of the parts, giving a flat frequency response and a good match. The attenuator is placed in line between the source-output and source-input ports. By making readings with the attenuator both in and out of the circuit, the gains of all three receivers can be calibrated. The receiver-gain procedure is handled in a small, separate program. The calibration program should only

Table 1—Typical Performance Details

Frequency Range	2-250 MHz
Frequency Resolution	1 Hz
Output Level	-15 to +15 dBm
(Lower outputs are available by using an attenuator on the source output)	
B-term Receiver 1-dB compression point	+17 dBm
B-term load match	> 30 dB return loss
Corrected A/R directivity	> 50 dB
Reflection Measurement Accuracy	
0 to –10 dB reflection:	± 1 dB
–10 to –20 dB reflection:	± 2 dB
–20 to –30 dB reflection:	± 5 dB
Transmission Measurement Accuracy	
Through line:	± 0.1 dB
± 40 dB:	± 1 dB
± 60 dB:	± 2 dB
Sweep time for 51-point display	
One parameter measured:	1.5 s
Both parameters measured:	2.4 s

need to be run once or at most, yearly as a recertification of the system calibration. The resulting gain factors are stored in a file for use by the main network-analyzer application.

To calibrate a measurement, only a through-line short circuit, open circuit and a load are required. For the open, I just leave the BNC input open circuit; at these frequencies, the fringing capacitance is low enough to be negligible. For a short circuit, I use one of those shorting end plugs that fit a BNC. For the load, I use a 50-Ω, 2-W through termination like that commonly used with oscilloscope inputs. A photo of the entire calibration kit is shown in Fig 8.

Firmware/Software

Most of the PIC firmware for this project is the same as was used in the VHF source published earlier (see Note 1). An additional set of commands dealing with the A/D converter was added. To keep the measurement speed high, I wrote some data-reduction routines in the firmware. Specifically: When the firmware is told to make a measurement, it holds off until the PLLs are locked. That allows the *Windows* software to set a frequency, then immediately request a measurement. The PIC firmware then waits until the source is locked on frequency then a measurement is made. When making a measurement, the firmware applies a simple digital filtering routine to acquire multiple A/D samples and then mathematically filters them to reduce the apparent trace noise.

The reflection (A/R) and transmission (B/R) measurements are ratios, so to increase the measurement speed the firmware makes both a digitally filtered R measurement and then the A or B measurement. Then the firmware subtracts the values and returns a signed result. The values can be subtracted instead of divided, because the detectors have already converted the measurements to log values. This allows a single 16-bit result to be sent over the EIA-232 connection instead of two 16-bit values. The *Windows* software can then apply the proper gain constant and error correction to the result before displaying the value.

The software that runs the *Windows* application is written in Agilent Technologies' *VEE* (see Note 5). *VEE* is a graphic-based programming language that is well suited for instrument control and data presentation because of its multitude of built-in graphing objects and built-in standard interface (including IEEE-488 bus) support.

The interface between *VEE* and the PIC firmware is via an ActiveX control. The ActiveX control was written in *Visual Basic* and it handles the calls to and from the PIC firmware via the EIA-232 port. Using an ActiveX control to build a high-level driver for the analyzer allows flexibility in that many programming languages and applications can directly import and use ActiveX controls.

VEE also includes a compiler that allows programs written in it to be distributed royalty-free. To run the analyzer application on any *Windows* PC, one need only download and install the ActiveX control, load the *VEE* run-time files and then run the compiled *VEE* applications.[6]

Using the VHF Network Analyzer

Using the analyzer first requires that the DUT be connected to the proper ports. If you require only a reflection measurement, the DUT may be connected just to the reflection port. For transmission measurements, the DUT must be connected between the reflection and transmission ports. The source-in and source-out ports can be connected with a straight BNC jumper or an attenua-

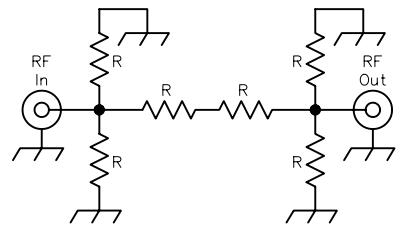

Fig 7—A high-performance 20-dB attenuator can be built with six 121-Ω, 1% resistors as shown. To preserve the bandwidth of the attenuator, you should minimize the lead lengths of all the resistors as shown below. This attenuator is used to calibrate receiver gain by measuring with it in circuit, then out of the circuit and deriving a gain factor for each receiver. During subsequent DUT testing, the attenuator is handy when inserted into the B-receiver path to raise its compression point to well over 37 dBm. Or, it can be used between the source and A/R couplers to reduce the source's output power when testing low-power amplifiers.

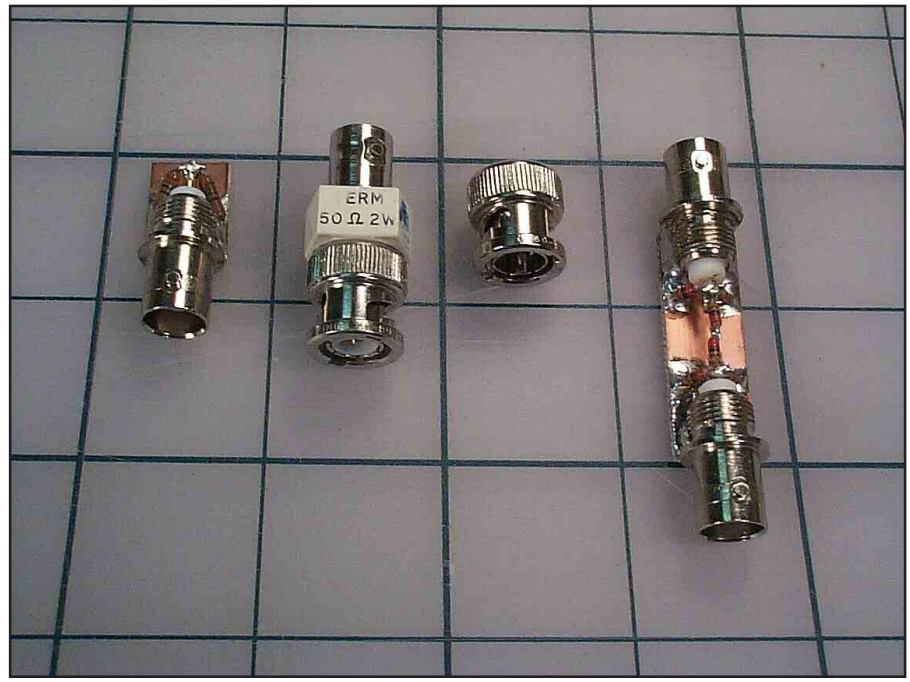

Fig 8—The half-homemade, half-purchased calibration kit for the network analyzer consists of (left to right): a 1.5:1 (75-Ω) mismatch standard, 50-Ω termination, shorting BNC end cap used for the short standard (the open standard just leaves the input port open) and lastly the 20-dB attenuation standard. I built the mismatch load and attenuator out of 1/4-W metal-film resistors with the leads trimmed as short as possible. This arrangement gave more than adequate results at 250 MHz. 1206 SMT resistors could have also been used with slightly less physical robustness.

tor may be inserted in line to reduce the incident power when measuring high-gain DUTs. Without the attenuator, the power to the DUT from the VHF source can be set within a –15 to +15 dBm range via the source's built-in PIN-diode attenuator. For passive DUTs, the power from the source should be set to the maximum value (+15 dBm) to maximize the measurement dynamic range.

The measurement to be performed may be selected from the setup screen (shown in Fig 9). The format of the measurement may also be selected: decibels, magnitude or SWR for reflection measurements. Full control over the sweep is possible by independently selecting the start frequency, stop frequency and number of sweep points. The source power may be set on this screen, also.

Once a measurement setup is defined, the analyzer must be calibrated by pressing the reflection and/or transmission-calibration buttons on the main screen and placing the proper terminations on the ports as requested (the calibration is "directed" by the software). At this point, the entire setup along with the calibration results may be saved to a setup file for later retrieval.

A sample measurement shows the versatility of the analyzer for amateur applications. Fig 10 shows the measurement of a six-pole crystal filter centered at 21.4 MHz. This filter was designed for 50-Ω input and output impedances, so it was directly connected to the analyzer. The markers show a passband loss of about 3 dB. The other marker was positioned at the –60-dB response point and the delta frequency read 44.67 kHz. The reflection is shown in the A/R trace as better than about 12 dB over the entire passband.

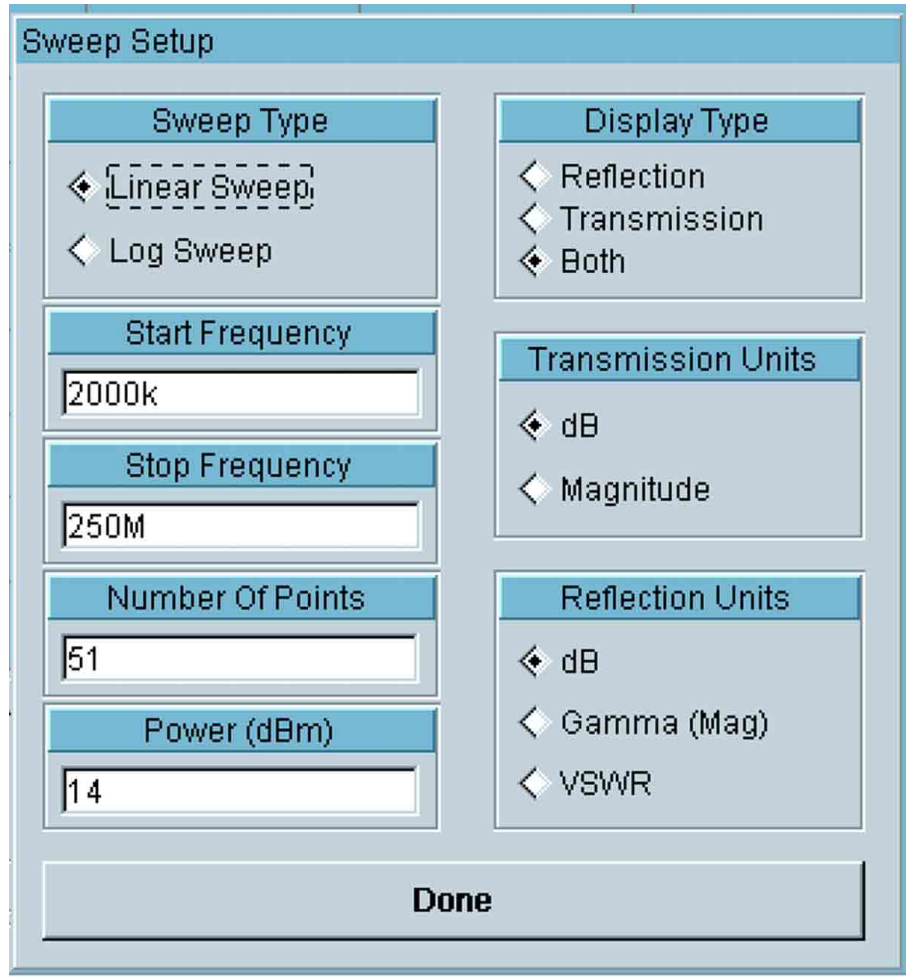

Fig 9—The setup screen from the main application shows all the parameters that may be used to define an instrument sweep. Multiple data formats are also available. Once a setup is defined, it may be saved to disk along with the calibration data for easy access later.

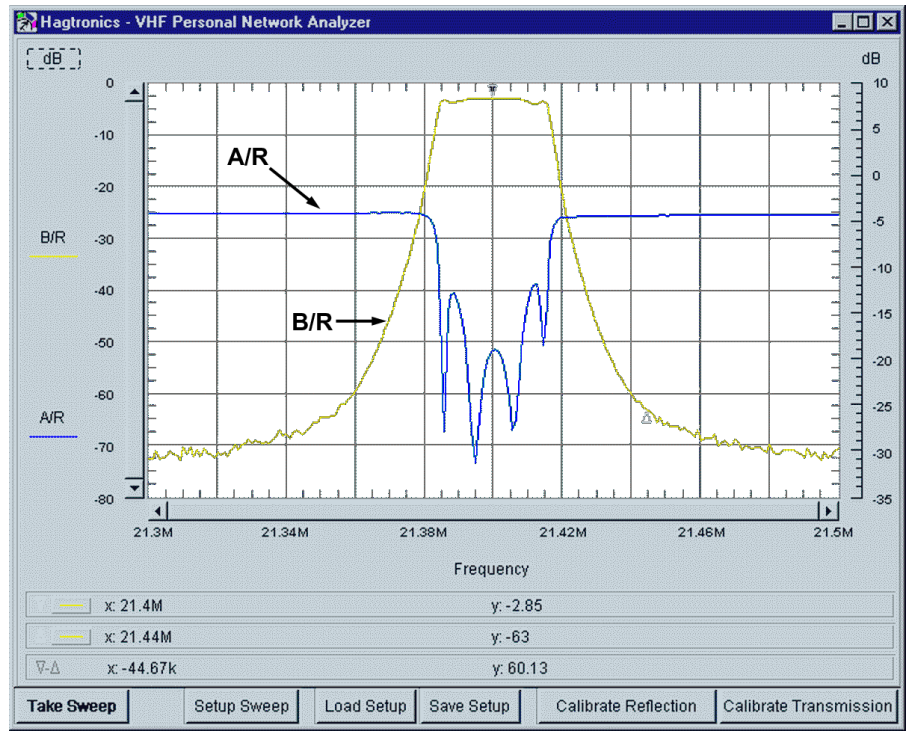

Fig 10—The analyzer in action! Here is the actual measured response of a six-pole, 21.4-MHz crystal filter. Here the lower trace is the transmission loss of the filter (B/R measurement) and the upper trace is the reflection (A/R measurement) of the filter in decibels (right-hand scale). The markers may be independently moved on either trace. They show absolute data at the point of placement and the delta between markers. The *VEE* application also allows printing of the plot to any *Windows* printer (color or black and white) and multiple sweeps may be displayed simultaneously.

PNA Parts List

Receiver Circuits (Three needed per Analyzer)

R1, R2—105 Ω, 1206, ±1% (Digi-Key, P1050FTR-ND)
R3—121 Ω, 1/4 W, ±1% (Digi-Key, P1210FTR-ND)
R4—22 Ω, 1/4 W, ±5%
R5—6.98 kΩ, 1/4 W, ±1 %
R6—11.0 kΩ, 1/4 W, ±1%
R7—1.0 kΩ, 1/4 W, ±5%
C1, C2—feedthrough capacitor
C3—0.1 µF, 50 V, ceramic
C4, C5—4.7 nF, 1206, X7R (Digi-Key #PCC472BCT-ND)
C6, 0.1 µF, 50 V, ceramic
C7, 1 µF, 35 V tantalum
U1, AD8307AN (Allied #AD8307AN)
U2, LMC7111BIN (Digi-Key #LMC7111 BIN-ND)

A To D Board

R1-R3, 1.0 kΩ, 1/4 W, ±5%
R4-R7, 330 Ω, 1/4 W, ±5%
C1, C2, C4-C7, C9—0.1 µF, 50 V ceramic
C3—1 µF, 35 V, Tantalum
C8—4.7 µF, 16 V, Tantalum
D1—1N4148 (or 1N914, 1N4448),
U1—LM2931AZ-5.0 (Digi-Key #LM2931AZ-5.0-ND)
U2—MAX186, 12-bit A/D converter (Digi-Key #MAX186DCPP-ND)
L1—EMI filter (Digi-Key, P9807CT-ND)

GENERAL PARTS

Couplers
0.2-250 MHz coupler (Mini Circuits Labs #ZFDC-20-3; 2 required for project)
RF Connectors
SMA PC-board launch (Digi-Key #J610-ND, 3 required for project)
Feedthrough Capacitors
2500 pF 50 V (Dan's Small Parts, 5 required for project)
Hardware
Die-cast enclosures for the receivers, 3.9×2.0×1.0 inches, (Jameco #11957, 2 required for project)

Notes

[1]S. Hageman, "Build this 250 MHz Synthesized Signal Source," *QEX*, Jan/Feb 2000.

[2]"Exploring the Architectures of Network Analyzers," Agilent Technologies application note 1287-2, **www.agilent.com**.

[3]1000-2500 pF feedthrough capacitors are available from Dan's Small Parts and Kits, Box 3634 Missoula, Montana 59806-3634, phone or fax (406) 258 2782, **www.fix.net/dans.html**.

[4]D. Rytting, "Effects of Uncorrected RF Performance in a Vector Network Analyzer," *Microwave Journal*, April 1991

[5]Agilent *VEE* is a graphical test and measurement development system, **www.agilent.com/find/vee**

[6]The size of the *VEE* runtime install program is too large to be practical to download over a dialup connection however it may be found at, **www.agilent.com/find/vee**. The other files that are required (including the PIC firmware) are available for free download from the VHF Analyzer FAQ page at **www.geocities.com/hagtronics**.

[7]A CD-ROM with all the applicable program files is available from the author for $5 (postage paid to the USA and Canada; add $10 postage and handling for shipment worldwide). If you order a preprogrammed PIC for the project I will supply the data CD with all the programs for free. A programmed PIC16C63 for the project is available for $25 (postage paid in the USA and Canada; add $10 postage and handling for shipment worldwide). For builders of the VHF Source, I will upgrade your firmware free of charge as long as you send the original PIC back to me with a SASE that includes return postage.

Steve Hageman has been interested in electronics since the fifth grade. A confirmed "analogaholic," Steve has always been fascinated by the magic of receiving signals from the "ether." Steve received a BSEE degree from the University of Santa Clara in 1978 and since then has spent his time designing everything from switching power supplies, to embedded systems, to most recently RF circuitry for test and measurement applications. Steve maintains a FAQ page on all his projects, including this one, at **www.geocities.com/hagtronics**. □□

A 455-kHz IF Signal Processor for SSB/CW

Come look at a modern IF with Collins mechanical filters.

By William E. Sabin, W0IYH

As part of a homebrew SSB/CW solid-state transmitter project for all nine HF bands, with an output of 100 W PEP or average, the 455-kHz IF circuitry described in this article provides the following functions:

- 20 dB of IF speech processing using two cascaded Collins miniature torsional-mode mechanical filters.[1] The microphone amplifier (not shown) has a compressor that does no significant speech processing, but it provides a nearly constant level into the IF-clipper circuit.
- A gain-controllable IF amplifier with linear decibels-per-volt control
- CW envelope shaping with backwave suppression
- ALC for a 100 W PA[2] and also for a 600 W PA (30L-1)
- Limiting of forward power at the PEP 100 W and 600 W levels with limiting of reflected power for transistor and tube protection
- Mode control, PTT, VOX and fast time-sequenced T/R switching and receiver muting in conjunction with a Parallax Basic Stamp OEMBS2 microcontroller[3]
- Frequency-spotting function
- All semiconductor devices are easily obtained DIP chips, or diodes
- Analog circuit design is used on the IF board

The emphasis in the SSB speech-processing mode is on maximum weak-signal articulation and intelligibility. The microphone amplifier has an 11-dB rise across the audio range to improve high frequency content and uses a voice-communications unidirectional dynamic microphone.[4, 5] No other audio processing is used. Previous articles[5, 6, 7, 8, 9] have discussed other modules for this transmitter.

[1]Notes appear on page 16.

1400 Harold Dr SE
Cedar Rapids, IA 52403
sabinw@mwci.net

Board Layout

Fig 1 shows the 4×6-inch PC board. The opposite side of the board has a solid ground plane with numerous interconnect wires. Input/output connections and ±12-V inputs are made via pressed-in Teflon terminals at various locations. Multiple-pin connectors are not used. Three-terminal +5-V (78L05) and –5-V (79L05) regulators are included. Aluminum angle stock is used to attach the card to the

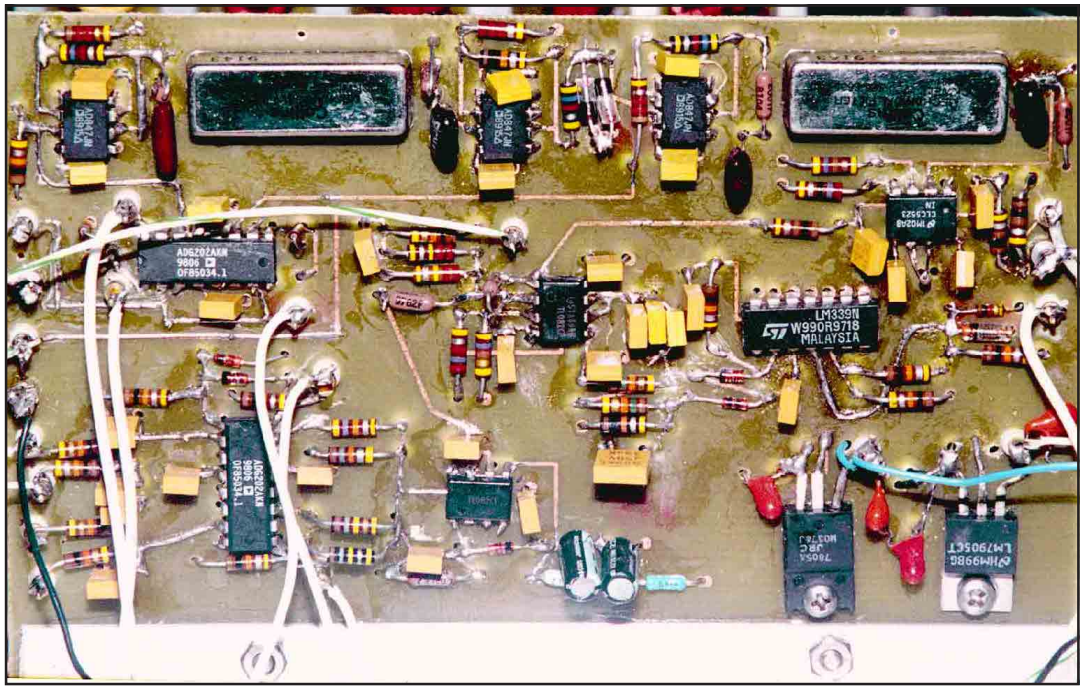

Fig 1—PC board construction of 455 kHz IF processor for SSB / CW.

chassis. IF signal paths have low levels of stray coupling. All components are through-hole versions that were on hand.

The Block Diagram

Fig 2 shows the functions of the IF board and the interconnections to the Basic Stamp controller board and other parts of the transmitter. Inputs from the front panel and both PAs are processed by the controller and applied to the IF board and other parts of the system in the correct sequence and timing. That prevents damage to the PA transistors, the relays and the receiver caused by hot-switching and spurious emissions during transmit-to-receive and receive-to-transmit transitions. When the 600-W PA is operational, an additional 10-ms delay allows time for its T/R relay to function. The ALC circuit prevents overload and nonlinearity in the signal path. Various other brief time delays allow all circuits to reach steady states at each point in operation. An adjustable VOX/CW hold-time of 0.25 to 2.5 seconds is provided by a 555 timer chip. I do not require true QSK (full break-in) operation.

Schematic Diagram

Fig 3 shows the various segments of the circuitry and their interconnections. Across the top are three AD847 (Analog Devices) high-frequency op amps, two mechanical filters (Collins 526-8694-010 miniature torsional-mode, see Note 1), and two 1N34A diodes (RadioShack) for IF clipping. The first two AD847s provide about 20 dB of voltage gain for speech processing. The SSB source resistance for the 455-kHz input signal (Fig 2) is 3.3 kΩ. In ordinary SSB operation, the signal is routed to a third AD847. The gain of this stage is set by the 1200-Ω resistor so that the peak-envelope-voltage (PEV) IF output is nearly equal in both modes. The *average* output, however, is about 3 dB greater in the processing mode because of the magnification of the weaker

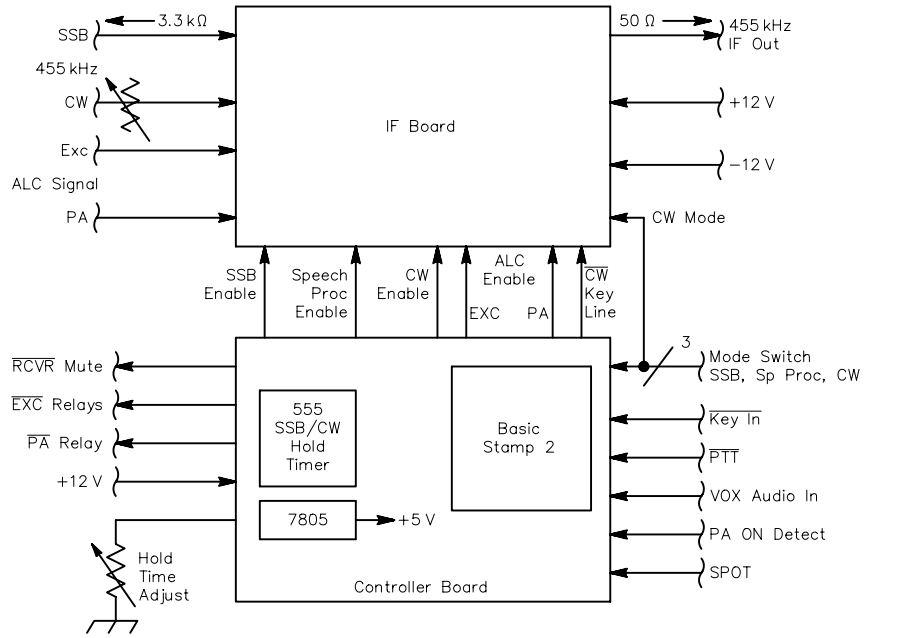

Fig 2—IF and controller board interconnections.

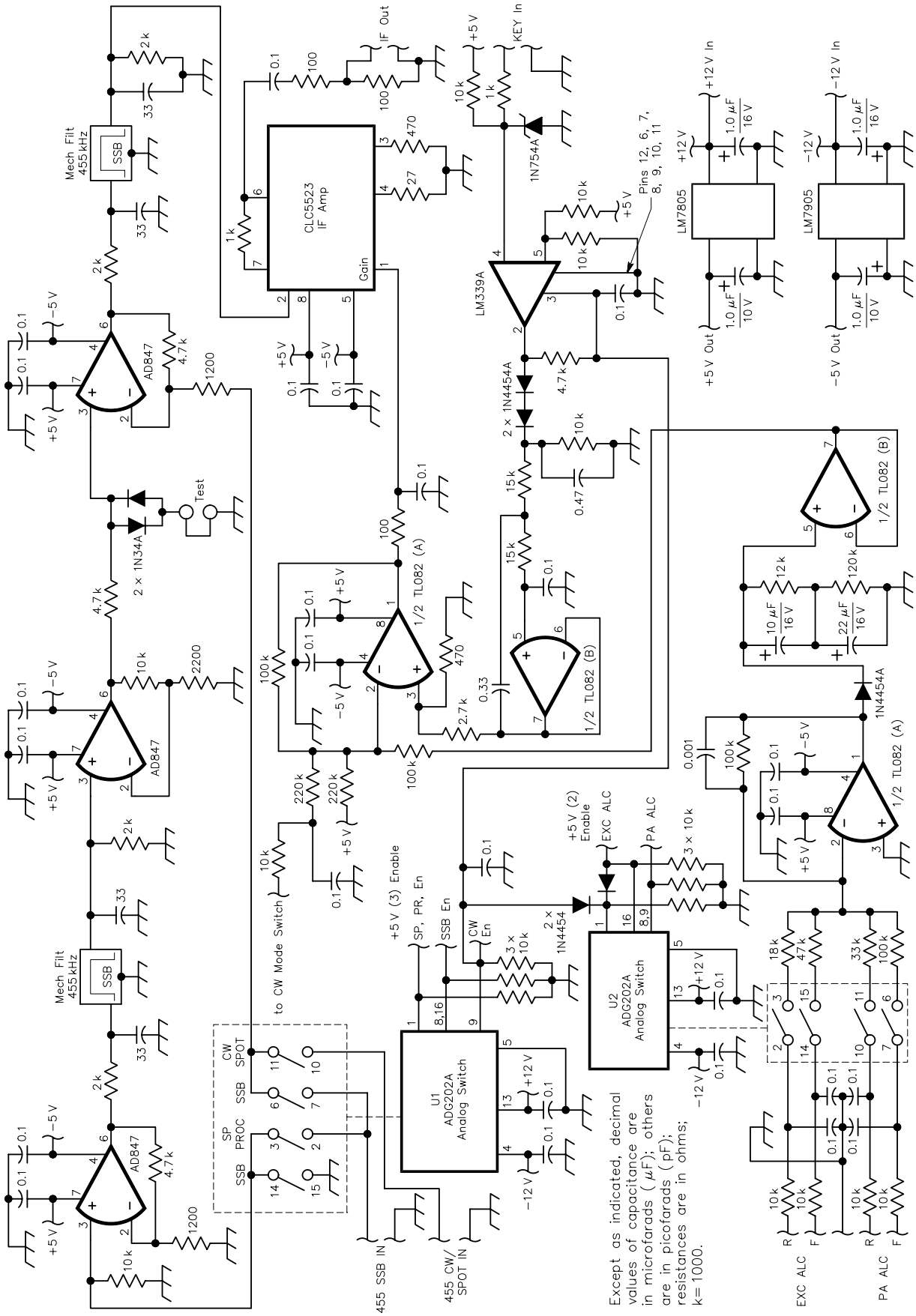

Fig 3—Schematic of 455-kHz IF processor.

speech components. In speech-processing mode, the voltage gain of this third stage is unity. It was a major effort to adjust signal levels and gain values to ensure a very clean signal path.

Signal switching is done by an Analog Devices ADG202A 4-pole SPST analog switch. This device uses ±12 V to maximize the linearity of the SSB signal by reverse biasing the built-in substrate diodes. The switches themselves use +5 V control signals. The double-sideband input (LSB and USB) from the balanced modulator is about 100 mV per sideband. The third-order IMD created by these switches is more than 70 dB below the PEV, which is negligible compared to other stages of the transmitter. In CW mode, the signal is routed to the third-amplifier stage.

After the second mechanical filter, the National Semiconductor CLC5523 gain-controlled current-feedback amplifier has a voltage gain of about two, set by the 1-kΩ and 470-Ω resistors. Pin 1 is the ALC input in SSB mode. The gain is a little less than maximum with no signal and is reduced a decibel or two by a negative-going ALC voltage that assures the PA output rating and linearity. The gain-control voltage (pin 1) can vary from +1.2 V to +0.4 V for a gain reduction of 60 dB, but a maximum of 40 dB is actually used. Beyond 40 dB, leakage and stray coupling effects become unnecessary nuisances.

Fig 4 shows the IF-board USB two-tone output, which is 70 mV PEV into 50 Ω. This level is correct for the next stage in the signal path. Fig 4A shows the output without IF processing and Fig 4B shows it with processing. Fig 4 includes very low level artifacts of my microphone amplifier/compressor and my two-tone audio generator. High-order IMD products created by the diodes are greatly attenuated by the second filter. In Fig 4, the two audio tones are 900 Hz and 1450 Hz (this spacing is required by my spectrum analyzer) which create third-order IMD at 350 Hz and 2000 Hz, close to the edges of the passband. In Fig 4A IMD products are not visible. Notice that in Fig 4B only odd-order products (3rd, 5th, 7th, etc) are visible. This is characteristic of IF clipping that improves articulation and intelligibility of weak signals, as compared to lower-cost audio clipping that creates large amounts of harmonic distortion and even-order IMD.

Fig 5 shows the spectra of broadband composite adult male and female speech signals from a broadband loudspeaker into my Shure "Highball" unidirectional microphone. The test used slow and repetitive (250) average-holding frequency sweeps (Fig 5A) and peak-holding (Fig 5B) and a USB signal. The reference levels for both figures are the same. My mechanical filters have a 3-dB passband from 300 to 2800 Hz. The passband ripples are caused by the receiver and loudspeaker, not the microphone or AF/IF circuitry. The high-frequency emphasis improves voice articulation and quality very significantly. I optimized the complete response experimentally for my voice and my microphone by setting R and C val-

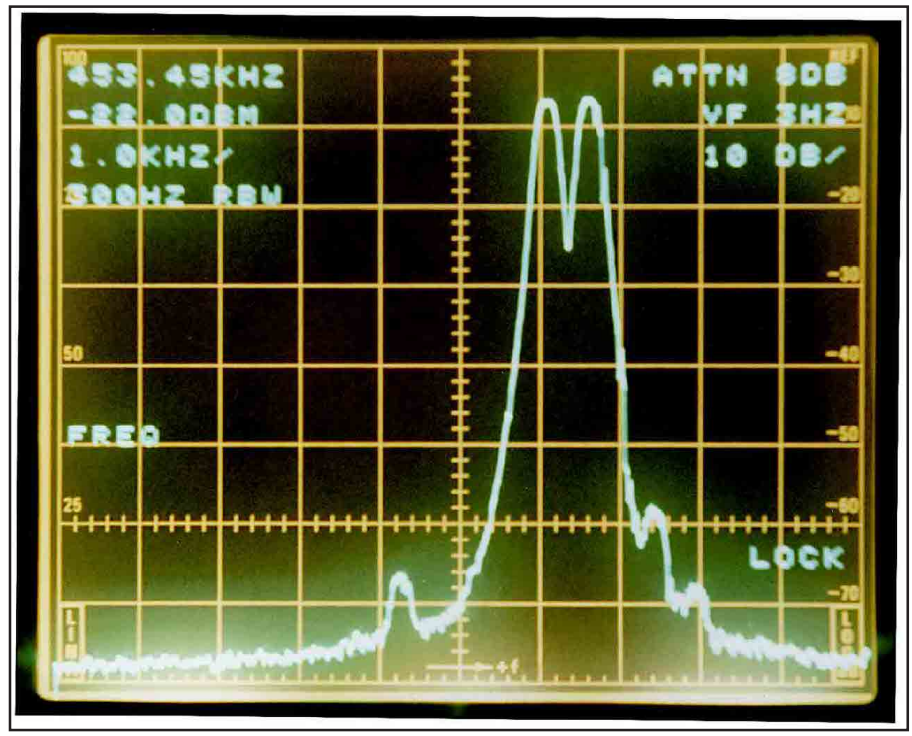

(A)

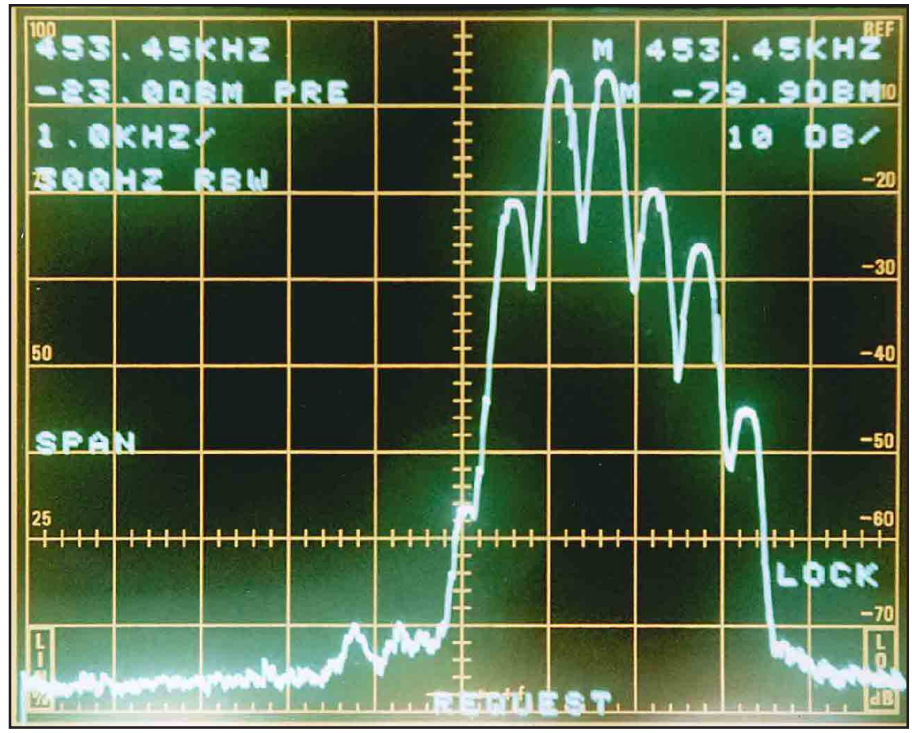

(B)

Fig 4—Two-tone intermodulation: At A, with no speech processing. At B, with 20 dB of speech processing.

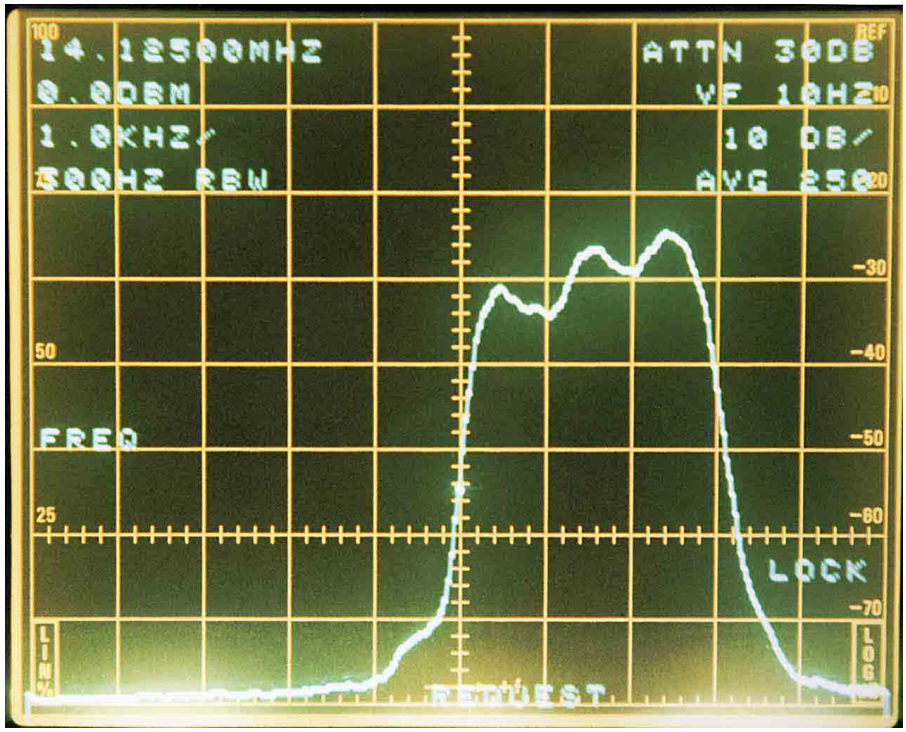

(A)

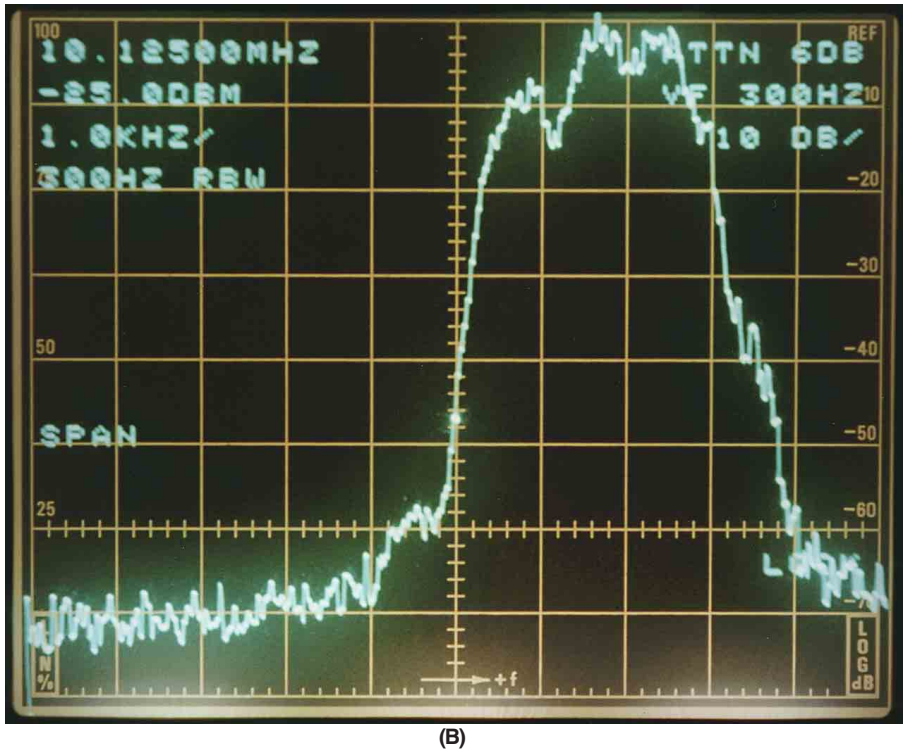

(B)

Fig 5—USB 455-kHz frequency response, from microphone input, of composite adult male and female voices with 20 dB of IF limiting. The frequency scale is 1 kHz per division. At A is an average-holding plot and at B is a peak-holding plot. The top-of-scale reference level is the same for both plots. These plots are at an RF frequency, but before power amplification.

ues in the microphone amplifier.

The adjacent-channel interference at 3.5 kHz above the carrier frequency is very small for two tones and also for the speech signal. My spectrum analyzer has a minimum resolution bandwidth of 300 Hz, which slightly widens the spectrum plot; that is especially noticeable at the low frequency end. Fig 5 also shows a small amount of LSB output, created by the balanced modulator and the filter response below the carrier frequency. The "re-peaking effect" (see Note 5) in the second filter reduces the IF clipping by a couple of decibels.

The level of the CW input signal is set by a front-panel control to achieve a PA output from 1 W to 100 W. In this mode the CLC5523 gain is set to nearly minimum at key-up and is increased by the key-down action. The keying waveform is set by a Sallen-Key second-order low-pass op-amp filter. Because of the logarithmic control characteristic of the IF amplifier, it was expedient to fine-tune the time constants experimentally. For this, I used a pulse generator to create a continuous string of dots so that the RF output envelope could be viewed on an oscilloscope. The rise and fall times are nearly equal at about 5 or 6 ms, between the 10% and 90% values. The 0.47 µF capacitor stretches and rounds the trailing edge just the right amount. This waveform produces a clean RF envelope shape; however, the signal does not go all the way to zero on key-up, which produces a –40 dBc "backwave."

The control board solves this problem with software. It operates the CW Enable input to the analog switch. The action is shown in Fig 6. At key-down time to the control board (Fig 2), the switch is closed, sending IF to the input of the CLC5523 amplifier. The RF envelope starts to rise in about 3 ms. At key-up time, the key line to the IF board goes high, but the switch remains closed for 12 ms to allow plenty of time for the waveform to fall smoothly. The results: no backwave and a well-formed CW envelope. Also, the software debounces the contacts on my old fashioned (1950) "side-swiper" key. These fixes show how the Basic Stamp improved CW performance. For a startup string of dots, 10 ms of the first dot is lost to allow time for receive-to-transmit switching, which is okay for my maximum code speed.

The ALC inputs are switched by the other ADG202A analog switch. In SSB mode, forward and reflected signals from the directional couplers at the 100 W PA and the 600 W PA outputs assure linear SSB operation and also protect against possible damage from excessive SWR. The control board detects that the 30L-1 PA is on and enables the appropriate ALC inputs at the ADG202A switch. In the CW mode, forward power is not sensed, but reflected power is detected and reduces the drive to the PA as necessary to protect the PA and the two-transformer type directional couplers (see Note 9).

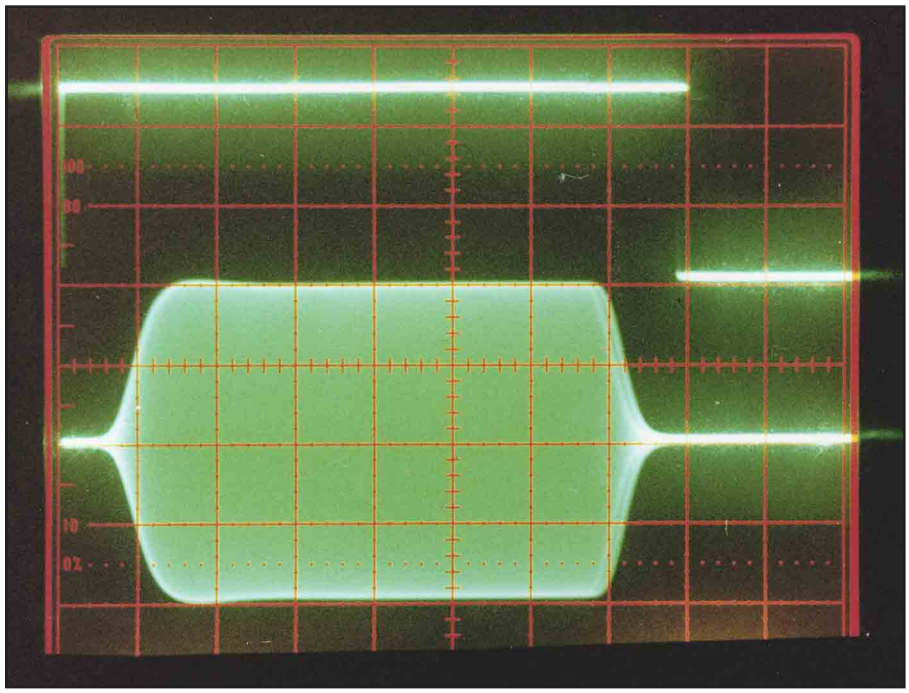

Fig 6—CW RF envelope and the CW Enable waveform that prevents CW backwave.

The ALC filter has a fast-attack (2 ms) and slow-decay (2.5 s) response using a diode and a dual time-constant RC circuit. In SSB, the fluctuations in the ALC that are applied to the CLC5523 amplifer are very small and do not noticeably degrade the quality of the SSB signal.

Also included is a frequency-spot function. The controller turns on the CW Enable signal and grounds the Key Input line (but does not activate the T/R relays) and sends an adjustable 455-kHz spot-signal level to the IF and low-level RF circuits.

Conclusions

Although the signal path is an analog design, reasonably modern devices and circuit design methods are used. In the interest of simple and straightforward design, I decided not to do any digital signal processing in this particular application. There is today still a lot to learn and a lot to accomplish using analog methods. The mechanical filters are a *little* on the expensive side, but the simplicity of the approach more than compensates, and the quality of the IF speech-processed signal and the cleanliness of the IF output spectrum are outstanding. For details of the mechanical filters that I used in this project, go to (**www.rockwellcollins.com/otherbusinesses/collins-filters/low-cost-series/**). Bob Johnson at the Rockwell Collins Filter department has been helpful in this project and previous projects (see Note 1). His expertise is always appreciated.

The OEMBS2 Basic Stamp (**www.parallaxinc.com/**) controller is easy to program if you understand simple *BASIC* programming methods, and it is much more than fast enough in this application. Delays (the PAUSE XX ms instruction) are introduced to slow the action where needed. It uses a PIC16C57C-20/SS microcontroller with a 20-MHz clock and a *PBASIC* interpreter. The EEPROM is very easily loaded, modified and debugged (without removal from the equipment) via an onboard 9-pin connector from a PC serial port using Parallax Editor software. Details of the Basic Stamp control board, including the *BASIC* code that I use, are not included in this article, but are available from me by e-mail.

Notes

[1]W. E. Sabin, W0IYH, "The Mechanical Filter in HF Receiver Design," *QEX,* March 1996, pp 14-20.

[2]W. E. Sabin, W0IYH, "A 100-W MOSFET HF Amplifier," *QEX*, Nov/Dec 1999, pp 31-40.

[3]A. Williams, WD5GNR, "An Introduction to Microcontrollers: Ham Radio Style!" *QEX,* Jul/Aug 1998, pp 28-31.

[4]R. Heil, K9EID, "High-Quality SSB Audio," *QEX,* Mar/Apr 2000, pp 38-44.

[5]W. E. Sabin, W0IYH, "A Logarithmic Audio Speech Processor," *Communications Quarterly*, Winter 1997, p 9. This unit has been modified for peak compression rather than speech processing.

[6]W. E. Sabin, W0IYH, "Power Supply for a MOSFET Power Amplifier," *QEX*, Mar/Apr 1999, pp 50-54.

[7]W. E. Sabin W0IYH "Diplexer Filters for an HF MOSFET Power Amplifier,"*QEX*, Jul/Aug 1999, pp 20-26.

[8]W. E. Sabin, W0IYH, "Narrow Bandpass Filters for HF," *QEX*, Sept/Oct 2000, pp 13-17.

[9]W. E. Sabin, W0IYH, "The Lumped-Element Directional Coupler," *QEX*, March 1995, pp 3-12.

TX RX SYSTEMS INC.

VARI-NOTCH® DUPLEXERS

FOR 2 METERS

The TX RX Systems Inc. patented Vari-Notch filter circuit, a pseudo-bandpass design, provides low loss, high TX to RX, and between-channel isolation, excellent for amateur band applications. TX RX Systems Inc. has been manufacturing multicoupling systems since 1976. Other models available for 220 and 440 MHz, UHF ATV and 1.2 GHz.

19" RACK MOUNT

MODEL 28-37-02A

144-174 MHz

92 dB ISOLATION AT 0.6 MHz SEPARATION

400 WATT POWER RATING

TX RX SYSTEMS INC.

8625 INDUSTRIAL PARKWAY, ANGOLA, NY 14006

TELEPHONE 716-549-4700 FAX 716-549-4772 (24 HRS.) e-mail: sales@txrx.com

A MEMBER OF THE BHD TECHNOLOGIES GROUP

About Monopoles and Dipoles

Do you want to put up a vertical antenna? Do you have one that's not performing well? Here are the hows and whys of verticals that work.

By Valentin Trainotti, LU1ACM

In 1895, Guglielmo Marconi made a spark transmission in the Italian countryside (achieving a distance of 100 meters), beginning a century of radio communications. His experiments were based on Heinrich Hertz' electromagnetic-wave discovery a few years before, validating the theory of James Clerk Maxwell.

Marconi wanted to achieve truly long-range communications for practical use and maximum range was a priority. At first, he saw that maximum range could be achieved by increasing the antenna height for both horizontal and vertical polarizations. At that time, the antenna was at once the radiating system and part of the generator or transmitter. The operating frequency was a function of the antenna's size. Maximum range was achieved by increasing antenna size, which lowers the generated frequency. When using dipoles, it was difficult to have an elevated spark system and a big antenna at the same time.

Therefore, Marconi started working empirically because science could give him no advice. Almost no one was working on these things before him. He found a practical method to get the spark equipment to the feed point using a monopole, sometimes called a Marconi, antenna. Figs 1 and 2 show sketches of a Hertzian dipole and a Marconi monopole, respectively.

The invention of the monopole permitted him to achieve a lower generated frequency and at the same time, a vertical polarization with a smaller antenna—half the size of a Hertzian dipole for the same frequency. Increasing the monopole's size was very simple: Increase its height. That effect permitted lowering the frequency and Marconi discovered an increase in range. The last years of the 19th century saw work toward lower and lower frequencies to achieve maximum range. Of course, as techniques improved, more power was injected into antenna systems. This work made possible transatlantic radio communication, which was finally obtained by the Marconi-Fleming team on December 12, 1901, linking Podhu, England, and St. John's, Newfoundland.

Bernardo de Irigoyen 650 2 10
Ciudad de Buenos Aires, CF 1072
Argentina
vtrainotti@ieee.org

The invention of the monopole and the vertical polarization it produced made possible the launching of a surface wave along the Earth's surface. Surface waves propagate with low attenuation, achieving long-range communications even beyond the horizon.

Monopoles

Marconi invented the monopole antenna by making a ground connection at one end of the antenna. How this antenna and wave propagation worked was a mystery at the time. Nevertheless, as more scientific and technical individuals became involved in the radio communications field, many questions were answered. In 1924, Stuart Ballantine wrote a wonderful paper in the *Proceedings of the IRE*, providing the basis for an optimum monopole antenna for AM broadcast stations operating at medium frequencies. Optimum monopole-antenna height does not necessarily yield maximum efficiency, because a monopole works with a ground plane as an integral part of it.

Supposing perfectly conducting ground, optimum monopole height is around 5/8 λ. This height gives maximum field strength along the Earth. Nevertheless, for MF broadcast use, the secondary lobe of its radiation pattern at this height was found excessive and detrimental to operation at night. This effect made possible the optimum antenna-height determination for broadcast use with maximum nocturnal service area. The service area depends on antenna height, the antenna height-radius relationship, operating frequency and ground conductivity and permittivity. This nocturnal service area is based on the distance from the transmitting antenna, where the surface-ionospheric wave relationship is 10 dB. Beyond that distance, the self-interference zone begins, producing distortion of the received signals.

In the *Proceedings of the IRE,* Dr. George Brown wrote an historical paper about increasing the efficiency of a monopole installed over real ground. From his results, a technique using an artificial, buried ground plane for a broadcast antenna was developed. The artificial ground plane consists of 120 copper-wire radials, close to λ/4 in length, placed uniformly on the ground along every three degrees of azimuth, starting from the monopole's feed point.

Ideal soil has an impedance of 0 Ω. Nevertheless, a real monopole with an artificial, buried ground plane has soil under it having a different surface impedance. That impedance is the parallel combination of the physical soil impedance and the artificial ground-radial impedance. Because of the divergent wire structure, the ground-radial impedance changes as a function of the distance from the monopole's feed point. The total ground impedance is very low at the feed point, theoretically approaching zero because the wires are very close to one another. As distance from the antenna base increases, the total ground impedance rises to the impedance of the soil itself.

The actual soil impedance depends on the frequency of operation and the

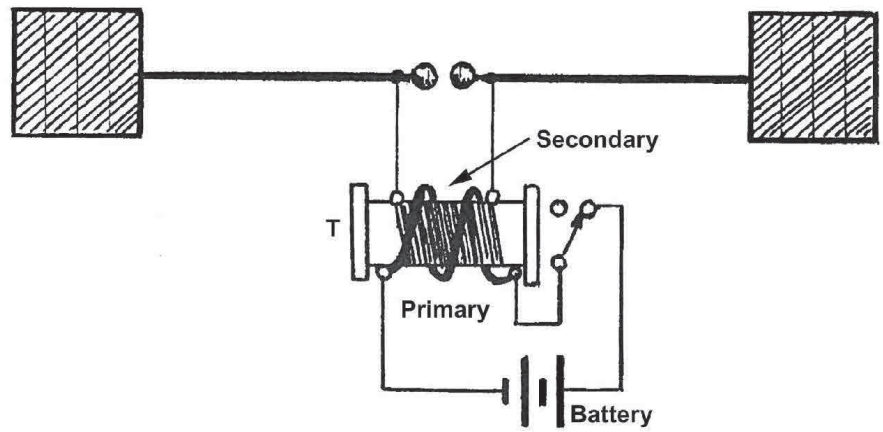

Fig 1—Sketch of Marconi's first dipole and transmitter (1887).

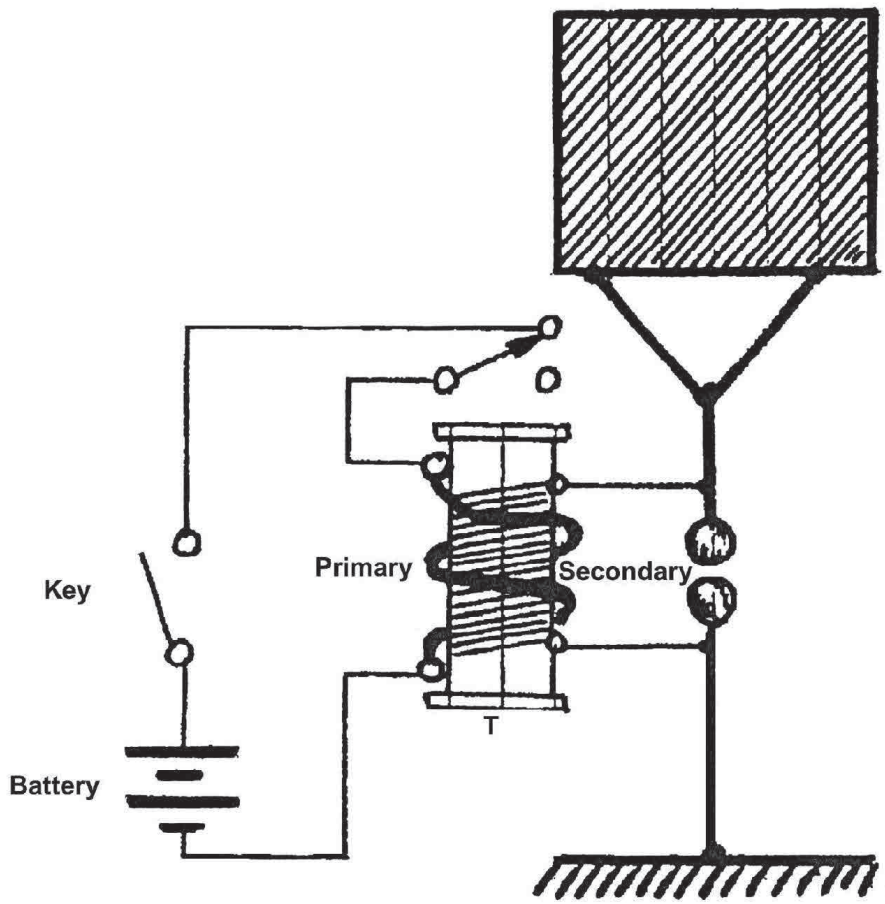

Fig 2—Sketch of Marconi's first monopole and transmitter (1896).

physical constants associated with the soil: conductivity, permittivity or dielectric constant. As an example, Fig 3 shows typical soil impedances, calculated at a frequency of 1 MHz for different numbers of buried ground-plane wires. Notice that when the wire number is low, the actual soil impedance is achieved closer to the feed point; in the higher-wire-number cases, increasing the number of wires does not decrease the total impedance. Notice also from this figure that a 120-wire artificial ground plane is almost optimal. Adding more wires does not increase the efficiency appreciably.

Near-field electric and magnetic calculations show a maximum for both fields at the monopole's feed point regardless of the monopole's height. That means the power density of the radiated wave is a maximum at the monopole's base. Fig 4 shows the antenna geometry.

Fig 5 shows the monopole's electric field circuit, where conduction current flows on the metallic part; the near-electric-field representation or displacement current flows in the surrounding space, and again, the conduction current flows in the ground plane. This permits closing the monopole's electric circuit and the production of an electromagnetic wave into the surrounding space.

To close the antenna circuit, all the force lines representing the near electric field intercept the ground plane at right angles, producing radial conducting currents in it, flowing toward the feed point. These radial conducting currents need a low-impedance medium to flow, so as not to lose energy. For this reason, a high-conductivity surface or metallic radials are needed. Radial length must be at least λ/4. Nevertheless, conducting currents at distances greater than one-half wavelength on the ground plane do not return to the feed point and do not increase the antenna's efficiency. Amateur monopoles generally do not get enough space for buried radials, or they use only a few to decrease the antenna's cost and, of course, achieve lower efficiencies than in the broadcasting-antenna case.

One important thing to remember is: Monopole ground planes should be of infinite conductivity, or as good as is possible, because it is part of the antenna itself. Any departure from this concept yields lower radiation efficiencies because of low Earth conductivity as compared to metallic conductors.

Dipoles

Dipoles are among the oldest antennas and they were the first radiating elements used since Hertz's experiments in 1885-1890. A dipole may be used for vertical or horizontal polarization, depending on its installation over ground. This is a quite old concept, because Earth was adopted as a reference and it is considered a hori-

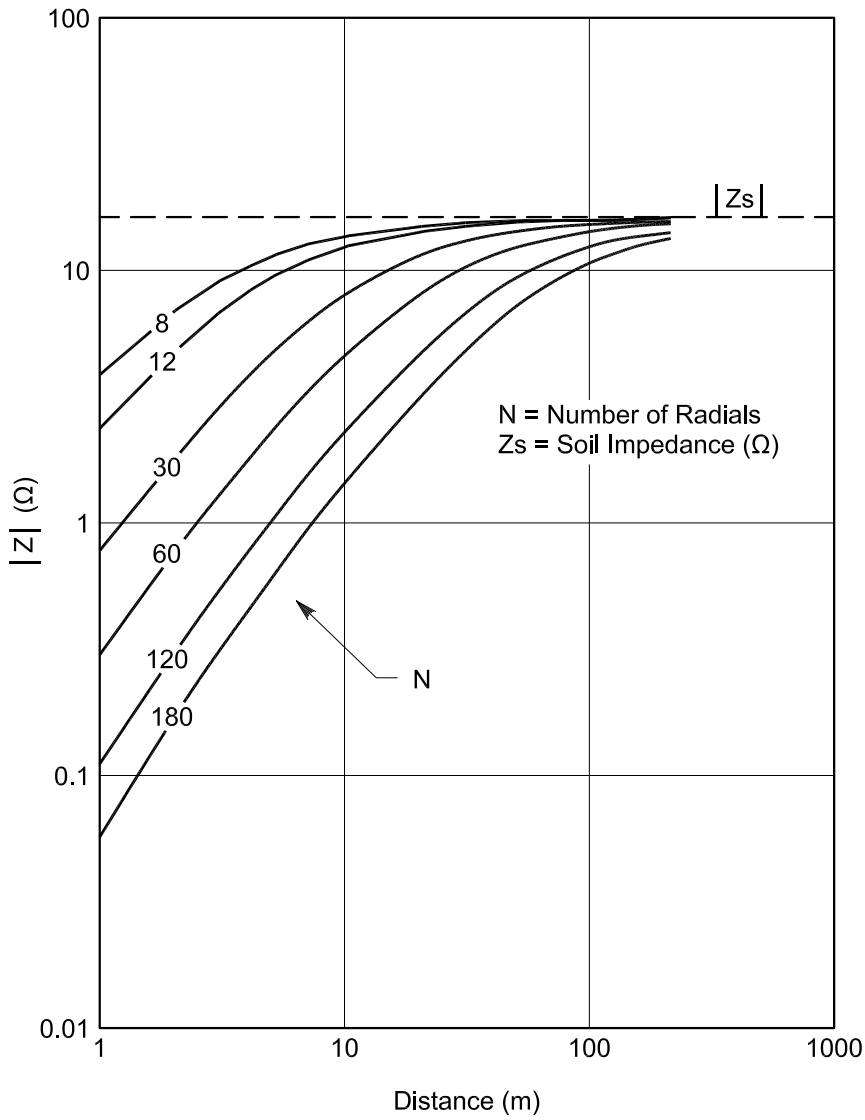

Fig 3—A graph of total ground impedance as a function of distance at 1 MHz (λ = 300 meters). Total impedance is due to metal-wire ground plane (radials) and real soil impedance (σ = 0.03 Siemens/meter ε_r = 30 at 1 MHz). Soil impedance, Z_s = 11.76 + j11.14 Ω. = |16.2| /43.45°.

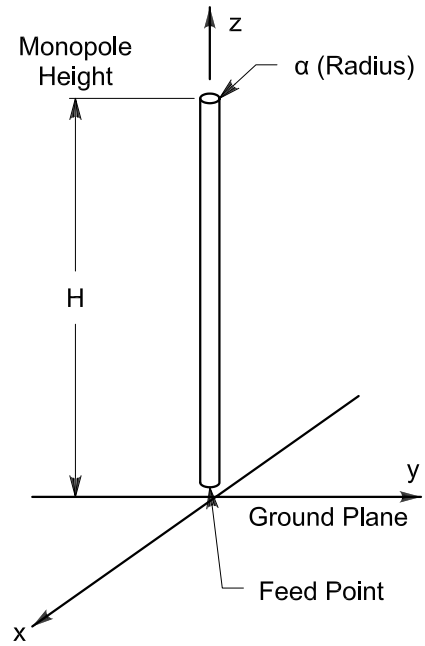

Fig 4—Monopole geometry.

zontal plane. Generally speaking, "horizontal polarization" means electric-field vectors are parallel to the Earth. Dipoles have been used successfully in the last century because they are high-efficiency antennas. For HF applications, most installations use horizontal dipoles, inverted-V dipoles or horizontal-dipole arrays.

A vertical dipole, installed over ground, produces near-electric-field lines that close a circuit over the dipole itself. Few lines connect with the image and they depend on the dipole's height over ground. This is a big difference from the monopole, where all the lines connect with the image. In the dipole case, fewer lines connect with the image as the dipole's height over ground is increased. That means that coupling between the dipole and its image lessens as its height increases: A dipole approaches free-space performance as its height increases. A vertical dipole and its image constitute a collinear array system and its mutual impedance is very low. A horizontal dipole and its image form a broadside array system, their mutual impedance is high and the dipole input impedance varies greatly as a function of height.

Fig 7 shows a representation of dipole electric-field lines. A big difference can be seen comparing this figure with that of the monopole (Fig 5). In the dipole case, electric-field lines close the antenna circuit in free space for the displacement current and—in low-loss

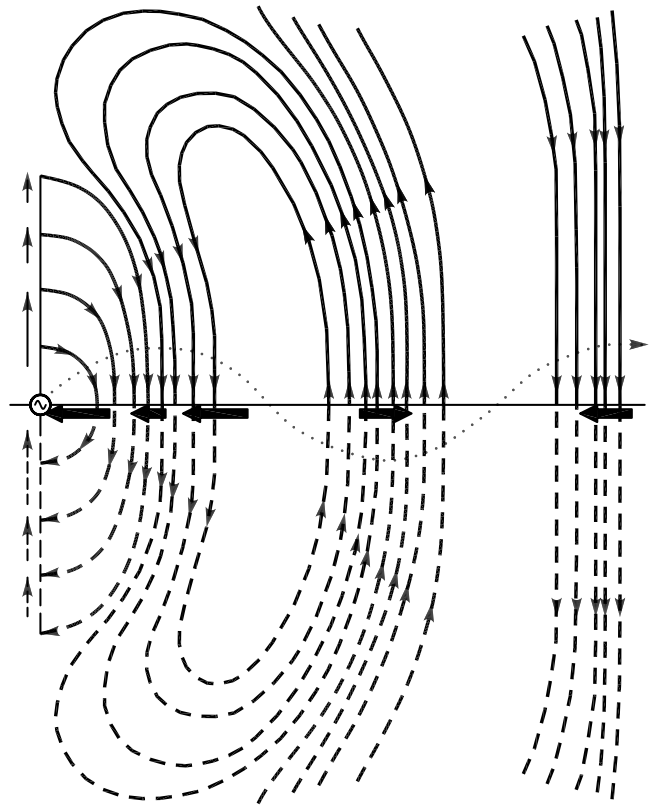

Fig 5—A simplified rendering of monopole near electric field and currents.

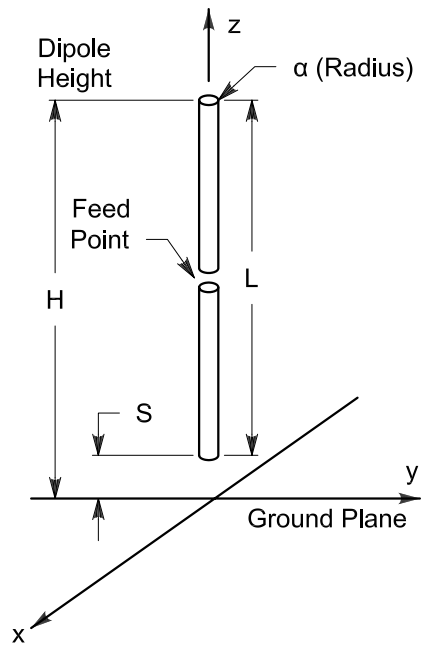

Fig 6—Dipole geometry.

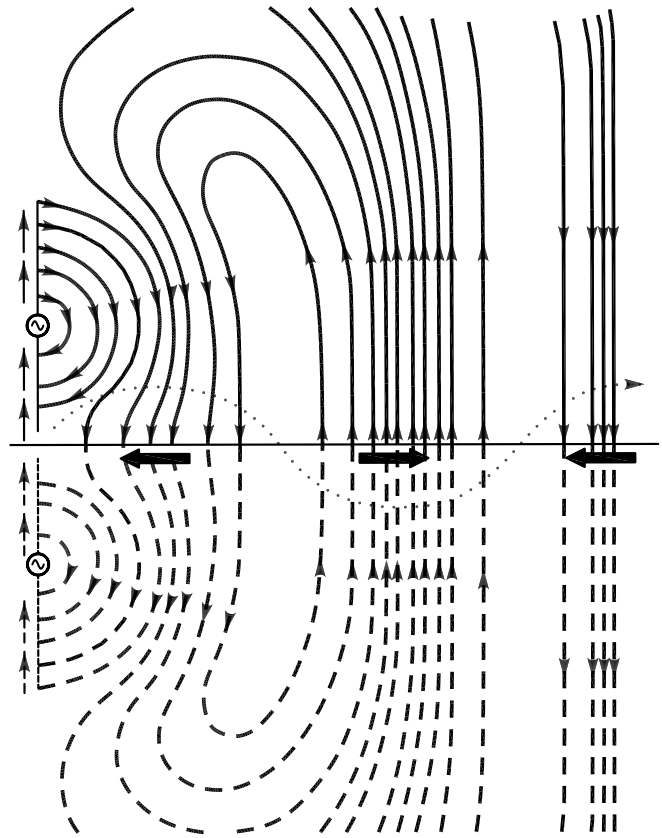

Fig 7—A simplified rendering of dipole near electric field and currents.

metallic conductors—for the conduction current. Weak conduction currents are in the ground plane under the vertical dipole and they depend on the separation of dipole's lower tip from ground. This is a reason why metallic radials should be avoided, especially when the dipole is raised above ground.

To conclude this part: Monopoles require very high-conductivity ground planes to produce high radiation efficiencies. That is not so important for vertical dipoles; their efficiencies depend on their heights above ground. In the latter case, ground radials should be avoided because of their small contribution to the dipole's radiation efficiency. Current and power densities in the ground plane depend on dipole height and physical shapes of lower antenna portions.

Fig 8 shows the calculated close-to-ground power-density comparison. In each case, infinite ground-plane conductivity has been considered. Each of the monopoles and dipoles in this simple example are operating at 10 MHz with 1 kW of input power. Monopole heights are 0.01, 0.25 and 0.5 λ. Vertical-dipole heights over ground are 0.503, 0.53, 0.6, 0.8 and 1.0 λ. Each dipole is λ/2 long, so that separation (s) from ground is increased. A monopole and dipole height/radius (H/a, slenderness) relationship of 200 has been chosen. Similar results can be obtained at other frequencies.

The dipole has more flexibility because it can be raised over the ground plane, and for this reason, the magnitudes of the fields and power density are even lower on the ground plane as height is increased. This can be seen clearly in Fig 9, where the calculated dipole power density over ground is shown as a function of the dipole's lower tip separation, s, at a distance of 1 m from the vertical dipole's base. Therefore, power density is reduced by around 30 dB when lower dipole tip reaches λ/2 and even lower as s is increased any further.

Empirical Evidence

Dipole behavior has been verified in practice because, during May 1994, an MF vertical dipole was designed and constructed for a 50-kW broadcast station, exhibiting high-efficiency radiation without the classical buried ground plane. Verification was obtained by means of very accurate surface-wave E-field measurements along the Earth. This achievement can be applied to Amateur Radio practice by having a simple, cheap, omnidirectional and practical antenna suitable for long-distance communications because of its low-elevation-angle radiation over real ground. The vertical radiation pattern, as a function of distance, was pointed out by Sommerfield, Norton and Jordan. The monopole vertical-radiation pattern shown is generally the corresponding far-field pattern where the surface-wave component has dropped out.

The radiated wave can be seen as the sum of a space wave and a surface wave. The space wave is the sum of a direct wave and a ground-reflected wave. For this reason, the wave along the Earth is entirely based on the surface wave because the space wave is almost zero. In turn, that results from the sum of the direct and out-of-phase reflected waves. On the contrary, in space or at high elevation angles, the radiated wave is entirely based on the space wave because the surface wave is relevant only very close to ground and decreases very sharply with elevation angle. Nevertheless, the total field strength is the sum of all wave components. It is well known that the surface wave decreases with distance as a function of polarization, frequency, conductivity and dielectric constant of the earth. Vertical polarization is used to produce a strong surface wave. Monopoles or vertical dipoles are used to generate it.

At high frequencies, the surface-wave range is generally short. Surface waves are more effective in the 160

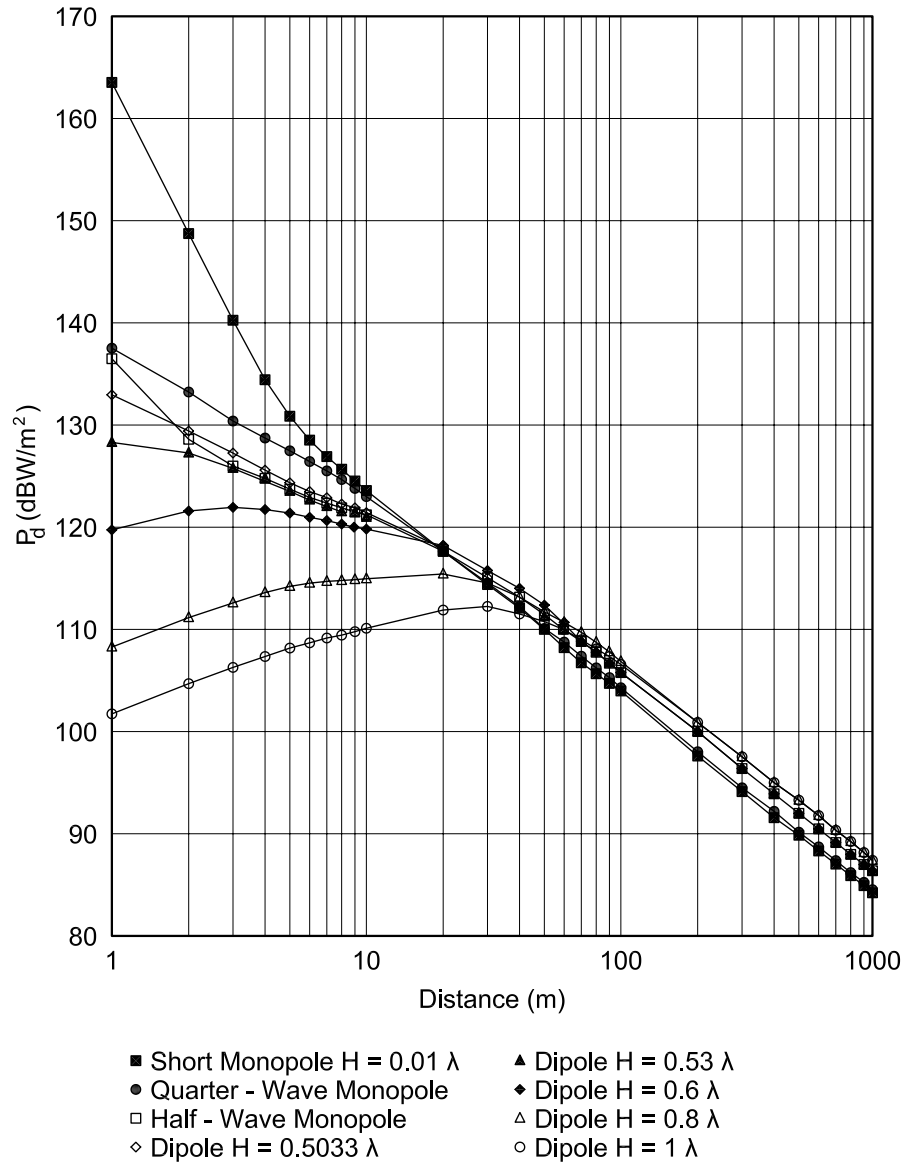

Fig 8—Calculated near power density in dB W / m² for different monopoles and vertical λ/2 dipoles (f = 10 MHz, λ = 30 meters, perfect ground).

and 80-m bands and for very-good-conductivity soils. Vertical antennas, especially λ/2 in height—either monopole or dipole—have low take-off angles that are useful for long-distance communication in the HF Amateur Radio bands, using the space wave refracted by the ionosphere.

Grounded Vertical Dipoles

A new, half-wavelength dipole has been developed for use as a vertical antenna. A λ/2 vertical dipole is a practical antenna to be employed in the HF bands. It is simple, cheap and very efficient. Dipoles have been made over the years of different shapes, but generally, the upper part of the dipole has been completely insulated from ground. This part of a dipole is very sensitive to stray, induced potentials that are very dangerous to electronic components—especially to sensitive preamplifiers because they are directly connected to the antenna through the transmission line. If this part of a dipole could be connected directly to ground, that would be very useful since it would avoid static-electricity problems associated with wind and atmospherics.

A solution to those problems can be obtained by designing an entirely grounded dipole. Such a grounded dipole can be seen in Fig 10. The dipole's central part is made of metallic tubing, at once forming its mechanical structure and having height H. This metallic structure can be connected to ground for static-discharge purposes. The dipole's skirt is made of three or four copper wires connected directly at the central metallic part close to its middle (H_G). Skirt wires are parallel to the central part and are separated by a distance from the vertical axis (S_S). The lower skirt-wire tips are separated from ground by dielectric isolators at a distance, S. The dipole is fed by means of a 50-Ω coaxial line connected directly to the proper point in the skirt (H_F), achieving a good impedance match with the band (SWR<2:1, transmission loss lower than 0.5 dB). Such a match is generally wider than necessary to cover an HF amateur band. Several models have been studied to optimize the dipole's dimensions, achieving a SWR (2:1) bandwidth of around 10% in any band. This permits operating with a good match, even in the 80-m amateur band from 3500-4000 kHz, which is the most difficult band to cover. In this band, a grounded supporting tower can be used if any metallic guys are broken into nonresonant lengths by insulators. An advantage of a grounded tower is that you can place other antennas at the top; but their effect must be compensated in the grounded dipole's impedance adjustment.

As an example, Table 1 and Fig 11 show the input resistance, reactance and SWR achieved for a grounded vertical dipole that was designed for the 15-m band. In this case, the resulting dimensions are: H=6.8 m, H_G=3.35 m, H_F=2.6 m, S_S=0.20 m, S=0.15 m and the supporting aluminum tube has a diameter of 50 mm. The skirt is made of four 4-mm copper wires attached to the supporting tube at a point H_G by means of four metallic spreaders. The coaxial UHF female connector is attached to the supporting tube at point H_F, where the four skirt wires are fed. Coaxial line can be installed inside the supporting tube through a hole placed close to the coaxial connector and close to the tube's bottom for weather protection. The supporting tube can be erected by means of three or four Dacron ropes or wires, conveniently broken by several insulators so as not to interfere with the antenna's near field. A picture of the antenna can be seen in Fig 12, which was taken during antenna-impedance measurements and adjustment. Fig 13 shows a best view of the feed point, where connections to the skirt wires and to the coaxial feed line can be seen.

Three other skirt-dipole models were built and tested for the 10- and 6-m bands, with similar input-imped-

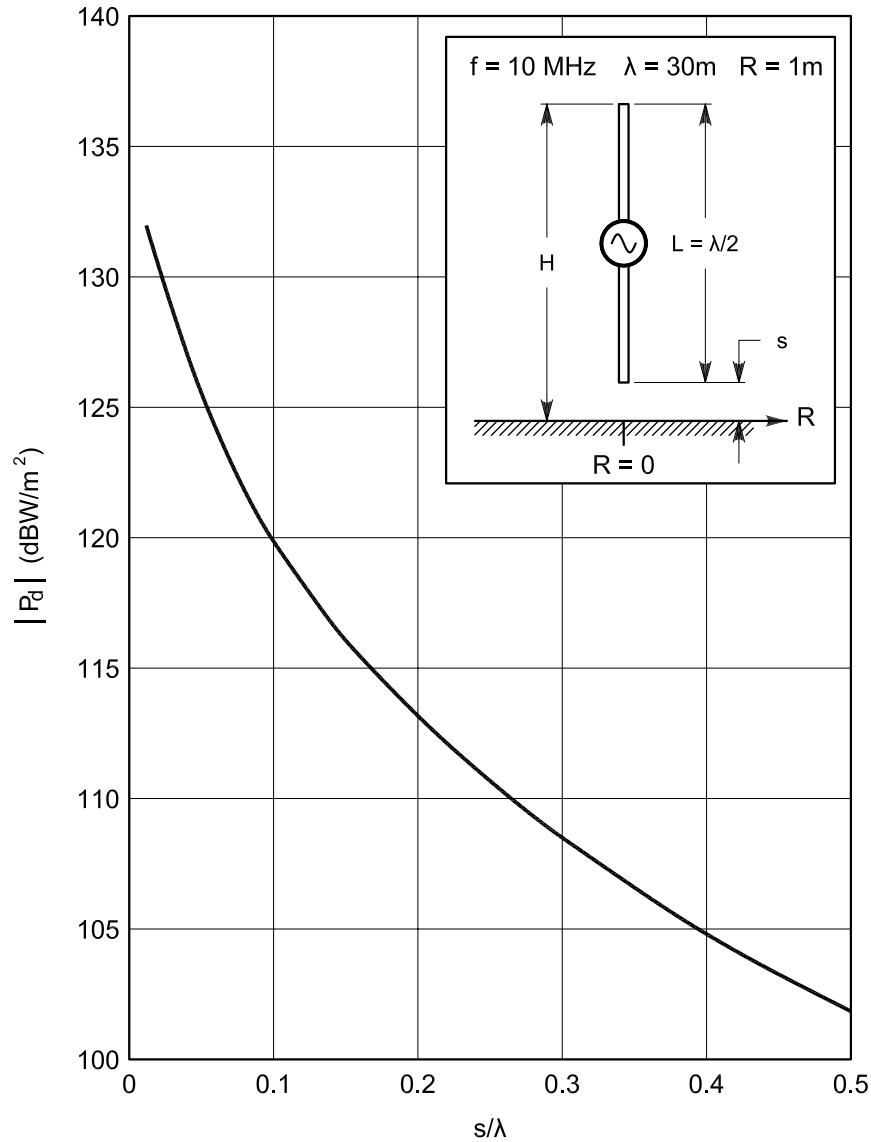

Fig 9—Calculated near power density at 1 meter from the dipole base as a function of the dipole lower tip height, *s*, in wavelengths.

Table 1—Grounded Vertical Dipole Input-Impedance Measurement

f (MHz)	*Rin (Ω)*	*Xin (Ω)*	*SWR*
20.5	96	20	2.00
20.6	91	17	1.89
20.7	86	15	1.80
20.8	80	13	1.65
20.9	75	12	1.55
21	70	10	1.44
21.1	65	9	1.34
21.2	65	6	1.33
21.3	59	4	1.20
21.4	56	2	1.12
21.5	53	1	1.06
21.6	51	0	1.02
21.7	48	1	1.04
21.8	46	3	1.11
21.9	44	3	1.13
22	43	4	1.18
22.1	40	5	1.27
22.2	40	8	1.30
22.3	36	10	1.49
22.4	35	11	1.53
22.5	33	12	1.63
22.6	31	13	1.78
22.7	29	14	1.90
22.8	27	15	1.98
22.9	27	16	2.12
23	26	17	2.20

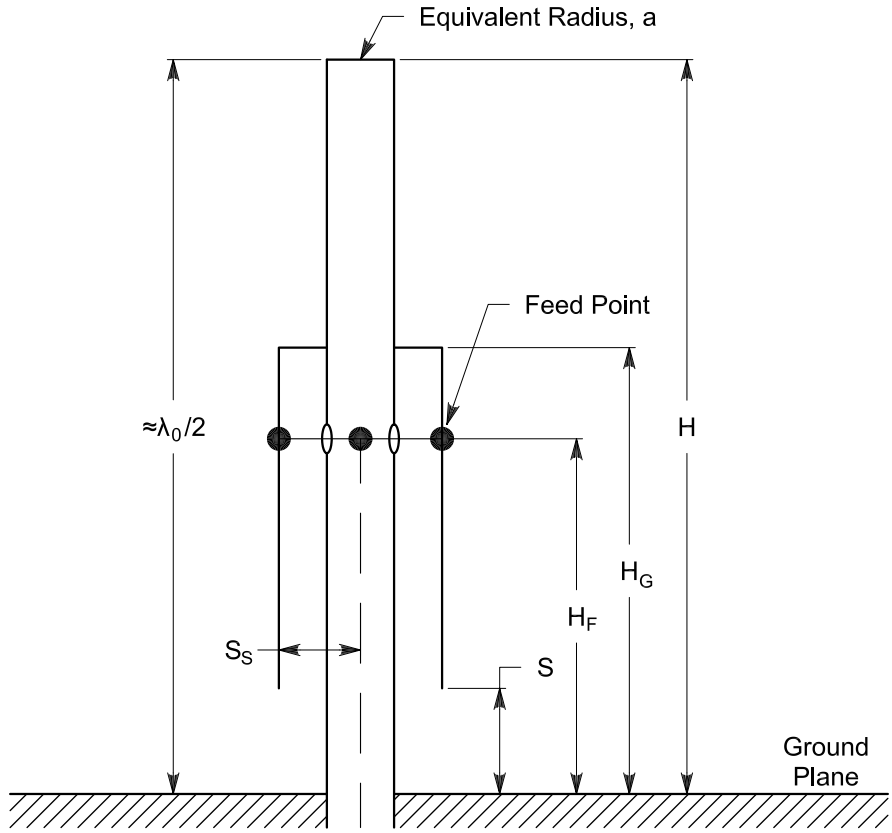

Fig 10—Sketch of a grounded λ/2 vertical dipole.

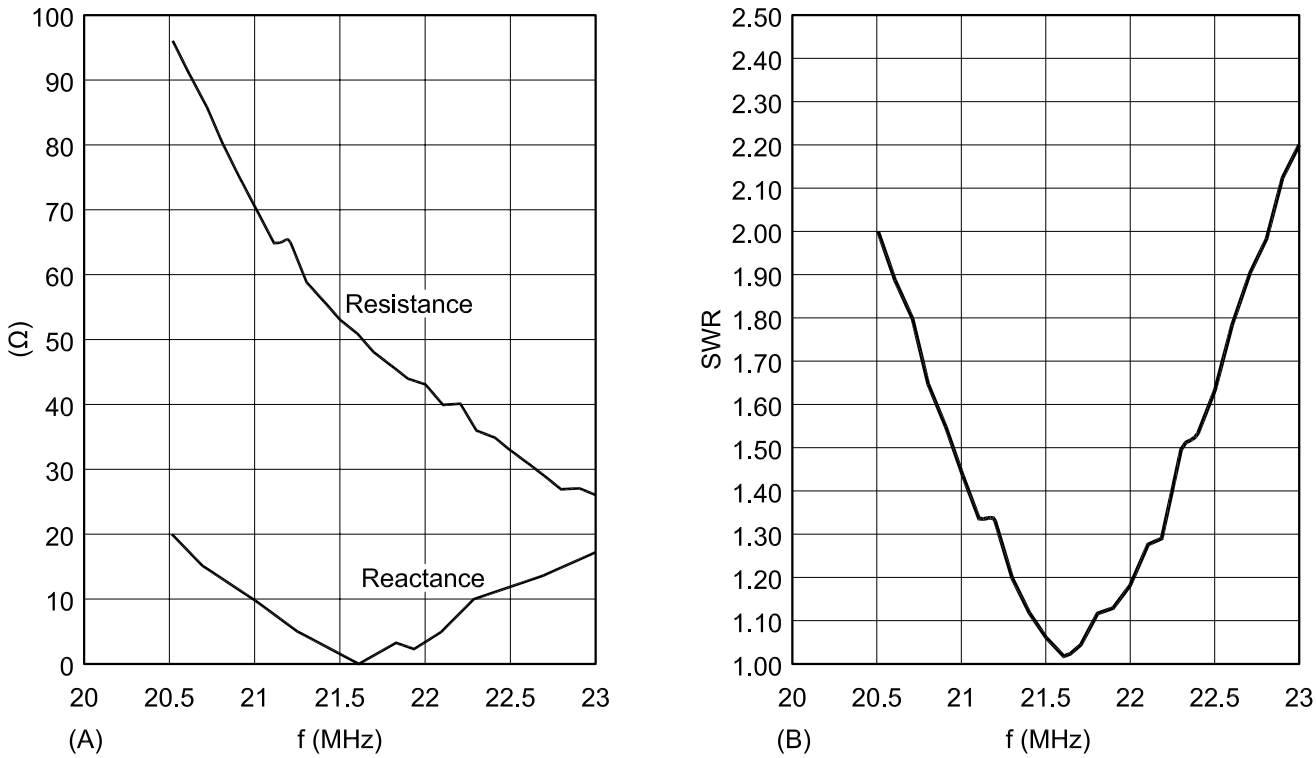

Fig 11—Characteristics of a 15-meter grounded vertical dipole. At A, measured input resistance and reactance. At B, SWR.

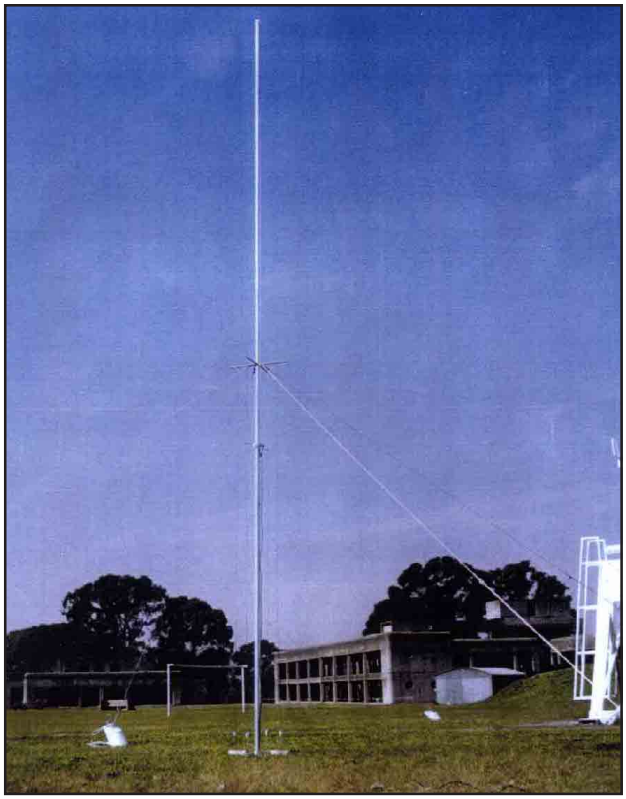

Fig 12—Photograph of a 15-meter grounded vertical dipole model during input impedance measurements.

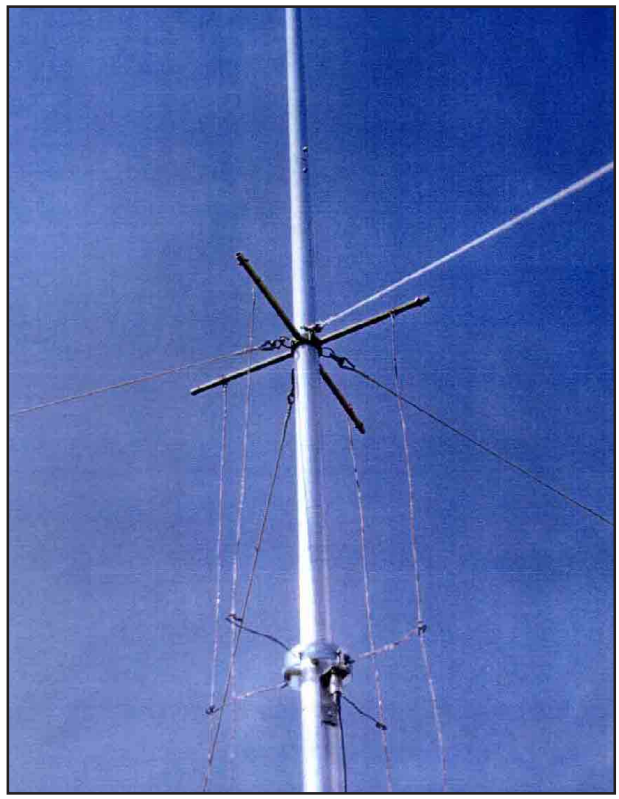

Fig 13—Photograph of a 15-meter grounded vertical dipole feed point.

ance behavior. A 6-m grounded vertical dipole is actually used for a 50.07-MHz beacon for the Citefa Radio Club in Buenos Aires, Argentina. This beacon has been received in Australia during good propagation conditions, permitting bilateral contacts on that band as soon as the beacon was received.

Two-meter and 75-cm models have been made. They are intended to be used on top of poles or supporting towers, taking advantage of their grounded structures and high radiation efficiency.

Conclusions

Monopole and dipole characteristics have been pointed out to promote understanding of their operation. I presented my thoughts in the hopes that they would help amateurs comprehend the operation of these kinds of antennas and that they would point out where antenna designers must be careful to achieve maximum antenna efficiency. In theory, monopoles and dipoles of similar height and over perfectly conducting earth have practically the same directivity and gain. Over real ground, though, a monopole has the disadvantage that it needs a metallic ground plane, as perfect as possible. This requirement is sometimes difficult to achieve.

For amateur purposes, the place where a monopole is installed is generally quite different from the ideal. For this reason, the creation of an artificial ground plane is a difficult—if not impossible—task. Dipoles, to the contrary, may be easily installed even on a rooftop, and they are not so dependent on a ground plane, making them the best selection where a simple and cheap antenna is desired. A grounded vertical dipole could be a simple, safe and practical solution to getting an Amateur Radio antenna on the air, especially for frequencies higher than 14 MHz, where dipole dimensions are reasonable.

Acknowlegements

I would like to express my gratitude to Ing. Juan Skora and to Diego Schweitzer and Pablo Perez for their support during the modeling, construction and measurement phases of this experiment.

References

A. Sommerfield, *Annalen der Physik*, Vol 128, Mar 1909.

S. Ballantine, *Proceedings of the IRE*, Vol 12, Dec 1924.

K. A. Norton, *Proceedings of the IRE*, Part I, Vol 24, Oct 1936.

K. A. Norton, *Proceedings of the IRE*, Part II, Vol 25, Sept 1937.

G. H. Brown et al., *Proceedings of the IRE*, Vol 25, June 1937.

E. Jordan, *Electromagnetic Wave and Radiating Systems* (Englewood Cliffs, New Jersey: Prentice-Hall, Inc, 1950).

V. Trainotti, *IEEE Transactions on Broadcasting*, Vol 37, No. 3, Sep 1991.

V. Trainotti, *IEEE Transactions on Broadcasting*, Vol 42, No. 4, Dec 1996.

V. Trainotti, *IEEE Transactions on Broadcasting*, Vol 45, No. 1, Mar 1999.

V. Trainotti, *IEEE Transactions on Broadcasting*, Vol 45, No. 3, Sep 1999.

Valentin Trainotti has been a radio amateur since 1954 (LU1ACM). He is an Electronic Engineer, working at Citefa Antenna and Propagation as Chief Engineer, full Professor (part time) of Radiating Systems on the Engineering Faculty of The University of Buenos Aires. A senior member of IEEE and Argentina Chapter of IEEE broadcast Technology Chair, he is a life member of Radio Club Argentino (RCA). Tino has studied many types of antennas, especially broadcast, including crossed-field arrays (CFAs). □□

The Fractal Loop Antenna: Understanding the Significance of Fractal Geometry in Determining Antenna Performance

Fractal antennas are visually interesting, but do they offer better performance than other geometries? Come learn how they compare.

By Dr. Steven R. Best, VE9SRB

Fractal antennas represent a class of electromagnetic radiators where the large-scale antenna structure is comprised of a series of repetitions of a single geometry (the geometry basis), and where each repetition may be on a different scale.[1, 2] Fractal antenna geometries are self-similar in that some portion of their geometry has the same shape as the large-scale geometry, only on a reduced scale.

The topic of fractal-loop antennas has been previously addressed by Dr. Nathan Cohen, N1IR, in a series of articles published in *Communications Quarterly*.[2, 3, 4] These articles describe the basic concepts and performance characteristics of a class of fractal-loop geometries known as *Minkowski Islands*. Dr. Cohen demonstrated that these fractal-loop antennas exhibit resonance compression and multiband behavior as a function of frequency. He concluded that this behavior is a result of the self-similar properties of the fractal geometry. The Minkowski Island fractal-loop antennas were also shown to have an impedance resonance at a frequency where the loop is of much smaller physical area than a resonant, nonfractal Euclidean square or circular loop.

Here, Minkowski Island fractal loops are considered from two perspectives. The performance properties of these fractal loops are examined in detail, and the performance tradeoffs associated with achieving a lower resonant frequency using fractal antenna geometries are considered. The performance tradeoffs are examined with respect to resonant resistance, bandwidth and efficiency. Second, the impedance and pattern performance properties of the Minkowski Island fractal loop are compared with nonself-similar, bent-wire loops having similar physical area and total wire length. This comparison reveals that the nonself-similar bent-wire geometries perform in a similar fashion to, or better than, their self-similar fractal counterparts. It also shows that the resonance compression and multiband behavior of fractal antennas is not a result of the self-similar

[1]Notes appear on page 34.

48 Perimeter Rd
Manchester, NH 03103
srbest@att.net

properties of that geometry. In fact, any loop antenna linearly loaded by increasing the total wire length while maintaining the same area would exhibit resonance compression and multiband behavior similar to that exhibited by self-similar fractal-loop antennas.

The Resonant Euclidean Loop Antenna

Before discussing the concepts and performance characteristics of fractal and other bent-wire loops, it is necessary to review the characteristics of a Euclidean, nonfractal loop geometry. In this case, the nonfractal loop antenna is the Euclidean loop depicted in Fig 1. This loop is slightly rectangular with dimensions of 2.8 × 2.66 meters. The total physical loop area is approximately 7.46 square meters.

Using *EZNEC Pro*,[5] the performance properties of the rectangular loop were determined for reference purposes. The *EZNEC* model for this antenna consists of 164 segments. The wire diameter is 3.2 mm and the wire-loss option is set for copper wire so that the antenna efficiency may be determined. The calculation engine used to model the antenna is *NEC 4.1*. A graph of the feed-point impedance properties of the rectangular loop is presented in Fig 2. The significant feature is that the rectangular-loop antenna exhibits four resonance points over the range from 2 to 60 MHz. Two of these resonance points are parallel resonances, where the feed-point resistance is very large and the reactance experiences a rapid transition between +X and –X. In these frequency regions, the antenna *Q* factor is high, the bandwidth is narrow and the impedance properties are sensitive to small variations in the antenna structure. The other two resonance points are series resonances, where the antenna exhibits more useful performance characteristics.

The performance properties of the rectangular-loop antenna at these two series-resonance points are summarized in Table 1. For reference purposes, the SWR is presented with respect to 50 Ω. The 2:1 SWR bandwidth is presented with respect to the resonant resistance, because bandwidth information presented in this manner provides a better indication of the antenna's inherent bandwidth performance. The behavior of the impedance properties of this antenna will be used as a reference for comparing and understanding the impedance properties of the fractal-loop antennas.

Minkowski Island Fractal Loop Antennas

The fractal-loop geometry chosen as a reference for comparison with non-self-similar bent-wire loop geometries is the Minkowski Island fractal-loop antenna (see References 2,3,4). Three Minkowski Island loop geometries are considered: the MI1, the MI2 and the MI3 fractal loops, as depicted in Figs 3, 4, and 5, respectively. The geometry basis for these fractal loops is a slightly rectangular shape having four indentations, one on each side. The

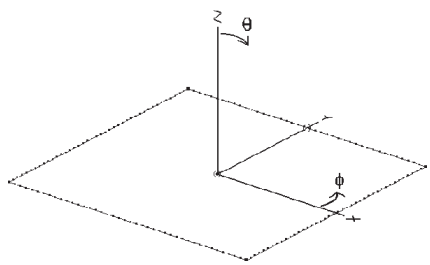

Fig 1—A simple, rectangular Euclidian loop antenna.

Table 1—Performance Properties of the Euclidean Rectangular-Loop Antenna

Resonant Frequency (MHz)	29.22	56.33
Feed-point Resistance (Ω)	134.2	268.6
SWR (50 Ω)	2.68	5.37
Peak Gain (dBi)	3.23	2.9
Overall Dimensions (λ)	0.273 x 0.259	0.526 x 0.50
Total Wire Length (λ)	1.065	2.054
2:1 SWR Bandwidth with respect to		
Resonant Resistance (%)	8	8.9
Radiation Efficiency (%)	99.3	99.6

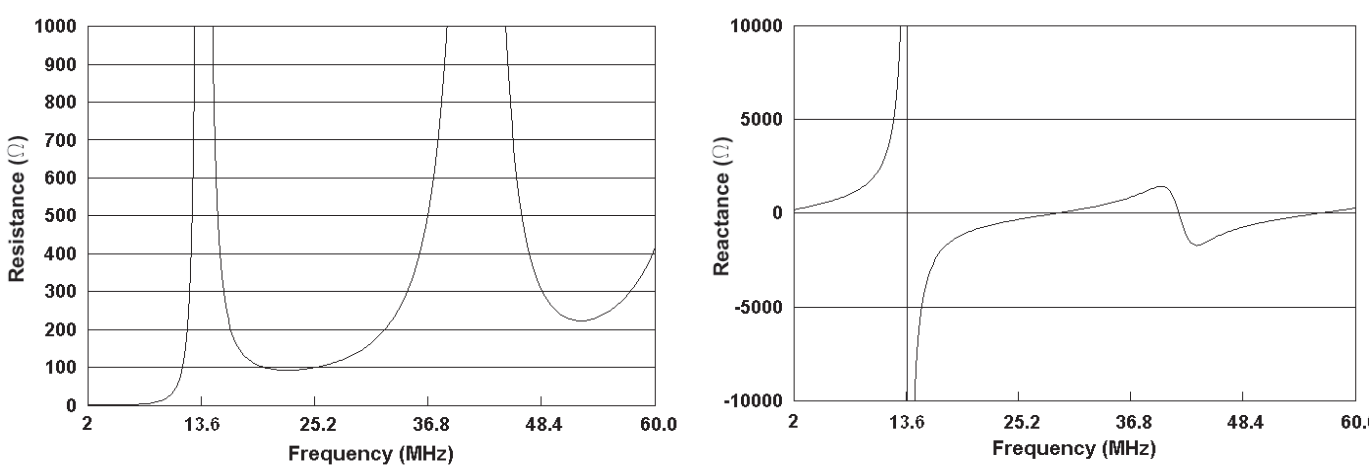

Fig 2—Feed-point impedance properties of a rectangular loop.

MI1 loop is the geometry basis for all of the Minkowski Island fractals. In the MI2 loop, this geometry basis is located in the center of the loop and is then repeated four times in the structure, once from each corner of the original basis. The MI3 loop is essentially comprised of five MI2 loops, one being located in the center of the MI3 and the other four extend from each corner of the center MI2 geometry.

To characterize the performance of the MI1, MI2 and MI3 fractal loop antennas, an *EZNEC* model of each was created. Loop dimensions of 2.8 × 2.66 meters were chosen to match the size of the Euclidean rectangular loop antenna discussed in the previous section. In replicating the MI3 loop geometry, the actual overall dimensions turned out to be 2.77 × 2.6 meters.

The *EZNEC* model created for the MI1 fractal loop consists of four wires and 164 segments. The wire diameter was set to 3.2 mm to match that of the nonfractal rectangular loop. Although the physical area of the MI1 loop is identical to that of the rectangular loop, the total wire length used to construct the MI1 loop is not. The total wire length in the rectangular loop is 10.93 meters, while the total wire length in the MI1 fractal loop is approximately 16.34 meters. The *EZNEC* model created for the MI2 fractal loop consists of 100 wires and a total of 500 segments. The total wire length in the MI2 loop is approximately 27.57 meters. The *EZNEC* model of the MI3 fractal loop consists of 500 wires and 500 segments. The total wire length in the MI3 fractal loop is approximately 45.67 meters. The wire-loss option in *EZNEC* was set to copper so that antenna efficiency could be determined at all fractal iterations.

The feed-point impedance properties of the MI1, MI2 and MI3 fractal loop antennas are presented in Figs 6, 7 and 8, respectively. From these impedance data, the changes over all fractal iterations are evident. As the fractal iteration and the total wire length in the loop increases, a compression of resonances from higher to lower frequencies occurs. The numerous resonant frequencies that occur with the Euclidean rectangular loop decrease in frequency and at the same time, they are spaced closer together in frequency. For the fractal antenna, this results in an increase in the number of resonances over a given fixed-frequency band. Over the same frequency band presented for the rectangular loop, the MI1 fractal loop exhibits six resonant frequencies, the MI2 fractal loop exhibits nine resonant frequencies and the MI3 fractal loop exhibits thirteen resonant frequencies. As with the Euclidean rectangular loop, the resonances alternate between a parallel and a series resonance with increasing frequency. The significant issue to consider and examine here is how much of this resonance-compression behavior is a direct result of the self-similar fractal geometry? At the same time, the performance tradeoffs associated with the lowering of the resonant frequencies are considered.

A detailed comparison of the performance properties of the Euclidean rectangular loop (designated MI0), the MI1 fractal loop, the MI2 fractal loop

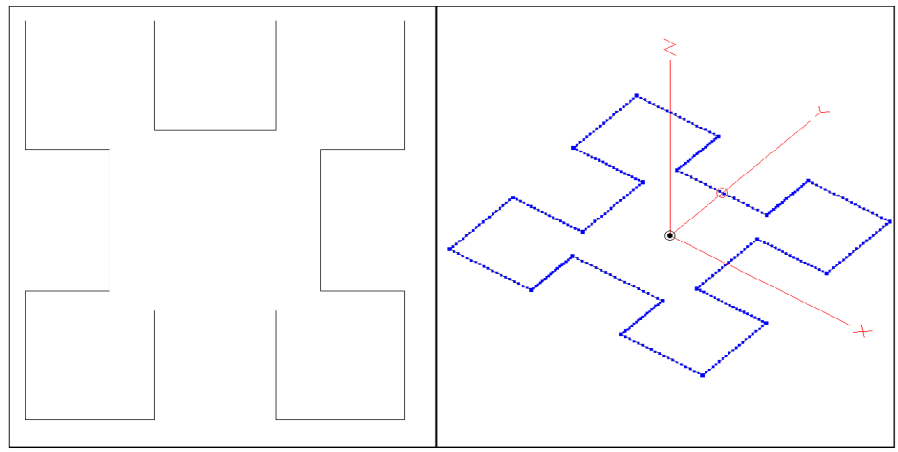

Fig 3—Minkowski Island loop geometry for the MI1 fractal loop.

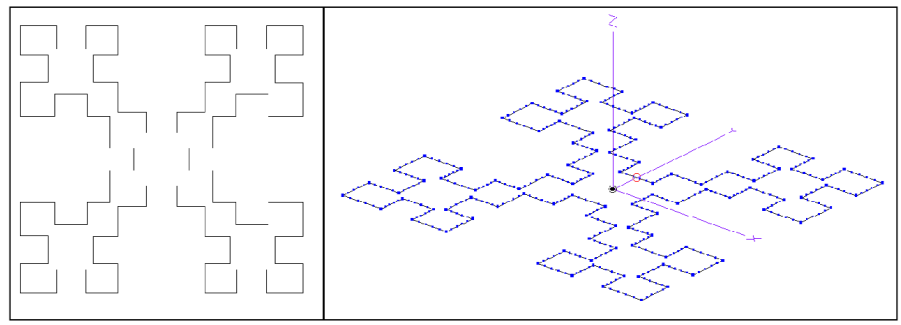

Fig 4—Minkowski Island loop geometry for the MI2 fractal loop.

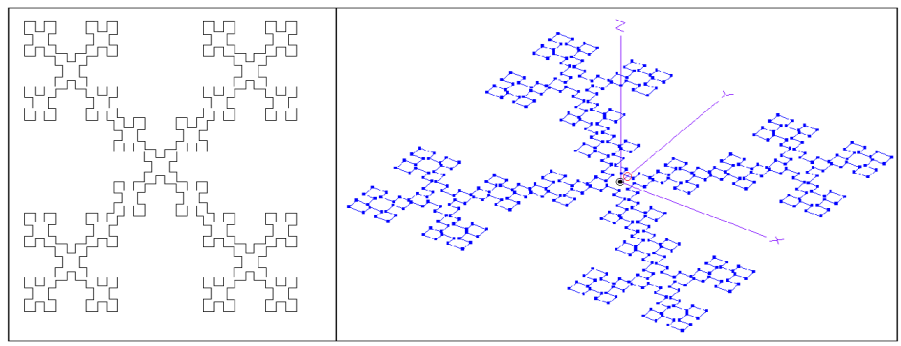

Fig 5—Minkowski Island loop geometry for the MI3 fractal loop.

and the MI3 fractal loop is presented in Table 2. The performance properties for each of these antennas are presented at the two lowest series-resonant frequencies. The performance properties presented for each antenna include the resonant frequency, resonant resistance, bandwidth, efficiency and gain. Dimensions of each loop with respect to the resonant wavelength are also presented.

Again, the significant point regarding the data presented in Table 2 is the progressive decrease in resonant frequency for the MI0, MI1, MI2 and MI3 loops. The lowest series-resonant frequency decreases from 29.22 MHz for the MI0 loop to 21.31 MHz, 15.19 MHz and 11.48 MHz for the MI1, MI2 and MI3 fractal loops, respectively. The second series-resonant frequency decreases from 56.33 MHz for the MI0 loop to 39.48 MHz, 27.89 MHz and 21.83 MHz for the MI1, MI2 and MI3 fractal loops, respectively. This progressive lowering of resonant frequency also illustrates another significant fact: As the fractal iteration increases, the resonant frequency decrease converges to a lower limit. This illustrates that the benefit of lowering resonant frequency diminishes with a progressive increase in the fractal iteration.[6]

The data in Table 2 also show that as the resonant frequency is lowered with each increase in fractal iteration, the resonant resistance, bandwidth, gain and efficiency decrease as well. The decrease in those parameters is more a function of the increase in total wire length in the antenna than the antenna's fractal geometry. The decrease in bandwidth and resonant resistance are a direct result of compressing more wire length into a smaller area (relative to the resonant wavelength). The decrease in efficiency and gain is simply a function of the increase in loss resistance (determined at the feed point) caused by the increase in total wire length.

These are the fundamental performance tradeoffs associated with lowering of an antenna's resonant frequency using fractal geometry or similar total wire-length compression technique. The fractal nature of the antenna's design is simply a mathematical methodology used to describe

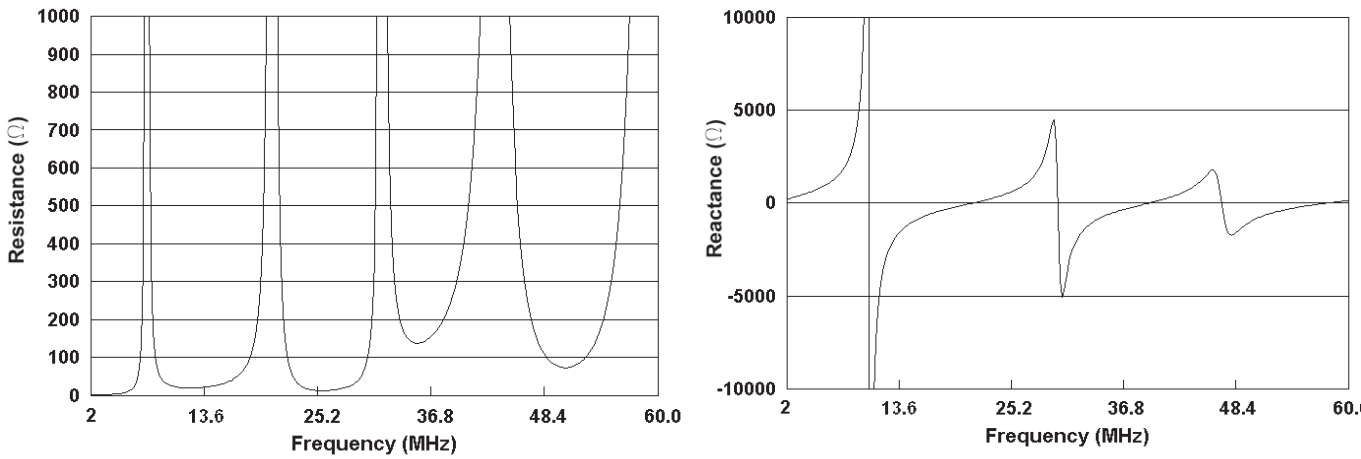

Fig 6—Feed-point impedance properties of the MI1 fractal-loop antenna.

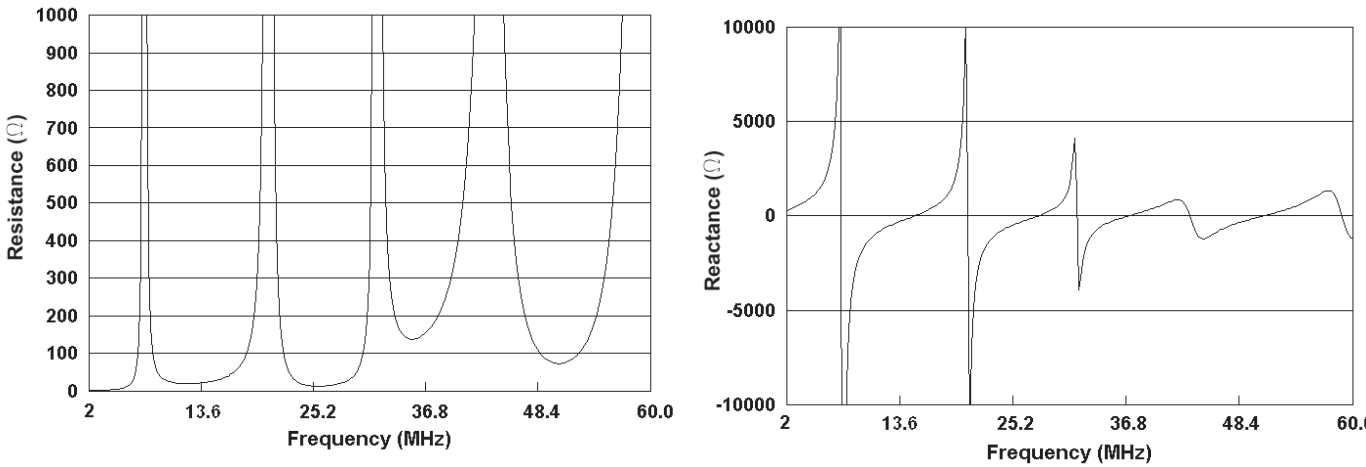

Fig 7—Feed-point impedance properties of the MI2 fractal-loop antenna.

Table 2—Comparison of the MI0, MI1, MI2 and MI3 Performance at their Resonant Frequencies

	MI0		*MI1*		*MI2*		*MI3*	
Resonant Frequency (MHz)	29.22	56.33	21.31	39.48	15.19	27.89	11.48	21.83
Feed-point Resistance (Ω)	134.2	268.6	57.8	77.8	28.1	19.1	17.6	9.6
Peak Gain (dBi)	3.23	2.9	2.38	4.5	1.83	3.5	1.0	2.1
Overall Dimensions (λ)	0.273 x 0.259	0.526 x 0.50	0.199 x 0.185	0.368 x 0.350	0.142 x 0.135	0.261 x 0.247	0.106 x 0.099	0.201 x 0.189
Total Wire Length (λ)	1.065	2.054	1.161	2.152	1.397	2.564	1.749	3.326
2:1 SWR Bandwidth with respect to								
Resonant Resistance (%)	8	8.9	3.14	2.1	1.18	0.39	0.61	0.13
Radiation Efficiency (%)	99.3	99.6	98.1	98.1	94.1	89.5	81.8	66.7

Table 3—Performance Properties of the Minkowski Island Fractal Loop Antennas

	MI2		*MI3 Mod*		*MI3*	
Resonant Frequency (MHz)	15.19	27.89	13.85	25.77	11.48	21.83
Feed-point Resistance (Ω)	28.1	19.1	23.1	13.8	17.6	9.6
Peak Gain (dBi)	1.83	3.5	1.46	3.4	1.0	2.1
Overall Dimensions (λ)	0.142 x 0.135	0.261 x 0.247	0.128 x 0.120	0.238 x 0.223	0.106 x 0.099	0.201 x 0.189
Total Wire Length (λ)	1.397	2.564	1.478	2.749	1.749	3.326
2:1 SWR Bandwidth with respect to						
Resonant Resistance (%)	1.18	0.39	0.96	0.26	0.61	0.13
Radiation Efficiency (%)	94.1	89.5	90.9	83.5	81.8	66.7

or determine how the increase in total wire length can be compressed into a predefined physical area.

Radiation patterns of the MI0, MI1, MI2 and MI3 loop antennas are presented in Figs 9, 10, 11 and 12, respectively. The patterns presented for the lower resonant frequency are cut in the θ-sweep plane with ϕ set at 90°. The patterns presented for the upper resonant frequency are cut in the ϕ-sweep plane with θ set at 90°. Radiation patterns for each of the antennas at their respective resonant frequencies are similar. The most notable difference in pattern shape and gain occurs between the MI0 loop and the MI1 fractal loop. The difference in gain is primarily a result of differences in pattern shape as both antennas have similar efficiencies. The difference in pattern shape can be attributed primarily to the difference in the size of the loop with respect to the resonant wavelength. Note that the MI0 loop is significantly larger with respect to the resonant wavelength than the MI1 loop. The radiation pattern shapes for the MI1, MI2 and MI3 fractal antennas are similar at their respective resonant frequencies because these loops are small and have similar size with respect to the wavelength. Because each of the loop radiation patterns has essentially the same shape at their resonant frequencies, gain differences can be attributed to the loop efficiency, which is primarily a function of the loop total wire length and the resulting loss resistance.

To further illustrate that the performance properties of the Minkowski Island fractal-loop antennas and the performance tradeoffs are more a function of the increase in total wire length than the loop geometry, a modification of the MI3 fractal loop was analyzed. This modification, the *MI3 Mod*, is depicted in Fig 13. The MI3 Mod loop has the same physical area as the MI3 fractal loop but significantly less total wire length: 32 meters compared to 45.67 meters. Examining the MI3 Mod geometry in detail, it is evident that it is essentially a hybrid of the MI2 and MI3 geometries.

A graph of the MI3 Mod loop's impedance properties is presented in Fig 14. A detailed summary comparison of the performance properties of the MI2, MI3 and the MI3 Mod loops is presented in Table 3. These results are consistent with the difference in total wire length between these two loop configurations. The MI3 Mod has less wire length than the MI3 antenna, a

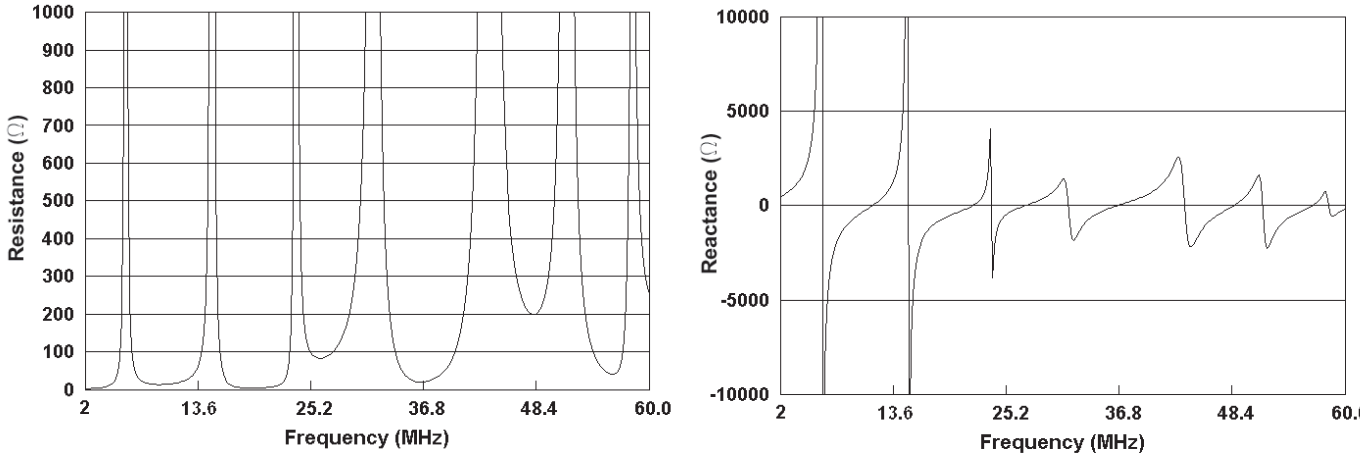

Fig 8—Feed-point impedance properties of the MI3 fractal-loop antenna.

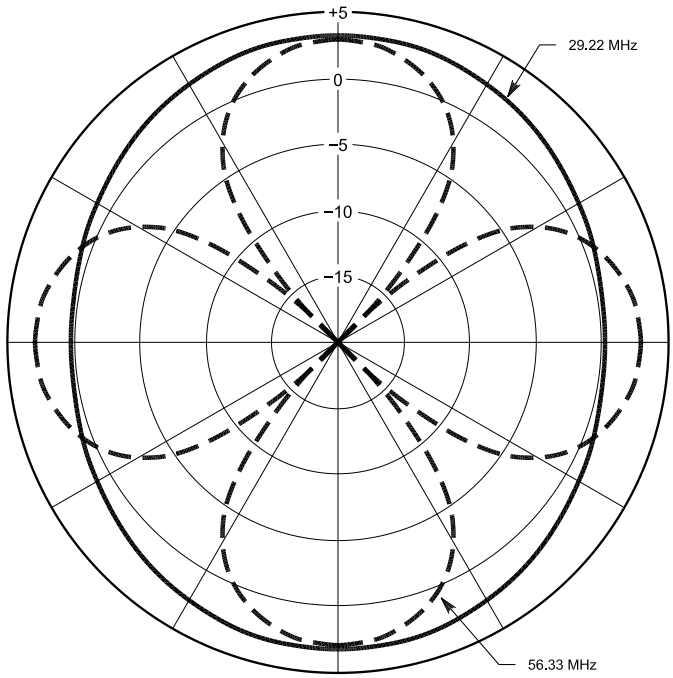

Fig 9—Radiation patterns of the MI0 loop antenna. (Notice that this is not on a standard ARRL grid—*Ed.*)

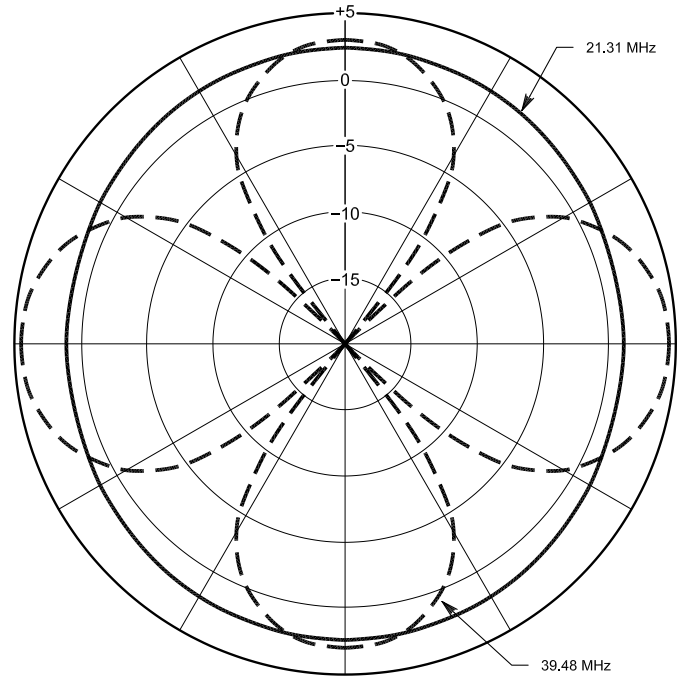

Fig 10—Radiation patterns of the MI1 loop antenna. (Notice that this is not on a standard ARRL grid—*Ed.*)

Table 4—Dimensional and Performance Properties of Nonself-similar, Bent-Wire Loop Configurations

	MI2 Loop		***BW1***		***BW2***		***BW3***	
Overall Dimensions (meters)	2.8 x 2.66		2.8 x 2.66		2.77 x 2.5		2.77 x 2.77	
Total Wire Length (meters)	27.57		27.57		26.35		27.37	
Resonant Frequency (MHz)	15.19	27.89	14.86	27.34	16.06	29.44	15.82	28.97
Feed-point Resistance (Ω)	28.1	19.1	27.0	17.6	32.8	20.2	33.9	23.9
Peak Gain (dBi)	1.83	3.6	1.83	5.45	1.91	5.23	1.9	5.34
2:1 SWR bandwidth with respect to								
Resonant Resistance (%)	1.18	0.39	1.37	0.56	1.63	0.60	1.64	0.71
Radiation Efficiency (%)	94.1	89.5	94.1	89.9	95.3	91.6	95.1	92.3

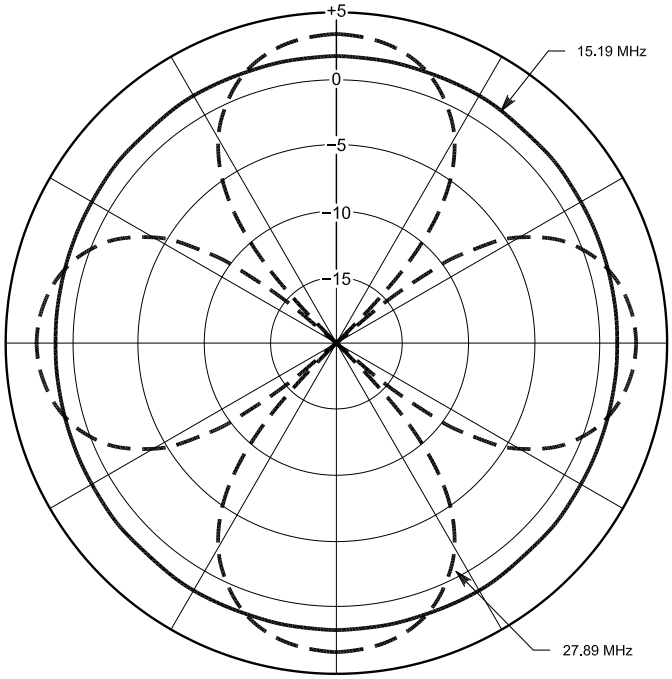

Fig 11—Radiation patterns of the MI2 loop antenna. (Notice that this is not on a standard ARRL grid—*Ed.*)

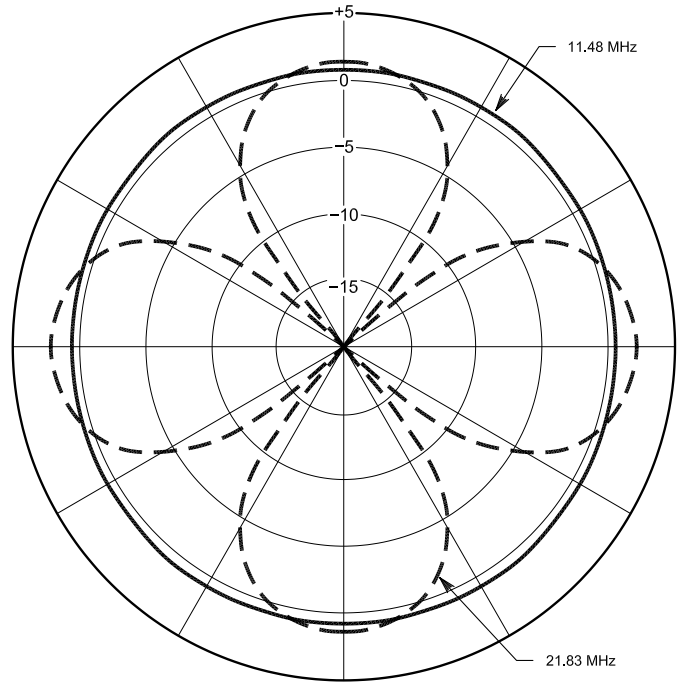

Fig 12—Radiation patterns of the MI3 loop antenna. (Notice that this is not on a standard ARRL grid—*Ed.*)

higher resonant frequency, increased resonant resistance, increased bandwidth and increased efficiency. By reviewing the impedance properties of the MI3 Mod and the data presented in Table 3, it is evident that the MI3 Mod antenna performs in a manner more similar to that of the MI2 fractal loop than the MI3 fractal loop. This is primarily so because the total wire length in the MI3 Mod loop design more closely matches that of the MI2 fractal loop than the total wire length of the MI3 fractal loop.

The performance advantage offered by the MI1, MI2, MI3 Mod and MI3 fractal-loop designs compared to the Euclidean rectangular loop is the lowering of resonant frequency when the antennas occupy the same area. It has been generally concluded that this reduction in resonant frequency and the associated multiple resonance compressions are solely a result of the fractal geometry of the antenna. From the analysis and data presented here, it is evident that this behavior is more a function of the total wire length in the loop rather than the geometry. Alternate, Euclidean loop geometries having the same overall physical area and total wire length as the fractal loop geometry provide similar performance.

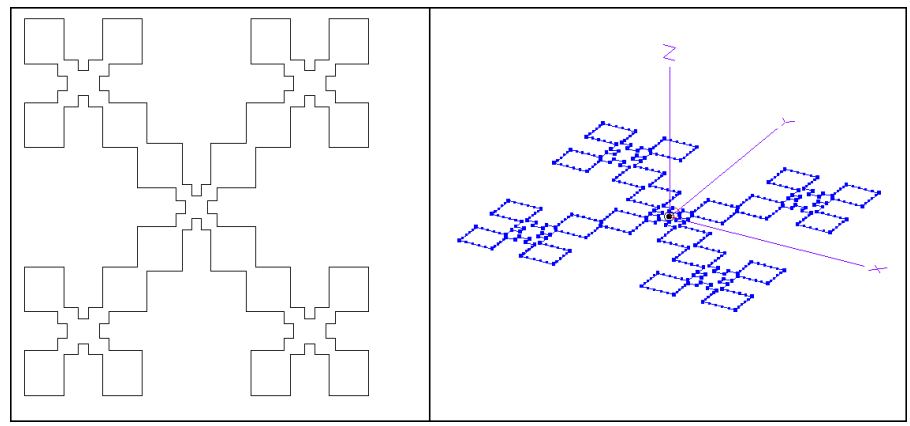

Fig 13—A modification of the MI3 fractal loop, the *MI3 Mod*, has the same physical area as the MI3 fractal loop but significantly less total wire length: 32 meters compared to 45.67 meters.

Beginning with a nonfractal rectangular loop, one could incrementally increase the total wire length in the loop and yet maintain the same overall area. The increase in wire length could be accommodated in the same area through an arbitrary and even symmetrical arrangement of the loop wire. It is intuitively obvious that increasing the total wire length in the loop would result in a lowering of the loop's resonant frequency. At some point, the argument would arise as to whether or not a fractal arrangement of the loop wire would provide optimum performance. Optimum performance could be determined through an evaluation of the loop's resonant frequency, resonant impedance, bandwidth and efficiency. Based on this perspective, the issue to consider further is whether performance similar to that of the MI2 fractal loop can be achieved using nonself-similar loop geometries where the same total wire length is compressed into the same overall physical area using an arbi-

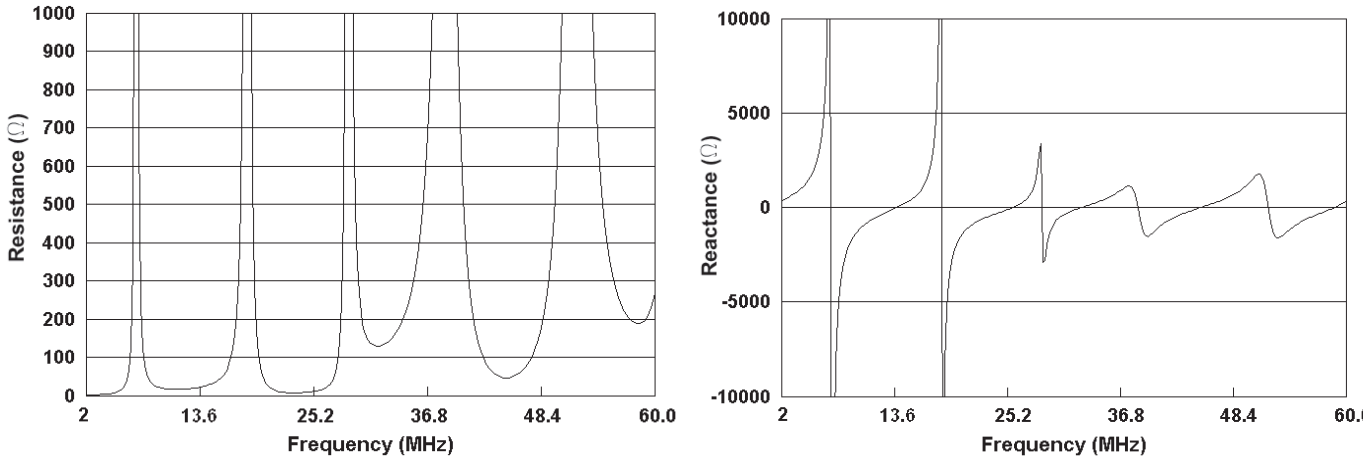

Fig 14—A graph of the MI3 Mod loop's impedance properties.

trary, yet symmetrical geometrical arrangement of wire.

Nonself-similar, Bent-Wire Loop Antennas

To investigate whether a nonself-similar, arbitrary, yet symmetrical arrangement of the loop wire would result in performance similar to that of a self-similar loop antenna, several arbitrarily shaped, bent-wire loop designs were created. Each loop had area and total wire length identical to the MI2 fractal loop, or nearly so. These nonself-similar, bent-wire loop designs were analyzed using *EZNEC* and their performance compared with that of the MI2 fractal-loop antenna.

Three nonself-similar, bent-wire loop configurations were designed. These are depicted in Fig 15 and designated as Bent-Wire Loop 1 (BW1), Bent-Wire Loop 2 (BW2) and Bent-Wire Loop 3 (BW3). The actual physical dimensions of these loop antennas and comparisons with the dimensions of the MI2 fractal loop are presented in Table 4. The performance characteristics and comparison with the MI2 fractal loop antenna are also presented there. A comparison of the impedance properties of these three loop antennas to those of the MI2 fractal loop is presented in Fig 16.

Table 4 shows that all four of the loop-antenna designs offer similar performance at their two lowest series resonances. The minor shifts in resonant frequency are to be expected because each antenna has a slightly different area and total wire length. Referring to Fig 16, it is obvious all four of the loop antennas exhibit similar resonance compression and multiband behavior as a function of frequency. As the operating frequency increases, differences in performance become more pronounced. This is a result of many factors, including that the antennas become larger with respect to the operating frequency and that they have different areas, total wire lengths and geometries. Although geometry is a factor in determining performance, it is clearly not the single reason for the resonance-compression behavior exhibited by these antennas. Additionally, if the wire length in a bent-wire loop is adjusted such that its resonant frequency identically matches that of the MI2 loop, the performance properties will essentially match those of the MI2 loop, independent of geometry (see Note 6).

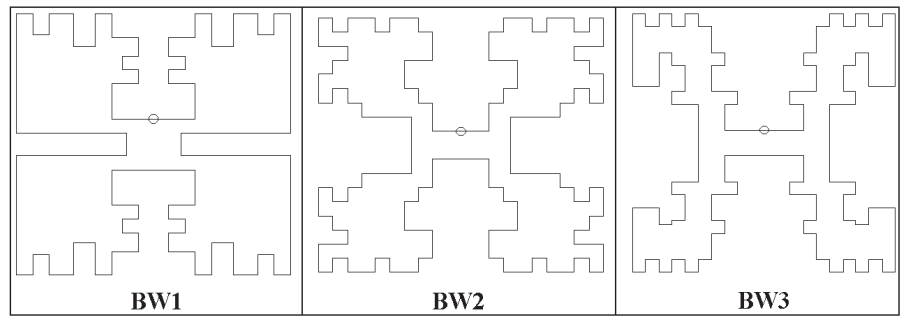

Fig 15—Three nonself-similar, bent-wire loop configurations designated as Bent-Wire Loop 1 (BW1), Bent-Wire Loop 2 (BW2) and Bent-Wire Loop 3 (BW3). These loop antennas are compared with the MI2 fractal loop in Table 4. The impedance properties of these loops are compared to those of the MI2 fractal loop in Fig 16.

At the upper series resonance, the most notable performance differences are the antennas' peak gains and radiation patterns. As the frequency increases, the geometry starts to become more significant in determining performance because the antenna is larger with respect to the operating wavelength. These differences can be minimized if the nonself-similar bent-wire loops are configured to be symmetrical about both the X and Y axes. Radiation patterns of all four antennas are presented in Fig 17. At the lower resonant frequency, the radiation patterns are cut in the θ-sweep plane with ϕ set at 90°, and the patterns are identical. At the upper resonant frequency, the radiation patterns are cut in the ϕ-sweep plane with θ set at 90° because maximum radiation occurs in this plane.

At the upper resonant frequency, the patterns are similar, with the most notable difference being the MI2 fractal loop's radiation pattern, which is symmetrical because of its more symmetrical geometry. The difference

in the azimuth radiation patterns at the upper resonance is the cause for the difference in the gain of each loop presented in Table 4. The efficiency of each loop at its upper resonant frequency is very similar to the others.

Discussion

This article presented an analysis of the Minkowski Island fractal loop antennas as well as an analysis of an MI3 Mod loop and three arbitrary nonself-similar bent-wire loop designs that essentially occupy the same physical area. An examination of the MI1, MI2, MI3 Mod and MI3 loops shows that as the total wire length in the loop increases while the area remains constant, the loop's resonant frequency, feed-point resistance, bandwidth and efficiency decrease. These are the performance tradeoffs associated with the lowering of resonant frequency through the use of fractal geometry or other similar wire-compression schemes. This behavior is clearly more a function of the increase in total wire length than a function of the loop geometry.

Through a detailed analysis of the MI2 fractal loop and the three arbitrary nonself-similar bent-wire loops, it was demonstrated that all of these loops have essentially the same perfor-

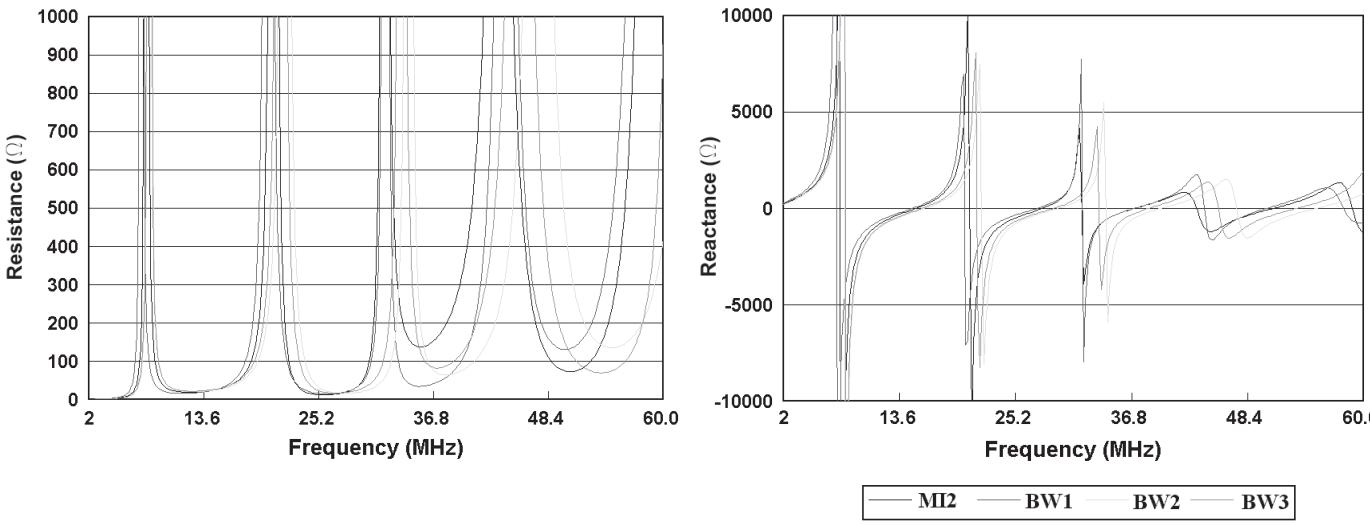

Fig 16—Impedance properties of the BW1, BW2 and BW3 fractal loops compared to those of the MI2.

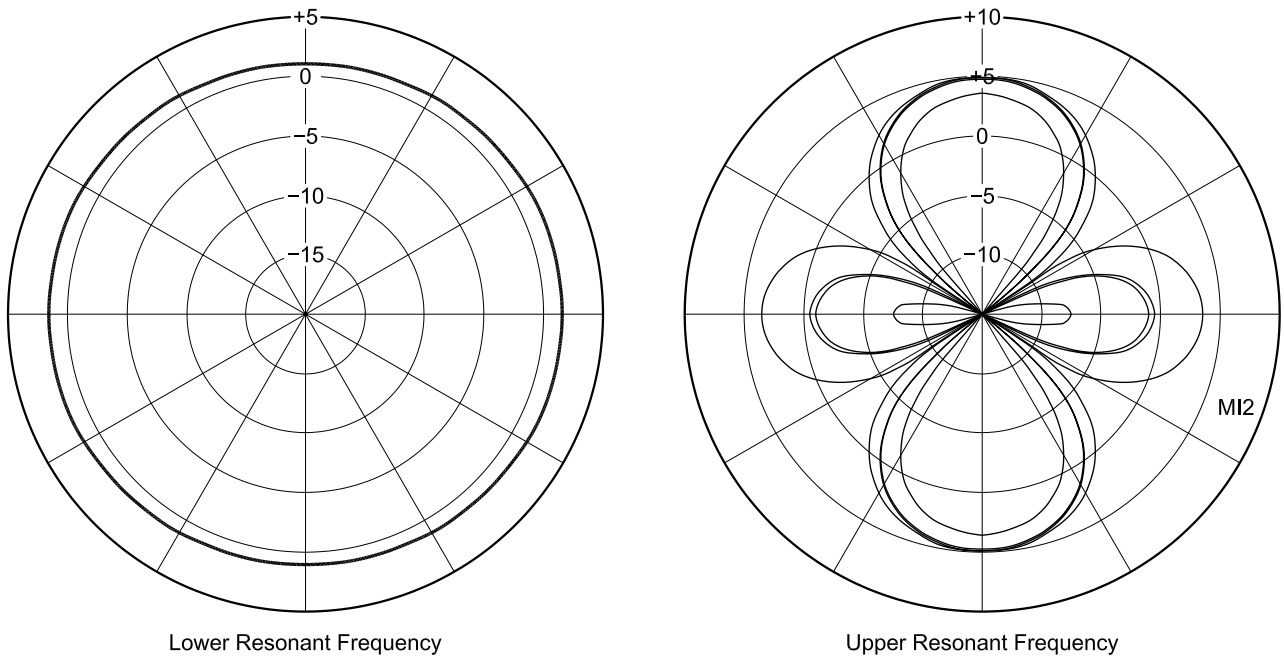

Fig 17—Radiation patterns of the BW1, BW2 and BW3 fractal loops compared to that of the MI2. (Notice that this is not on a standard ARRL grid—*Ed.*)

mance in terms of resonant frequency, radiation resistance, bandwidth, efficiency, gain and radiation pattern. It can be concluded that while the loop geometry is one factor in determining the antenna performance, it is not as significant as the loop's area and total wire length. Other factors affecting the loop performance include the feed-point location and the loop's wire diameter. From this, arranging the loop geometry into a self-similar fractal shape rather than an arbitrary shape does not provide significant benefits at the lower resonant frequencies. Fractal geometry is not the sole factor determining compressed resonance behavior. Fractal geometry is clearly defined as a large-scale structure comprised of a series of repetitions of a single geometry (the geometry basis), where each repetition is on different or the same scale. These fractal geometries are self-similar in that some portion of their geometry has the same shape as the large-scale geometry.

Acknowledgement

I would like to thank Mr. Roy Lewallen, W7EL, and Mr. Rick Littlefield, K1BQT, for their valuable comments and discussions regarding the content and format of this article.

Notes

[1]C. Puente-Baliarda, J. Romeu, R. Pous and A. Cardama, "On the Behavior of the Sierpinski Multiband Fractal Antenna," *IEEE Transactions on Antennas and Propagation*, Vol. 46, pp 517-524, April 1998.

[2]N. Cohen, "Fractal Antennas Part 1," *Communications Quarterly*, pp 7-22, Summer 1995.

[3]N. Cohen, "Fractal Antennas Part 2," *Communications Quarterly*, pp 53-65, Summer 1996.

[4]N. Cohen and Robert Hohlfeld, "Fractal Loops and the Small Loop Approximation," *Communications Quarterly*, pp 77-81, Winter 1996.

[5]*EZNEC*/4 Antenna Modeling Software, Roy Lewallen PE, W7EL, **www.eznec.com**. You can download the *EZNEC* desciption files uased in this article from the ARRLWeb at **www.arrl.org/qex/**. Look for 0302Best.zip.

[6]S. Best, "On the Performance Trade-offs Associated with Fractal Antenna Designs," *Antenna Application Symposium*, Allerton Park, University of Illinois, Oct 2001.

TAPR

Join* the effort in developing Spread Spectrum Communications for the amateur radio service. *Join TAPR and become part of the largest packet radio group in the world. TAPR is a non-profit amateur radio organization that develops new communications technology, provides useful/affordable kits, and promotes the advancement of the amateur art through publications, meetings, and standards. Membership includes a subscription to the *TAPR Packet Status Register* quarterly newsletter, which provides up-to-date news and user/technical information. Annual membership US/Canada/Mexico $20, and outside North America $25.

TAPR CD-ROM

Over 600 Megs of Data in ISO 9660 format. TAPR Software Library: 40 megs of software on BBSs, Satellites, Switches, TNCs, Terminals, TCP/IP, and more! 150Megs of APRS Software and Maps. RealAudio Files. Quicktime Movies. Mail Archives from TAPR's SIGs, and much, much more!

Wireless Digital Communications: Design and Theory

Finally a book covering a broad spectrum of wireless digital subjects in one place, written by Tom McDermott, N5EG. Topics include: DSP-based modem filters, forward-error-correcting codes, carrier transmission types, data codes, data slicers, clock recovery, matched filters, carrier recovery, propagation channel models, and much more! Includes a disk!

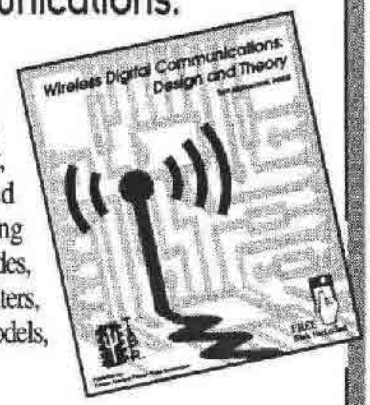

Tucson Amateur Packet Radio Corp.

Tucson Amateur Packet Radio
8987-309 E. Tanque Verde Rd #337 • Tucson, Arizona • 85749-9399
Office: (940) 383-0000 • Fax: (940) 566-2544 • Internet: tapr@tapr.org www.tapr.org
Non-Profit Research and Development Corporation

Some Notes on Turnstile-Antenna Properties

Turnstiles are popular antennas for satellite work and Earth-bound omnidirectional applications, but getting the desired results requires more than simply parallel connecting dipoles. Come learn why.

By L. B. Cebik, W4RNL

The turnstile antenna is one solution to the occasional need for an omnidirectional, horizontally polarized antenna. Often described as a "fairly simple" antenna consisting of two dipoles and a 90° phasing line, the turnstile has often disappointed builders. In the belief that much of the disappointment stems from a poor understanding of how the turnstile does its work within its limiting factors, I have compiled the following design and performance notes. I hope that they will lead to better turnstile antennas.

1434 High Mesa Dr
Knoxville, TN 37938-4443
cebik@cebik.com

Why Does the Turnstile Seem So Simple?

The most usual turnstile antenna design consists of two resonant horizontal dipoles for a given frequency. We set them at right angles to each other, using any convenient form of support. The main feed line goes to one of the two dipoles. A 90° length of transmission line—the phasing line—connects the feed point of dipole 1 to dipole 2. Fig 1 shows the general scheme.

If we construct such an antenna and place it 1 λ above ground, then the lowest elevation lobe will form—at 14° above the horizon—an azimuth pattern similar to the one shown in Fig 2. Because the beamwidth of each of the dipoles is less than 90°, there is not quite enough signal strength from each dipole on the 45° axes to completely circularize the pattern overall. However, the difference between the peaks broadside to each dipole and the null between peaks is only about 1 dB. For virtually all purposes, the pattern is omnidirectional. The maximum gain of the model used to produce this pattern is about 4.7 dBi, about 3 dB below the maximum gain of a single dipole under the same conditions. In part, the gain reduction is the price of spreading a single dipole's bidirectional pattern over the full horizon.

A turnstile presents a very broad SWR curve, as illustrated by Fig 3. Perhaps this fact, more than any other, lures casual builders into be-

lieving that the turnstile is an easy antenna to build successfully. However, the very shallow SWR curve is very misleading. Even poorly constructed turnstiles with woefully distorted patterns relative to the omnidirectional ideal will exhibit very low SWR values.

We may list the conditions for achieving a successful (omnidirectional) standard dipole-turnstile antenna briefly. First, the individual dipoles should be resonant; that is, they should show virtually no reactance at each feed point. Second, the phase line's characteristic impedance should equal the feed-point impedance of the individual dipoles. The length of the line should be 1/4 λ or 90° (electrically). The physical length of the phase line should be adjusted by multiplying the required electrical length by the velocity factor of actual line used. For most coaxial cables, the range of velocity factors runs between 0.66 for solid-dielectric cables, to 0.78 for many foam-dielectric cables, to 0.84 for some specialty cables (such as RG-63).

The impedance presented by the main feed point of the assembly will be one-half the impedance of each individual resonant dipole. The key model with which we shall perform our investigations consists of two 50.5-MHz dipoles of 0.44-inch-diameter aluminum. (The diameter results from estimating the effective diameter of elements composed partially of ½-inch tubing and partially of ⅜-inch tubing.) The element lengths are 111.6 inches (0.4775 λ) for each dipole. The elements are vertically separated in the model by a little over one inch (0.005 λ) to avoid inaccuracies that occur when modeled crossing wires (even at 90°) are too close to each other. To use the electrical length of the line throughout, the transmission line is set with a modeled velocity factor of 1.0. Hence, the line of this initial model is 0.25 λ long at 70 Ω impedance. With the model 1 λ above good ground, the antenna shows a feed-point impedance of 35.07 –*j*0.03 Ω. The overly precise numbers for the source impedance suggest how little reactance the turnstile feed point may present.

Although often thought of as an impedance matching line, the cable connecting the dipoles of a standard turnstile is a true phasing line. As such, its task is to present the second dipole with a certain current magnitude and phase angle relative to the first dipole. Essentially, the current magnitude on the second dipole should be equal to that on the first dipole with a phase angle difference of 90°. As we shall see, many of the difficulties that we may encounter with turnstiles result from not fully appreciating the fact that current, and not impedance, is the key parameter for the system. The primary model shows on dipole 1 a current magnitude of 0.489 at a phase angle of –0.07°. Dipole 2 shows 0.501 at –90.05°. The current ratio of the two elements is 0.976, with a phase angle difference of 89.98°, and the azi-

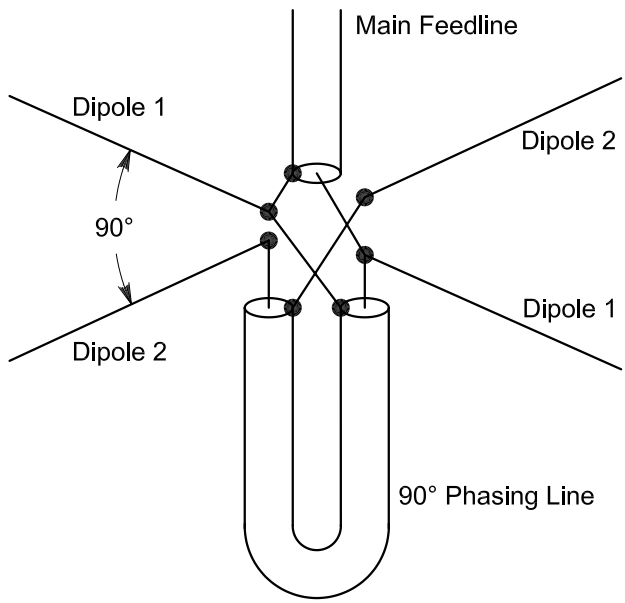

Fig 1—The general outline of a dipole-turnstile antenna.

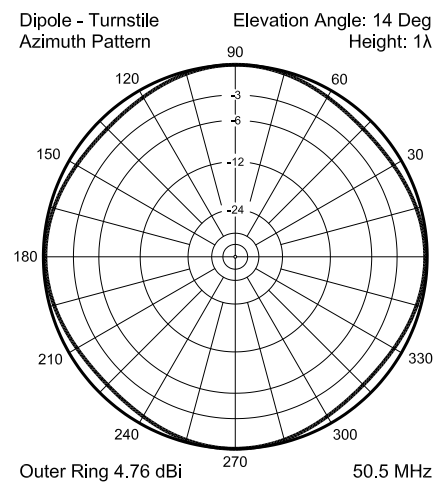

Fig 2—The azimuth pattern (14° elevation angle, 50.5 MHz) of a well-constructed dipole-turnstile antenna modeled 1 λ above good ground.

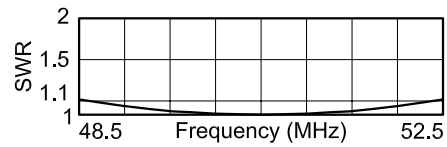

Fig 3—The 35-Ω SWR curve of a well-constructed dipole-turnstile antenna modeled 1 λ above good ground.

Table 1—Turnstile Current-Magnitude and Phase-Angle Conditions at 50.5 MHz ±2%

Frequency	***Dipole 1***		***Dipole 2***		*I Ratio*	*Phase*
(MHz)	*I Mag.*	*I Phase (°)*	*I Mag.*	*I Phase (°)*		*Difference (°)*
49.5	0.507	14.99	0.518	–87.96	0.979	102.95
50.5	0.489	–0.07	0.501	–90.05	0.976	89.98
51.5	0.460	–15.14	0.513	–93.90	0.897	78.76

muth pattern of Fig 2 is the result. Although the current magnitude and phase-angle values may seem superfluous at first sight, they are at the heart of understanding turnstile performance.

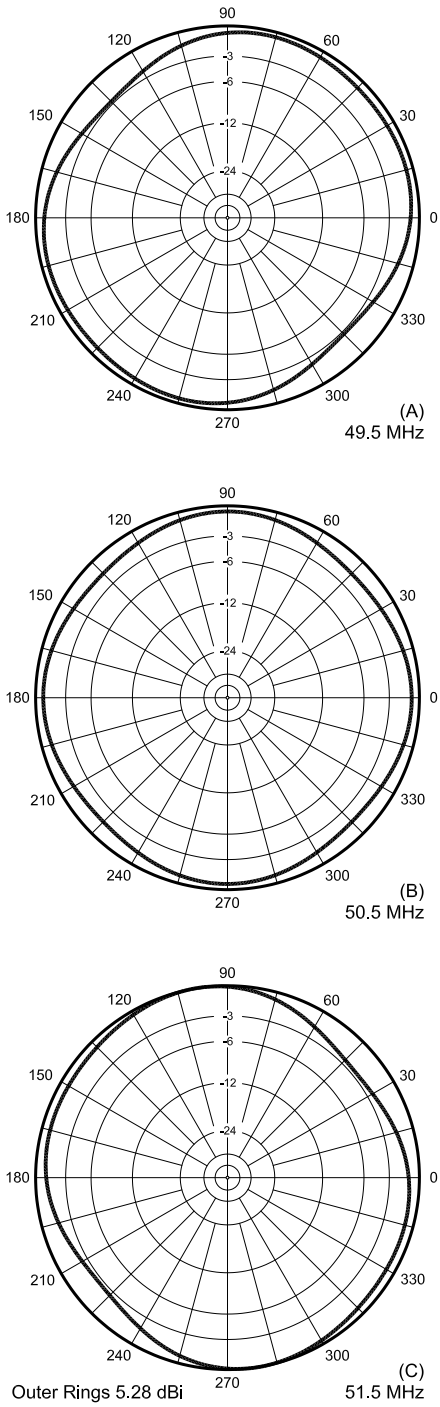

Fig 4—Azimuth patterns (14° elevation angle) of a dipole-turnstile antenna designed for 50.5 MHz operated (A) 1 MHz below, (B) at and (C) 1 MHz above the design frequency. The antenna is modeled 1 λ above good ground.

The Basic Properties of Turnstile Antennas

One useful technique to increase our appreciation of the performance of any antenna type is to systematically vary some of the operating parameters. Since the SWR curve in Fig 3 is so flat—barely 1.1:1 at 2 MHz above and below the design frequency of our basic model—let's examine other properties as we move away from the center frequency. Table 1 lists the current conditions of the primary model 1 MHz below and above the design frequency—about a 2% frequency change per step. Although we note some change in the ratio of current magnitudes for the dipole elements, the most drastic change occurs with respect to the phase angle between the two elements—about 12° in each case.

As Fig 4 demonstrates, the change in phasing has consequences for the azimuth pattern of the antenna. Whereas at the design frequency, the maximum gain differential around the pattern was 1.03 dB, the gain differential at 49.5 MHz is 2.21 dB and at 50.5 MHz is 2.51 dB. The differential grows as we further depart from the design frequency, resulting in bidirectional oval patterns rather than an omnidirectional pattern. How much "ovalizing" of the pattern one may tolerate is a user judgment based on operating requirements. However, –3 dB is the standard half-power level and the patterns in Fig 4 are fast approaching this level of distortion of the ideal pattern.

Notice as well that the azimuth angle of maximum gain shifts in opposite directions above and below the design frequency. A larger phase angle tends to force the pattern clockwise relative to the ideal, while a smaller phase angle tends to shift the pattern counter-clockwise.

The exercise in varying the frequency of the dipole-turnstile is equivalent to one in which we might begin with antennas that are not very close to resonance. At 50.5 MHz, the 111.6-inch dipole impedance is 71.8 + j0.0 Ω. At 49.5 MHz, the dipole shows an impedance of 68.7 –j 18.0 Ω, while at 51.5 MHz, the dipole impedance is 75.1 + j 18.4 Ω. Dipoles that are off resonance by the same degree at the design frequency but that use an accurately cut phase line will show similar patterns to the distorted ones in Fig 4.

A second way in which we may systematically alter the parameters of dipole turnstiles is to vary the length of the phase line from its desired electrical length of 0.25 λ. Table 2 shows the results of varying the line length up to a limit of 20% shorter and longer. It is very noticeable in the table that the current-magnitude ratio between the dipoles does not vary within the limits of the decimal places to which I have carried out the values. In contrast, the relative phase angle between the elements does change very significantly—and virtually linearly. Fig 5 shows the linear change of relative phase angle with a linear change in phase-line length.

A change in line length corresponds roughly to errors in the construction of the phase line that may result from simple slips to failing to take the velocity factor of the line into account when measuring the physical line length. Such errors result in azimuth patterns that depart from the ideal. Notice that despite a similarity in phase angles between certain line in Table 2 and Table 1, the azimuth-pat-

Table 2—Turnstile Current-Magnitude and Phase-Angle Conditions with Changing Phase-Line Lengths

Line Length	***Dipole 1***		***Dipole 2***		*I Ratio*	*Phase*
(λ)	*I Mag.*	*I Phase (°)*	*I Mag.*	*I Phase (°)*		*Difference (°)*
0.20	0.490	–0.41	0.501	–72.05	0.978	71.64
0.21	0.490	–0.35	0.501	–75.65	0.978	75.30
0.22	0.489	–0.29	0.501	–79.25	0.978	78.96
0.23	0.489	–0.22	0.501	–82.85	0.978	82.63
0.24	0.489	–0.14	0.501	–86.45	0.978	86.31
0.25	0.489	–0.07	0.501	–90.05	0.978	89.98
0.26	0.489	+0.00	0.501	–93.65	0.978	93.65
0.27	0.489	+0.08	0.501	–97.25	0.978	97.36
0.28	0.489	+0.16	0.501	–100.8	0.978	100.96
0.29	0.489	+0.23	0.501	–104.4	0.978	104.63
0.30	0.489	+0.30	0.501	–108.0	0.978	108.30

Note: Phase-line characteristic impedance: 70 Ω

tern distortion increases more rapidly as we increase the line length above the optimum value than when we shorten the line. However, notice that the 51.5-MHz pattern in Fig 4 and Table 1 shows a greater departure from the ideal current-magnitude ratio than do those for the lines in Table 2 that approximate the 103° phase angle. As a consequence, errors that result in slightly short phase-line lengths are less harmful to pattern shape than those that result in lines that are too long.

A comparable set of distortions occurs whenever we press into service phase lines having characteristic impedances other than the required value. The available lines for an accurately built dipole-turnstile consist of RG-11, RG-59 and similar 70 to 75 Ω cables. A 5-Ω range of characteristic impedance creates no significant variations in patterns. However, let's suppose that we try to use a 50-Ω cable (RG-8, RG-58, etc) or a 93-Ω cable (RG-62).

Table 3 shows the results of our little experiment. Phase-line characteristic impedances that are off the required value result in very little change in the relative phase angle of the currents on the two dipoles. However, they do result is radical changes in the ratio of current magnitudes, with the low Z_0 resulting in a ratio 30% below ideal and the high Z_0 yielding a current magnitude ratio that is 30% too high. When the phase angle remains very close to the desired 90° value and only the current ratios change, the patterns do not bend clockwise or counterclockwise. Instead, as shown in Fig 6, the patterns become oval bidirectional patterns in the broadside direction to the dipole with the higher relative current. (In all azimuth patterns, 0° is to the right and 90° is straight up, according to the conventions used in *EZNEC*, the software used for these studies. Think of dipole 1 as extending vertically on the plot grid, with dipole 2 extending horizontally across the grid.) The 50-Ω sample shows a gain differential of about 3.1 dB, while the 93-Ω example shows a gain differential of about 2.3 dB.

These notes have related various imperfect conditions of relative current magnitude and phase angle to ways in which we can construct or operate a dipole-turnstile in a non-ideal mode. For a brief discussion of the direct relationship of turnstile azimuth patterns and current conditions, see the Appendix at the end of this article.

Matching a Turnstile to a Main Feed Line

Our survey of basic dipole-turnstile properties has displayed some of the sources and effects of current-magnitude and phase-angle offsets relative to optimized values. However, the survey has so far not tackled the fact that the overall feed-point impedance of the dipole turnstile is 35 Ω (with virtually no reactance). Although numerous users are content with an SWR of about 1.43:1 relative to a 50-Ω main feed line—especially since it does not

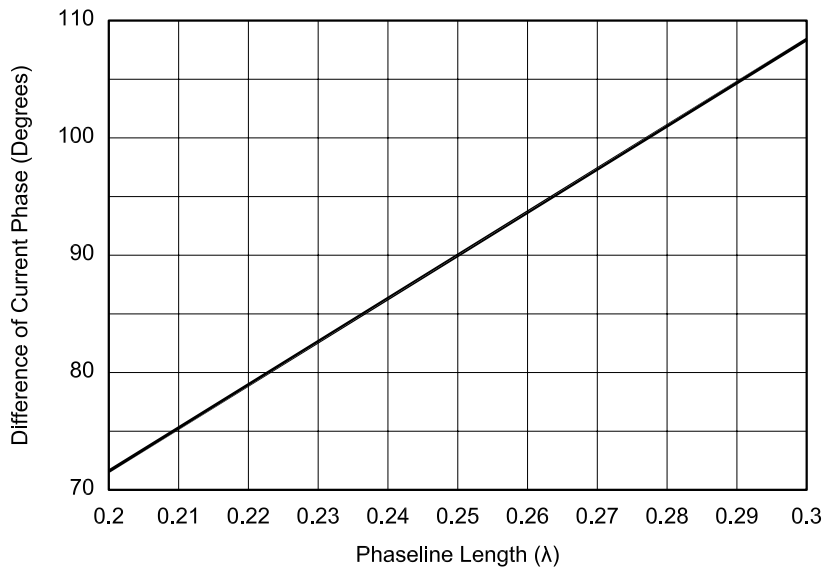

Fig 5—The relationship of the relative current-phase angles on the dipoles of a turnstile antenna to variations in the length of a 70-Ω phasing line from 0.2 to 0.3 λ.

Table 3—Turnstile Current Conditions with Phase Lines of Different Characteristic Impedances

Line Z_0	***Dipole 1***		***Dipole 2***		*I Ratio*	*Phase*
(Ω)	*I Mag.*	*I Phase (°)*	*I Mag.*	*I Phase (°)*		*Difference (°)*
50	0.328	–0.09	0.470	–90.07	0.698	89.98
70	0.489	–0.07	0.501	–90.05	0.978	89.98
93	0.628	–0.05	0.484	–91.14	1.298	91.09

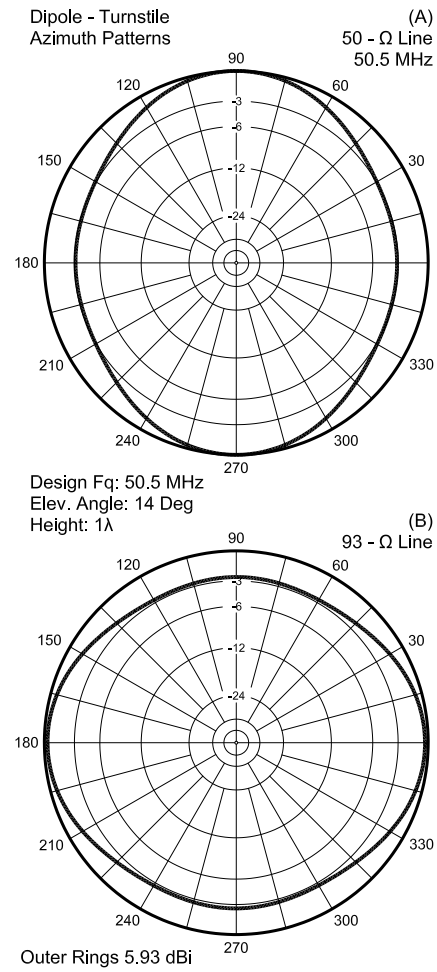

Fig 6—Azimuth patterns (14° elevation angle, 50.5 MHz) for a dipole-turnstile antenna when using phase lines of common but erroneous values of characteristic impedance (Z_0): (A) for 50-Ω lines and (B) for 93-Ω lines.

significantly change over a large bandwidth—other users strive for a closer match to their main feed line.

One scheme with several variations appears in Fig 7. The principle is to calculate line lengths of a cable that will achieve two goals. First, the selected line and line lengths, when combined in a parallel connection, will yield close to a 50-Ω impedance. The line used in our example will be a 93-Ω cable (RG-62). Second, the relative line lengths to the individual dipoles will preserve a 90° impedance differential between the two dipoles, thus providing the conditions for an omnidirectional pattern. The required line lengths are 0.125 λ for the short cable and 0.375 λ for the long cable.

When we model this system using our basic 50.5-MHz dipole turnstile, we obtain some interesting results. Version A of Table 4 shows the numerical results of the dual-cable feed system. As calculated, the feed-point impedance of the parallel combination of the lines is very close to 50 Ω. However, the relative phase angle between the two dipoles is seriously low. The top azimuth pattern in Fig 8 shows the degree to which the pattern has lost its desired omnidirectional properties.

The failure of the impedance-based calculations to achieve the desired omnidirectional pattern results from a failure to appreciate that the phasing of a turnstile antenna rests upon current transformations along transmission lines. Only when the cable impedance is a relatively perfect match with the individual-dipole-feed-point impedance will the current and impedance track along a line. Since the dual-cable technique requires a mismatch to achieve the desired feed-point impedance overall, the current will not change its magnitude and phase angle at the same rate as the impedance.

We can correct the current values by changing the lengths of one or both cables. Table 4 shows the limiting cases—that is, a correction by changing only one of the two cables. Version B of the dual-cable system lengthens the longer cable to 0.418 λ while leaving the short cable unchanged. Version C shortens the shorter cable to 0.080 λ while leaving the long cable unchanged. The table shows phase differentials

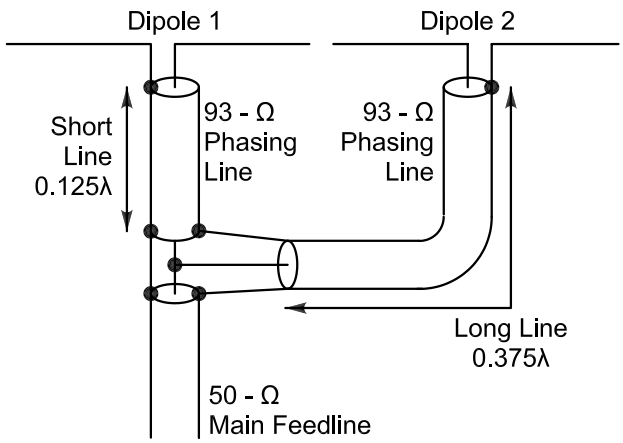

Fig 7—One (of several possible) impedance-based schemes for simultaneously phasing the dipoles of a turnstile antenna and matching the array to a 50-Ω main feedline.

Table 4—Simple and Modified Feed-System Properties for a Dual-Cable Turnstile Feed System

Version	***Short Cable***		***Long Cable***		*Feedpoint*
	Length (λ)	*Z_0 (Ω)*	*Length (λ)*	*Z_0 (Ω)*	*Impedance (Ω)*
A	0.125	93	0.375	93	48.3 –*j*0.2
B	0.125	93	0.418	93	44.6 –*j*0.1
C	0.080	93	0.375	93	44.5 –*j*0.2
D	0.102	93	0.397	93	44.6 –*j*0.1

Version	***Dipole 1***		***Dipole 2***		*I Ratio*	*Phase*
	I Mag.	*I Phase (°)*	*I Mag.*	*I Phase (°)*		*Difference (°)*
A	0.587	–53.25	0.589	–127.2	0.997	73.95
B	0.542	–53.17	0.587	–143.2	0.923	90.03
C	0.585	–36.40	0.542	–127.2	1.079	90.80
D	0.564	–44.93	0.565	–135.10	0.998	90.17

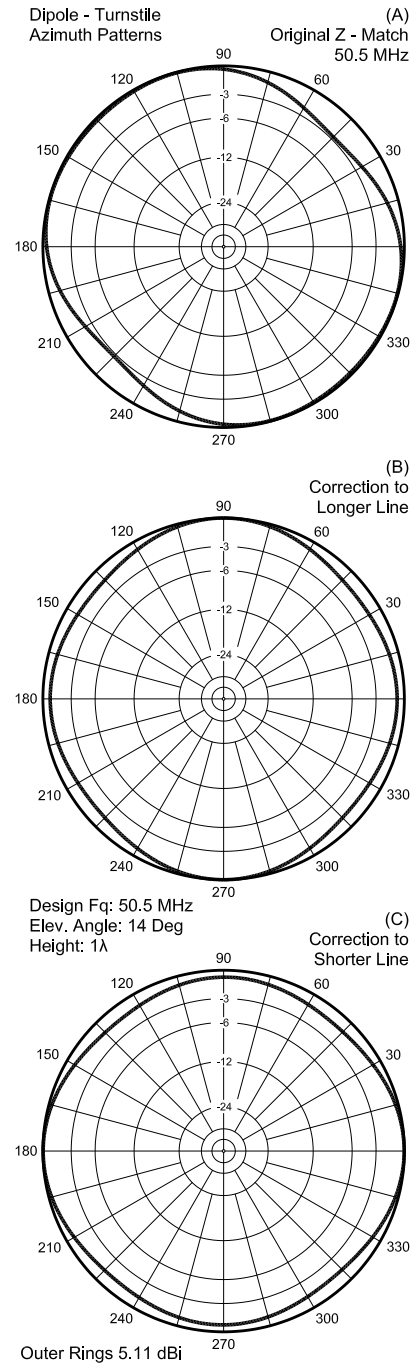

Fig 8—Azimuth patterns (14° elevation angle, 50.5 MHz) representing the results of the scheme shown in Fig 7 (A), and two forms (B, C) of correction to achieve a better relative phase angle between the dipole currents.

between the two dipoles within 1° of the ideal phase angle, with current magnitude ratios within 10% of ideal. The lower azimuth patterns in Fig 8 display the improvements.

Many combinations of shortening the short and lengthening the long cable in the system will also yield the desired phase-angle differential between the two dipoles. A combinatory change will also remove the 0.7 dB differential between pattern peaks at 90° angles from each other. Although in principle, one may calculate the combination of cable lengths required, trial modeling will likely uncover them more rapidly. Entry D in Table 4 shows a combination of lines that yields a very good result, with only a 0.01 dB variation between peak gain values at azimuth headings of 0° and 90°.

There are a number of matching techniques that we may employ to raise the 35-Ω dipole-turnstile impedance to 50 Ω without altering the original 0.25-λ 70-Ω phase line. One system, owing to Bramham, appears in Fig 9A. The system requires two cable sections, one matching the impedance of the load (which should be purely resistive), the other matching the main feed line. For our example, we shall use 35-Ω cable (RG-83) and 50-Ω cable (RG-8 or equivalent). Fig 9A shows a length of the 35-Ω cable between the turnstile feed point and the beginning of the matching sections. However, we may reduce that length to zero.

To calculate the required lengths, L_1 and L_2, we begin by calculating a special term, M:

$$M = \left(\frac{Z_2}{Z_1} + 1 + \frac{Z_1}{Z_2}\right) \qquad \text{(Eq 1)}$$

where Z_1 is the load impedance, 35 Ω, and Z_2 is the main-feed-line impedance, 50 Ω. The line lengths then follow from the equation:

$$L_1 \propto L_2 = \arctan\left(\frac{1}{\sqrt{M}}\right) \qquad \text{(Eq 2)}$$

where the answer emerges as an electrical length in degrees for conversion into a fraction of a wavelength and then into a physical line length. L_1 and L_2 will always be under 30°, and the values required for the present case are 29.48°. This length translates into 0.082 λ, or just over 14.1 inches before adjustment for the cable velocity factor.

The Bramham series-matching technique requires a line that matches the load. Often, such lines may not be available conveniently, and sometimes not at all. A more general series solution uses the Regier technique, fully described in *The ARRL Antenna Book* since the 1980s (pages 26-4 and 26-5 in the most recent editions). Fig 9B illustrates the technique. We need a section of the main feed line (Z_1 at length L_1) and a second section of a line of choice (Z_2 at length L_2). Not all choices will work, but for our case, we can use sections of 50-Ω line and 70-Ω line. We presumably have both lines, since we already have the dipole turnstile phase line and the main feed line for the system. Since our feed-point impedance is virtually purely resistive, we can simplify the calculations somewhat.

First, we calculate a pair of normalized values, n and r:

$$n = \frac{Z_2}{Z_1}; r = \frac{R_L}{Z_1} \qquad \text{(Eq 3)}$$

where Z_1 is the impedance of the main feed line, Z_2 is the impedance of the selected line, and R_L is the resistive component of the dipole-turnstile feed-point impedance. We next calculate the length, L_2, of the series section:

$$L_2 \propto \arctan\sqrt{\frac{(r-1)^2}{r\left(n-\frac{1}{n}\right)^2 - (r-1)^2}} \qquad \text{(Eq 4)}$$

The series length of feed line, L_1, requires the length L_2 for its result:

$$L_1 \propto \arctan\frac{\tan L_2\left(n - \frac{r}{n}\right)}{r-1} \qquad \text{(Eq 5)}$$

Although the Regier calculations appear more forbidding, even without their reactance terms, utility programs such as *HAMCALC* from VE3ERP contain the necessary steps and require only a few inputs for accurate outputs.

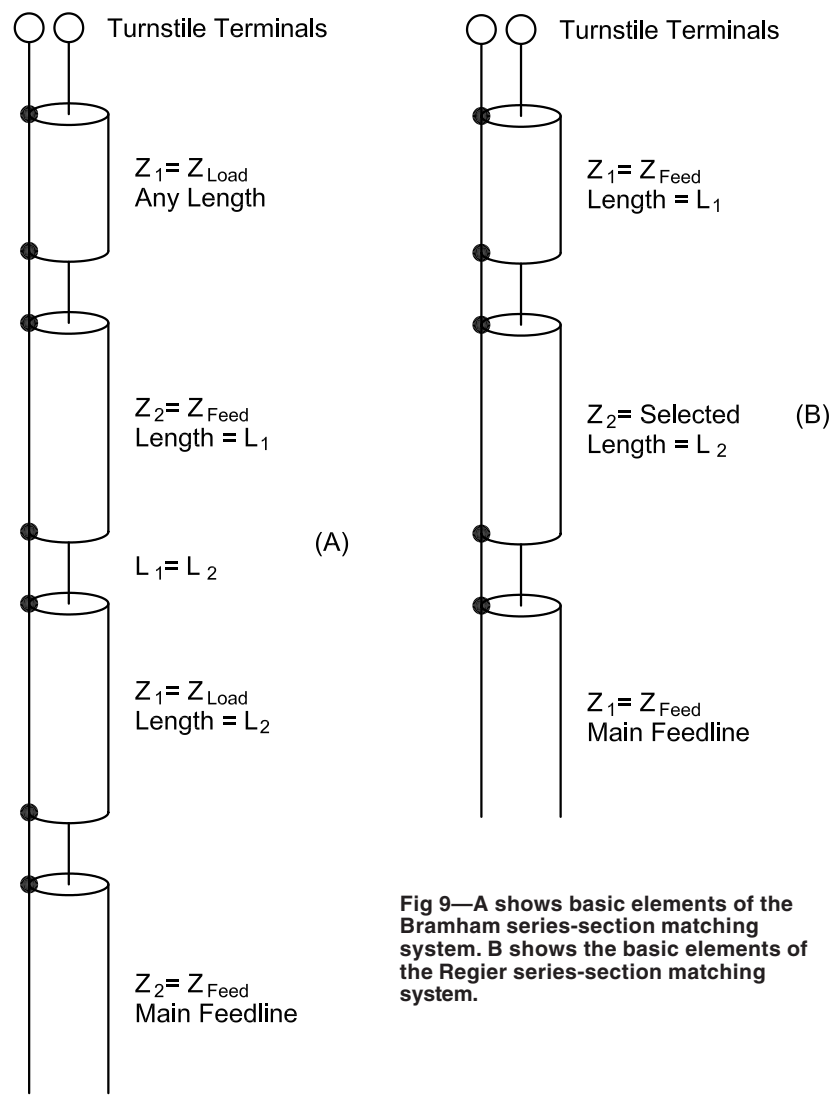

Fig 9—A shows basic elements of the Bramham series-section matching system. B shows the basic elements of the Regier series-section matching system.

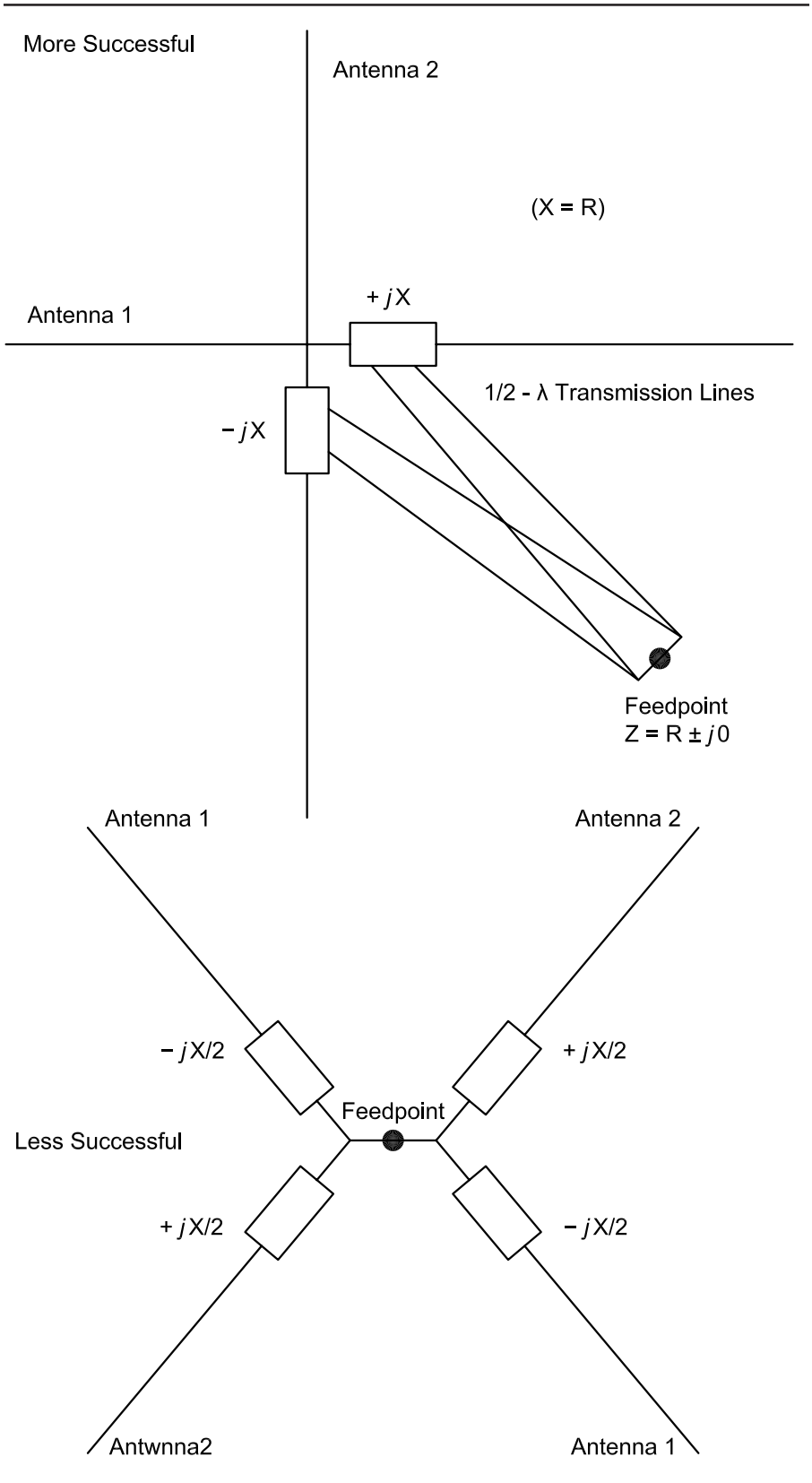

Fig 10—Two turnstile antennas intended for satellite operation at 145.9 MHz.

For our situation, using 50-Ω and 70-Ω cables, L_1, is 0.329 λ of 50-Ω line, while L_2 is 0.088 λ of 70-Ω cable.

Both the Bramham and Regier series matching networks yield a 50-Ω SWR curve that does not reach 1.05:1 at 49.5 and 51.5 MHz. As well, they have the advantage of not altering the current magnitude and phase angle established by the original 70-Ω phase line. Equally usable, but at a higher SWR level, would be a ¼- λ matching section composed of paralleled lengths of RG-62. The resulting 46-Ω line will transform the 35-Ω turnstile terminal impedance to about 61.8 Ω. If a 1.24:1 SWR is acceptable and if the requisite cable is available, the quarter-wavelength series section may be the simplest system of all.

Besides handling the dipole-turnstile matching challenge, the series matching systems may also be useful in other cases of turnstile antennas. Not every turnstile involves only dipoles.

A Special Case of Obtaining a Match and Quadrature

Zack Lau, W1VT, brought to light a special case that will yield the 90° phase shift while maintaining equal current magnitudes on the turnstile elements in *QEX* for Nov/Dec, 2001 (p 55). The required conditions are that antenna 1 have a feed-point impedance of $R + jR$ and that identical antenna 2 have an impedance of $R - jR$. Ordinarily, R is the resonant impedance of the individual antenna, and $+jR$ and $-jR$ are inductive and capacitive reactances introduced at the feed point of each antenna. Under these conditions, from a single source, the individual antennas will have equal magnitude currents and voltages that are 90° apart, along with a resistive impedance that is the value of the resonant impedance of an individual unloaded antenna.

The parallel combination of the two independent loaded impedances with equal but opposite reactive components equal to the resistive component meets the following condition:

$$\frac{(R+jR)(R-jR)}{(R+jR)+(R-jR)} = \frac{2R^2}{2R} = R \qquad \text{(Eq 6)}$$

Although there may be numerous combinations of R and $\pm jX$ for each antenna that will yield a 90° phase difference and equal current magnitudes and likewise many impedance combinations that will result in a parallel feed-point impedance R, the joint requirement severely restricts the system implementation possibilities.

Fig 10 sketches both a right and a

wrong way to implement the phasing system. The correct way (but not the only correct way) shows the conditions under which the system will work. That is, with each antenna isolated from the other. The simple system used to arrive at isolation in this case is to use λ/2 lines from each antenna to a parallel junction of the two. Half-wavelength lines or any reasonable characteristic impedance (such as 50-75 Ω) will replicate the feed-point conditions at their junction. The net source impedance for two 72-Ω dipoles in a turnstile arrangement will be 72 Ω with this system.

The system is more sensitive to some changes than others. Using reactances other than values equal to R will yield a noncircular pattern, regardless of whether the inductive or capacitive reactances are equal or unequal. Line lengths other than multiples of ½-λ also yield pattern distortions, since the impedance progression along the two lines is not the same.

A less successful means in Fig 10 of achieving the desired results—that is, one where the pattern is far less circular—reflects ordinary amateur building practice. It shows a single parallel connection of the two antennas, which use split balanced loads in their respective legs. Unfortunately, this system does not isolate the legs from each other, resulting in a noncircular pattern and in currents of unequal magnitude and considerably off from a 90° phase-angle difference. Test models of the non-isolated system showed current-magnitude ratios of about 1.25:1 with an 80° phase-angle difference. As well, the source impedance showed nearly 20 Ω inductive reactance. Increasing the inductive impedance circularized the pattern, but at a penalty: the source impedance moved well away from the resonant impedance of the individual dipoles in isolation.

The complementary-reactance system of obtaining quadrature requires the care of a precision instrument. The key to successfully implementing this system of quadrature lies not only in the selection of reactances for each antenna, but as well in maintaining a satisfactory isolation of the individual antennas. In this small account, I have not insisted upon using dipole turnstile elements, since the system has applications to quadrifilar and other antennas as well.

Which Antennas Can We "Turnstile" and Why?

In principle, we may turnstile any pair of identical antennas that we may set at right angles to each other. Creating a turnstile version of a complex array—such as a long-boom Yagi—usually requires a good reason. Very often, we find that reason in the elevation patterns of turnstile antennas.

Fig 11 shows two turnstile antennas designed for satellite reception. The dipole-turnstile over a large screen has been around since the 1970s, while the Moxon-rectangle-turnstile was recently featured in *QST* (Aug 2001, pp 38-41). Structural simplicity is only one of the reasons for suggesting a change from the dipole to the Moxon version.

The other reason appears in Fig 12, which presents the elevation patterns for the two antennas at 145.9 MHz, 2 λ above ground. The Moxon shows a somewhat smoother dome of coverage at higher elevation angles. The individual Moxons have feed-point impedances of 50 Ω, so the system feed-point impedance is 25 Ω overall. A ¼-λ section of 35-Ω cable (possibly composed of parallel sections of 70-Ω cable if RG-83 is not handy) transforms the impedance to 49 Ω for a standard co-

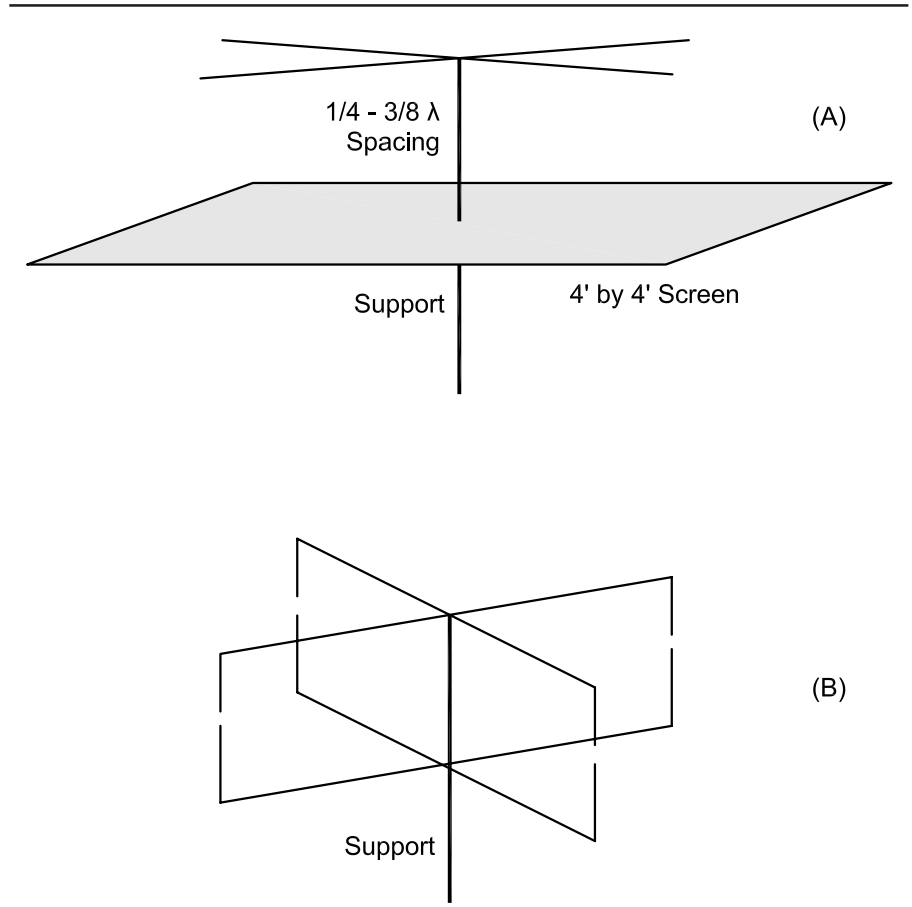

Fig 11—(A) dipole and (B) Moxon-rectangle turnstile antennas intended for satellite operation at 145.9 MHz.

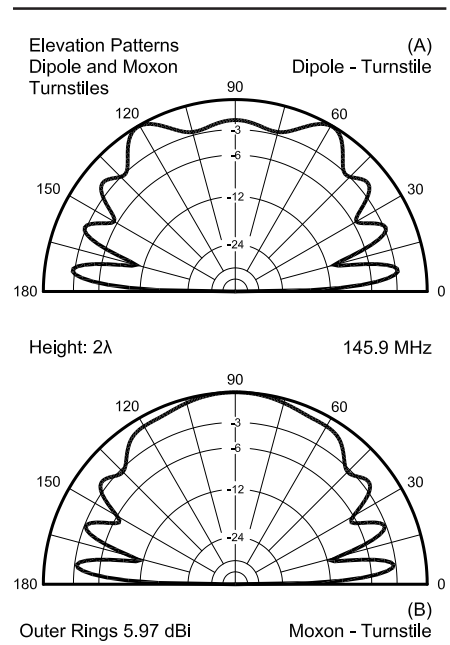

Fig 12—Elevation patterns for the two antennas in Fig 11, with each modeled 2 λ above ground.

axial main feedline.

One limiting factor of a dipole-turnstile for point-to-point communications in omnidirectional service is the relatively modest gain: about 4.7 dBi when the antenna is 1 λ above ground. We can increase the gain by a full decibel if we turnstile quad loops instead of dipoles. Fig 13 shows the outlines of such an arrangement, but without the phase line. When composed of #14 AWG copper wires for 50.5 MHz, the individual quad loops have impedances of 125 Ω, and a phase line made from RG-63 is ideal. The net system feed-point impedance is about 62 Ω, for a very wide-band 50-Ω SWR of about 1.25:1.

The improvement of the quad-turnstile over its dipole cousin involves more than gain. Fig 14 shows elevation patterns for both a dipole-turnstile and a quad-turnstile with their bases 1 λ above ground. At first sight, the quad elevation pattern seems normal, with the lower lobe being stronger than the second elevation lobe. However, notice the beamwidth of the second lobe. Now examine the dipole-turnstile pattern. With the simpler turnstile, the strongest lobe is actually the one with the higher elevation angle. Not only is the gain slightly higher than for the lower lobe, but as well, the higher-angle lobe has a wider beamwidth.

The dipole and quad elevation patterns should arouse some suspicions concerning the direction of strongest radiation relative to the structure of a turnstile antenna. As well, the utility of the turnstile for satellite reception should add to our suspicions. The simplest way to resolve the issue is to place a dipole-turnstile model in free space and examine the resulting pattern.

Fig 15 shows a free-space elevation pattern or H-plane pattern for our 50.5-MHz dipole turnstile. I have superimposed a sketch of the antenna to ensure that we orient ourselves correctly to the pattern. The dipole-turnstile has more gain broadside to the dipole pair than it does edgewise, the orientation we use for omnidirectional coverage. The difference in gain is well over 3 dB. Only ground reflections allow us to achieve a usable amount of gain at low elevation angles when we place the antenna over real ground.

The quad-turnstile improves both the gain and the elevation pattern by virtue of its form. It consists of two dipoles stacked 1/4 λ apart vertically, with the ends bent to meet. Essentially, we feed the two dipoles in phase. Any two dipoles stacked vertically and fed in phase will tend to suppress some high-angle radiation, with consequent increases in low angle radiation. However, the 1/4-λ spacing is not ideal if our goal is to suppress as much of the high angle radiation as possible. A spacing of 1/2 λ is superior, but it has a few pitfalls if we do not design our new array carefully.

Stacking Dipole-Turnstiles

Fig 16 shows the outline of two dipole-turnstiles stacked 1/2 λ apart. For our examination, we shall place the lower array at 1 λ above ground, with the upper array at 1.5 λ. We must supply each turnstile with a phasing line. As well, we shall need to contrive a system for feeding the arrays in phase.

If our efforts are successful, we shall obtain the elevation pattern shown in Fig 17. Low-angle gain increases as the upper lobes decrease in strength, and the stacked-dipole turnstiles show a considerable improvement even over the quad-turnstile. The cost is added overall array height.

With many antennas, stacking at a distance of 1/2 λ requires only that we take our original antennas and set them the proper distance apart. However, the dipole-turnstile shows very high levels of radiation both up and down. If we stack our 111.5-inch dipole system with its 70-Ω phase lines, we shall likely be disappointed. The upper portion of Fig 18 shows why. The resulting pattern displays considerable distortion rela-

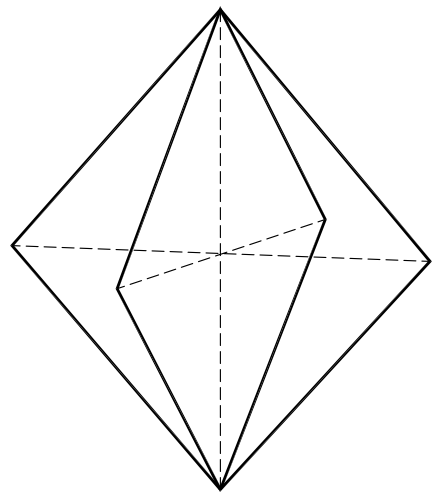

Fig 13—General outline of a quad-turnstile for 50.5 MHz, omitting the necessary phase line.

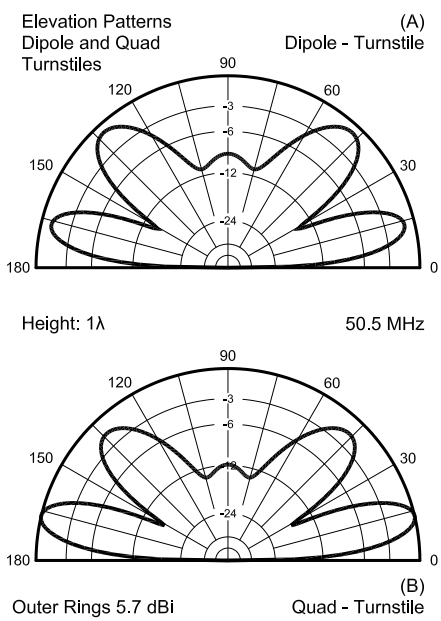

Fig 14—Elevation patterns for a dipole-turnstile (A) and a quad-turnstile (B) with each antenna mounted 1 λ above good ground at its base.

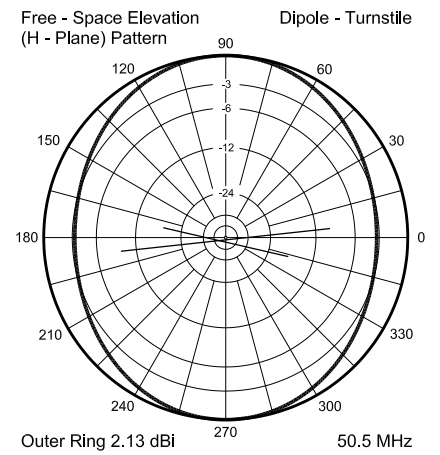

Fig 15—Free-space H-plane pattern of a dipole-turnstile antenna, showing the stronger radiation broadside to the dipole pair.

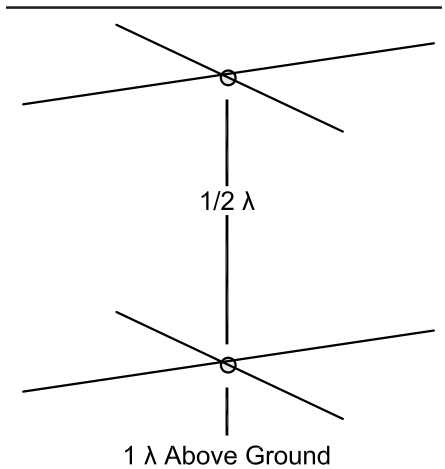

Fig 16—General outline of a stacked pair of dipole-turnstile antennas.

The Relationship of Dipole-Turnstile Azimuth Patterns to Relative-Current Magnitudes and Phasing of the Dipole Elements

A well-constructed dipole-turnstile antenna consists of two dipoles oriented at right angles. For this discussion, dipole 1 designates the element at the center of which we find the system feed point and the beginning of the phase line. Dipole 2 is be the element at the far end of the phase line. Ideally, the two dipoles will show currents of equal magnitude (a 1:1 ratio of currents from dipole 1 to dipole 2). Dipole 2 will show a net phase difference of 90° relative to dipole 1. Operationally, it does not matter whether dipole 2 is phased +90° or –90° relative to dipole 1. However, for consistency in this discussion, we shall use +90° as the ideal phase difference.

Under ideal phasing conditions, the azimuth pattern of a dipole-turnstile will be nearly circular. We cannot eliminate the pattern flattening between 90° points on the compass due to beamwidth limitations of the dipoles making up the array. Under ideal conditions, the differential in gain between points of maximum radiation and points of minimum radiation will be about 0.9 to 1.0 dB.

There is a systematic relationship between azimuth-pattern properties and the degree that dipoles depart from ideal phasing conditions. A given dipole-turnstile may have a less-than-ideal current ratio between dipoles or a relative phase angle that is greater or less than 90°—or a combination of both. As we move either variable away from ideal, the gain differential between maximum and minimum values increases and is a useful marker of the degree of azimuth-pattern distortion.

Fig A graphs the gain differential in azimuth patterns for the two variables. As with other 50.5-MHz dipole-turnstiles used in these notes, the antenna is 1 λ above ground. The range of current ratios from dipole 1 to dipole 2 is 0.75 to 1.25 in linear steps of 0.05. The upper region above a 1:1 ratio of current magnitude becomes a smaller percentage difference and hence yields a shallower curve than the ratios below 1:1. The relative phase-angle increments are 10° from 70° to 110°.

As is evident from the graph, a 90° phase angle between the currents on the dipoles yields the shallowest curve with the least distortion. Notably, the two curves that represent 10° departures from the ideal overlay each other, as do the two curves representing 20° departures from ideal. Equal departures from the ideal phase angle above and below that level result in equally great distortions to the azimuth pattern when the relative current-magnitude ratio is the same. However, the pattern shapes will differ.

Fig B shows azimuth patterns for a current ratio of 0.75. In viewing the patterns, consider dipole 1 to extend vertically through the center of the graph, with dipole 2 extending horizontally. Because the current on dipole 2 is higher, patterns will be distended vertically and pinched horizontally. At a relative phase angle of 90°, the pattern is symmetrical, with a gain differential of about 2.5 dB.

With the same current ratio, relative phase angles above and below 90° will bend or push the azimuth pattern as indicated in Fig B. At first sight, the patterns appear to be bidirectional ovals. However, the higher-gain portions of the patterns are not symmetrical about a centerline. Instead, the current ratio yields an offset in peak gain in a broadside direction relative to the dipole with the higher relative current magnitude.

Fig C presents comparable information for the situation in which dipole 1 (a vertical line for each plot grid) has a current magnitude that is 1.25 times that on dipole 2 (a horizontal line). With a phase angle of 90°, we obtain the same symmetry shown in Fig B, but at right angles to the earlier pattern. Phase angles of 70° and 110° yield distorted bidirectional patterns with the peak gain once more nearly broadside to the dipole having the higher current.

For a 20° phase-angle error and a 25% offset in the ideal current ratio, pattern distortion yields 4 dB or more differential between maximum and minimum gain. The level of pattern distortion is serious relative to a desire for omnidirectional horizontally polarized coverage. However, this level of distortion is not difficult to obtain under conditions of haphazard dipole-turnstile construction or operation. As with any phased array, turnstile performance is a function of the care with which we establish the conditions of correct current phasing between the elements.

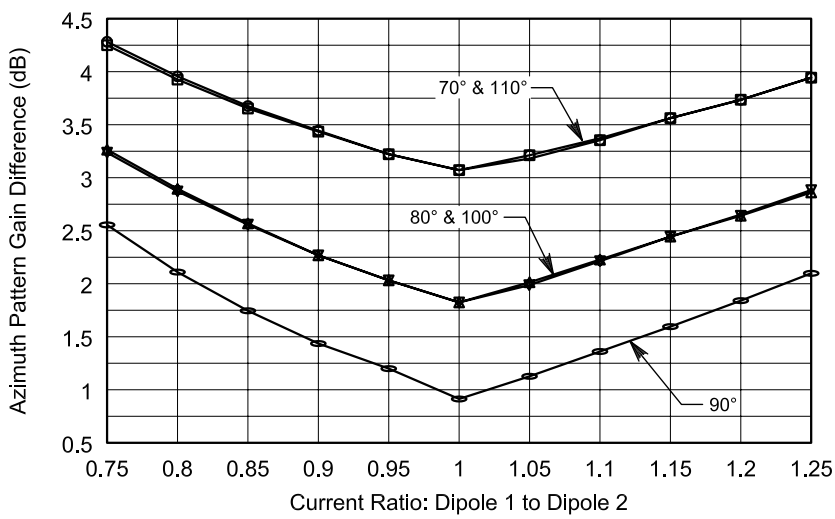

Fig A—A graph of the azimuth-pattern distortion as measured by the differential between maximum and minimum pattern gain resulting from changes in the relative phase angle and the current-magnitude ratio between antenna elements of a dipole-turnstile for 50.5 MHz mounted 1 λ above ground.

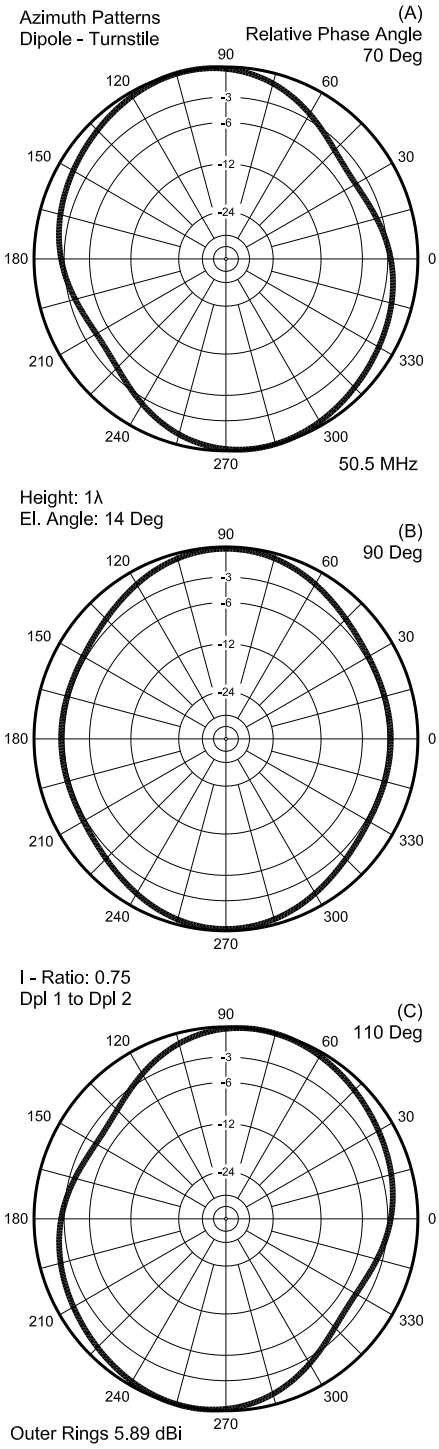

Fig B—Samples of azimuth-pattern distortion (14° elevation angle, 50.5 MHz) for a current-magnitude ratio of 0.75 from dipole 1 to dipole 2 and for relative phase angles of 70°, 90° and 110°.

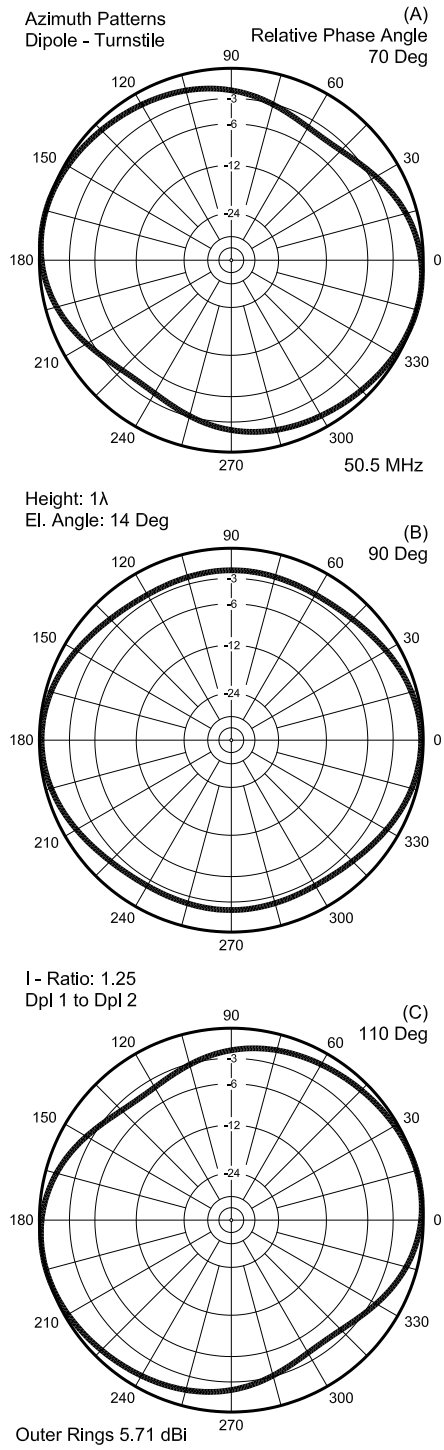

Fig C—Samples of azimuth-pattern distortion (14° elevation angle, 50.5 MHz) for a current-magnitude ratio of 1.25 from dipole 1 to dipole 2 and for relative phase angles of 70°, 90° and 110°.

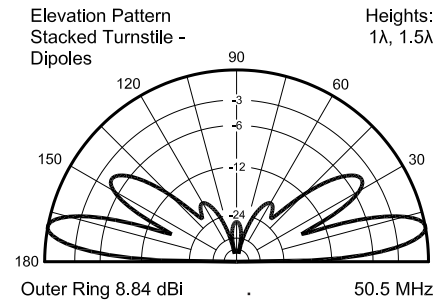

Fig 17—Elevation pattern of the stacked turnstiles shown in Fig 16.

tive to the desired omnidirectional pattern. In fact, the differential between maximum and minimum gain is over 3.8 dB. This situation would not show up well in mere SWR curves, since the feed-point impedance for each array is about 37.1 Ω, very close to the value of individual turnstile-dipole pairs.

Table 5 shows the reason why we obtain such a distorted pattern. Within each dipole-turnstile, the current magnitude ratio and phase angle differentials are far from ideal. What we have neglected to take into account is the relatively strong mutual coupling between the dipoles in each array of the stack. The mutual coupling will alter the required element lengths and also the required phase-line characteristic impedances.

Perhaps the simplest way to account for the mutual coupling is to create a stack of two simple dipoles in a model. Each dipole will be in its final position relative to the eventual stack of turnstiles, that is, 1 λ and 1.5 λ above ground. Now we can adjust the element lengths to obtain resonance. Under these conditions, we obtain a resonant length of 114.7 inches (0.491 λ), with individual feed-point impedances of $62.2 - j0.5\ \Omega$ (bottom) and $63.4 + j0.9\ \Omega$. Not only will our stacked dipole-turnstile array need longer elements, it will need a 63-Ω phase line. Modeling such a line is simpler than constructing one, although we might well parallel sections of RG-63 (Z_0 = 125 Ω) for the requisite impedance.

The current conditions for our revised stack of dipole-turnstile arrays appears in the lower part of Table 5. The current ratio between elements in each turnstile is much closer to the ideal value of 1.0, and the relative phase angles are within about 2° of ideal. The lower portion of Fig 18 shows the effects of our work upon the azimuth pattern. The gain variation totals just about 1 dB, with a maxi-

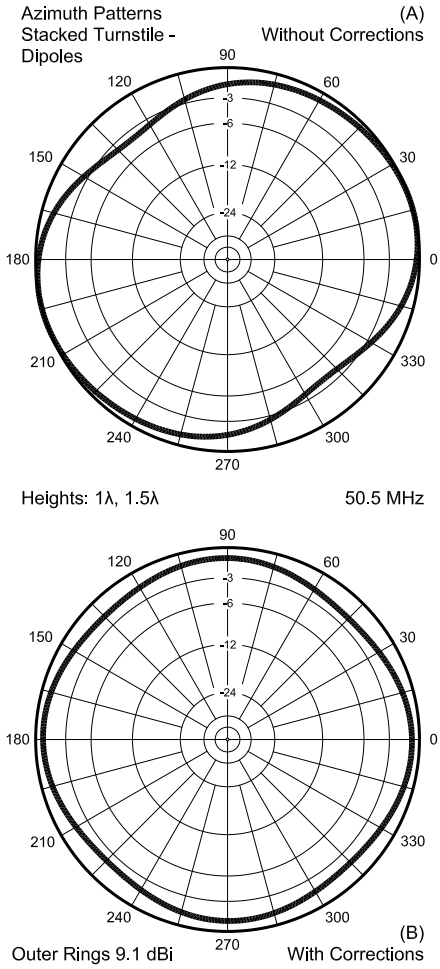

Fig 18—Azimuth patterns of stacked dipole-turnstile antennas before (A) and after (B) introduction of required corrections to element lengths and phase-line construction.

Table 5—Current Magnitudes and Phase Angles for Casual and Careful Stacks of Dipole-Turnstiles ½ λ Apart

A. Casual Version: each Dipole Length 111.5″ (0.477 λ)

Position	***Dipole 1***		***Dipole 2***		*I Ratio*	*Phase*
	I Mag.	*I Phase (°)*	*I Mag.*	*I Phase (°)*		*Difference (°)*
Bottom	0.620	18.39	0.530	–93.33	1.170	111.72
Top	0.612	17.50	0.529	–93.35	1.157	110.85

B. Careful Version: each dipole length 114.7″ (0.491 λ)

Position	***Dipole 1***		***Dipole 2***		*I Ratio*	*Phase*
	I Mag.	*I Phase (°)*	*I Mag.*	*I Phase (°)*		*Difference (°)*
Bottom	0.521	–1.35	0.500	–89.73	1.042	88.38
Top	0.512	–2.24	0.500	–90.19	1.024	87.95

mum gain of about 8.4 dBi. We have gained nearly 4 dB relative to a single dipole-turnstile and nearly 3 dB over the quad-turnstile array, all with a very acceptable pattern for virtually any omnidirectional purpose.

The feed-point impedance for each array is very close to 31.5 Ω. A pair of 50-Ω lines, each ¾ λ long will yield a parallel impedance of about 40 Ω. For this case, however, we might wish to use a Regier series match. A 0.037-λ section of 93-Ω cable (RG-62) followed by a 0.165-λ section of 50-Ω cable (RG8/58) would yield a 93-Ω line impedance. Once we include the velocity factors, we can create a short, straight pair of matching lines to a T junction for a 46-Ω impedance presented to the main feed line.

Conclusion

The turnstile array is, like all phased arrays, dependent upon the relative current magnitudes and phase angles of each element for proper operation as an omnidirectional, horizontally polarized antenna. We have examined a number of conditions of construction and operation that create distorted azimuth patterns, as well as corrective measures we might apply to restore near-ideal patterns. Among the conditions we explored were impedance-based combined matching and phasing systems, which led to the consideration of numerous alternatives that do not affect the desired antenna pattern.

We also looked at a number of candidate antennas for turnstile configuration, as well as the performance they promise. Except for satellite operation, where we wish to enhance the vertical field, most omnidirectional operations seek increased low-angle radiation. While the quad-turnstile offers some improvement with simple construction, stacked-dipole turnstiles offer the most improvement. However, the very factor that leads us to stack turnstiles—a high level of radiation vertically or perpendicular to each turnstile element pair—requires us to redesign the stack elements to account for mutual coupling among elements, with consequential changes in the required phase lines.

The turnstile configuration turns out not to be nearly so simple as we might imagine it to be. However, as we better understand its place among phased arrays we can better exploit its potentials. □□

A Low-Loss VHF/UHF Diplexer

Why use two lengths of expensive feed line when one will do? This handy box lets you use one feed line for both VHF and UHF energy, simultaneously!

By Pavel Zanek, OK1DNZ

Do you need to operate 145-MHz and 433-MHz transceivers simultaneously with one dual-band antenna? Do you require a dual-band 145/433-MHz transceiver to operate with two separate antennas? Do you have a dual-band transceiver with high RF output power? No problem: Here is a description of a simple VHF/ UHF diplexer with good RF parameters. You need only 50-Ω coaxial cable and some enameled #20 AWG copper wire to build your own diplexer circuit.

Features

- Characteristic impedance is 50 Ω
- Operating VHF frequency range: 144 to 146 MHz, UHF range: 432 to 440 MHz
- Low insertion loss (IL): 0.15 dB at VHF and 0.40 dB at UHF
- High isolation: The UHF band is isolated by 70 dB from the VHF path. The VHF band is isolated by 70 dB from the UHF path.
- All ports are well matched to 50 Ω with a maximum SWR of 1.26
- All ports are dc grounded
- Maximum RF power at VHF or UHF or VHF/UHF port is 100 W CW at 25°C
- Fully shielded construction
- Easy-to-produce, low-cost solution

All the parameters above were measured in a laboratory on the first sample of the diplexer. The measurements were performed by means of a vector network analyzer (HP-8714B) with an output level of 0 dBm. Two additional 10-dB pads for transmission measurement were used to avoid

Slovenska 518
Chrudim
Czech Republic, 537 05
Zanek.pavel@worldonline.cz

Table 1—Cable Lengths

Cable	*Electrical Length*	*Physical Length [mm]*
CC1, CC3	0.242 λ_{UHF}	113
CC2, CC4	0.250 λ_{UHF}	120
CC5, CC7	0.500 λ_{UHF}	241
CC6, CC8	0.250 λ_{VHF}	362

mismatch error when a low insertion loss (IL) was measured. The HP-8714B was calibrated before impedance measurements.

VHF/ UHF Diplexer, Design Requirements

The VHF/ UHF diplexer is a three-port device. The functional schematic diagram is shown in Fig 1. The VHF path (between the VHF and common ports) provides low IL at VHF and high isolation to the UHF port. Similarly, the UHF path (between UHF and common ports) yields low IL at UHF and high isolation to the VHF port. If we consider that both bands are sufficiently distant ($f_{UHF} / f_{VHF} \approx 3$ in this case), several possibilities arise to solve the diplexer design problem. We could use lumped design with low and high-pass filters, a distributed solution or the combination of lumped and distributed design. Let's find a solution that makes construction very simple and does not require special elements. Of course, good RF parameters must be achieved. An IL of less than 0.5 dB is expected. The isolation must be better than 65 dB and the SWR lower than 1.40. My design solution was analyzed and optimized by using the *SUPER COMPACT* program.[1]

Circuit Description

The full schematic diagram of the circuit is shown in Fig 2. The lengths of the coaxial cables (CC*x*) are shown in Table 1. All sections of coaxial transmission lines used have a characteristic impedance of 50 Ω. We will consider only a single-frequency design for the first simplified description. Transmission-line theory is not intimately discussed here; further discussion is available elsewhere.[2]

We can write the following equations to express the basic relationships between VHF and UHF frequencies, *f*, and wavelengths, λ:

$$f_{UHF} = 3 f_{VHF} \qquad \text{(Eq 1)}$$

and

$$\lambda_{UHF} = \frac{\lambda_{VHF}}{3} \qquad \text{(Eq 2)}$$

$$\lambda_{VHF} = \frac{300}{f_{VHF}} \qquad \text{(Eq 3)}$$

and

$$\lambda_{UHF} = \frac{300}{f_{UHF}} \qquad \text{(Eq 4)}$$

where frequencies are in megahertz and lengths in meters. The single-frequency design is computed for a geometric center frequency in each band. For the 2-meter (144 to 146 MHz in Czech Republic) and 70-cm bands (432 to 440 MHz in Czech Republic), we get:

$$\lambda_{VHF} = \frac{300}{\sqrt{144 \cdot 146}} = 2.069\ \text{m} \qquad \text{(Eq 5)}$$

and

$$\lambda_{UHF} = \frac{300}{\sqrt{432 \times 440}} = 0.688\ \text{m} \qquad \text{(Eq 6)}$$

VHF Section

Imagine that a UHF signal is passing through the diplexer. The shunt λ/4 coaxial cable stub CC1 (λ/4 at UHF) is open at the far end and acts as a short circuit for UHF at the VHF port. The open end of CC1 is transformed to a short at the VHF port according to:

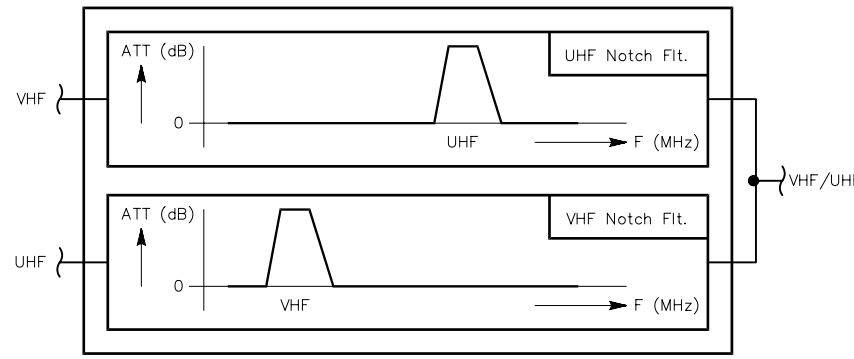

Fig 1—A functional diagram of the VHF/UHF diplexer.

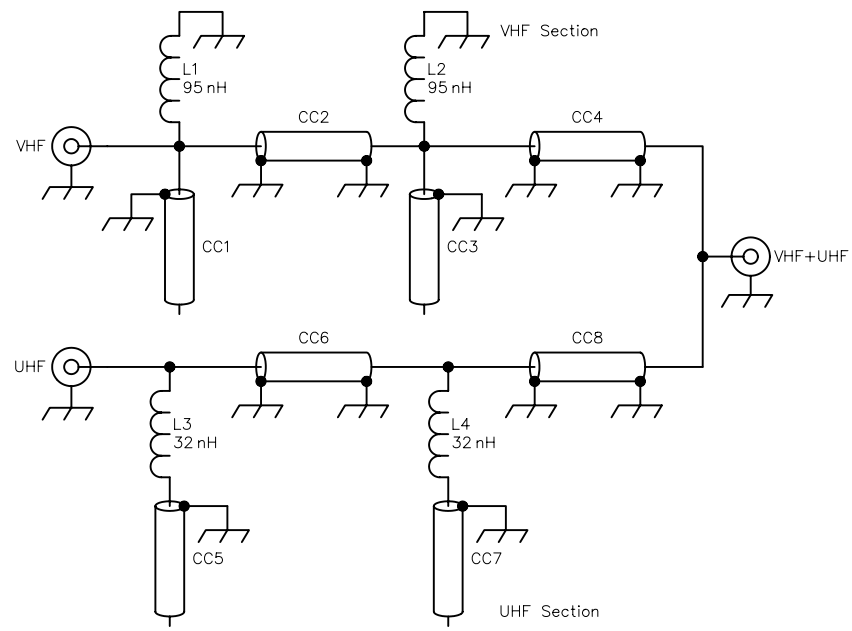

Fig 2—A schematic diagram of the VHF/UHF diplexer.

L1, L2—95 nH air-core coil 5½ turns #20 AWG (0.80 mm) enameled copper wire wound on a 3-mm-diameter drill with approximately 1 mm of space between turns (95 nH at 145 MHz)
L3, L4—32 nH air-core coil 2½ turns #20 AWG (0.80 mm) enameled copper wire wound on a 4-mm-diameter drill with approximately 2 mm of space between turns (32 nH at 145 MHz)
CC1-CC8—Transmission line sections cut (see Table 1 for lengths) from 2.0 m of hand-formable semi-rigid cable (Sucoform 141 Cu, Order Number: 22511635 from Huber and Suhner; see Table 1 and Note 2)
J1-J3—Panel-mount female N flange jacks Rosenberger #53 K 403-200 N3
Misc—Tinned steel box, WBG 40 DONAU, 74×148×30 mm, 0.5 mm thick

[1]Notes appear on page 51.

$$Z = -jZ_0 \cot\left(\frac{2\pi l}{\lambda}\right) \qquad \text{(Eq 7)}$$

where

Z_0 = characteristic impedance of coaxial cable

l = electrical length of coaxial cable

The λ/4 coaxial cable CC2 ($l = \lambda_{UHF}/4$ and $\lambda = \lambda_{UHF}$) transforms this theoretically zero impedance at UHF to infinite impedance at the top of the next shunt $l/4$ coaxial cable stub CC3 according to:

$$Z = jZ_0 \tan\left(\frac{2\pi l}{\lambda}\right) \qquad \text{(Eq 8)}$$

There is again a short circuit for UHF because of CC3 ($l = \lambda_{UHF}/4$ and $\lambda = \lambda_{UHF}$) according to Eq 7. Theoretically zero impedance at UHF is transformed again to high impedance at the common VHF/UHF port by CC4 ($l = \lambda_{VHF}/4$) according to Eq 8. Thus, the UHF transmission between UHF and VHF/UHF ports is not affected. Both inductors L1 and L2 have no influence now. They are shorted for UHF. The VHF port is well isolated now at UHF.

Now consider a VHF signal passing through the diplexer. The shunt cable stub CC1 presents at VHF an electrical length of about $\lambda_{UHF} / 4 = \lambda_{VHF} / 12 \approx 0.083\ \lambda_{VHF}$. Thus, CC1 works like a parallel capacitor at VHF. From Eq 7, we get the impedance: $Z = -j86.6\ \Omega$; for example, C = 12.7 pF at f_{VHF} = 145.0 MHz. This capacitance must be eliminated at VHF by using a parallel-resonant circuit tuned at f_{VHF}. From Thomson's well-known formula, we obtain:

$$L = \frac{1}{4\pi^2 f^2 C} \qquad \text{(Eq 9)}$$

where L is in Henries, f in Hertz and C in Farads. Then L1 = L2 = 95.1 nH. Now the VHF signal passes through CC4 to the common port.

UHF Section

Imagine a VHF signal is passing through the diplexer. The shunt λ/4 coaxial-cable stub CC5 (with its end open) has electrical length $l = \lambda_{UHF} / 2 = \lambda_{VHF} / 6 \approx 0.167\ \lambda_{VHF}$. This length presents the impedance given by Eq 7: $Z = -j28.9\ \Omega$; for example C = 38.0 pF at f_{VHF} = 145.0 MHz. The VHF signal must be shorted by the series resonance of CC5 and L3. We obtain the desired L3 from Eq 9: 31.7 nH. The λ/4 coaxial cable CC6 ($l = \lambda_{VHF} / 4$ and $\lambda = \lambda_{VHF}$) transforms this theoretically zero impedance at VHF to infinite impedance at the top of L4 according to Eq 8. Next, the same VHF series-resonant circuit (L4 and CC7) again shunts the VHF voltage. Theoretically VHF zero impedance is transformed to infinity at the common port by CC8 ($l = \lambda_{VHF} / 4$) according to Eq 8. Thus, the VHF transmission between the VHF and common ports is not affected. The UHF port is well isolated at VHF.

Now consider a UHF signal passing through the diplexer. The open shunt cable stub CC5 with electrical length $\lambda_{UHF} / 2$ presents, according to Eq 7, infinite impedance at the top end (the impedance is the same as at the open end). Then no UHF current can flow via the series combination of L3 and CC5. The situation is the same for L4

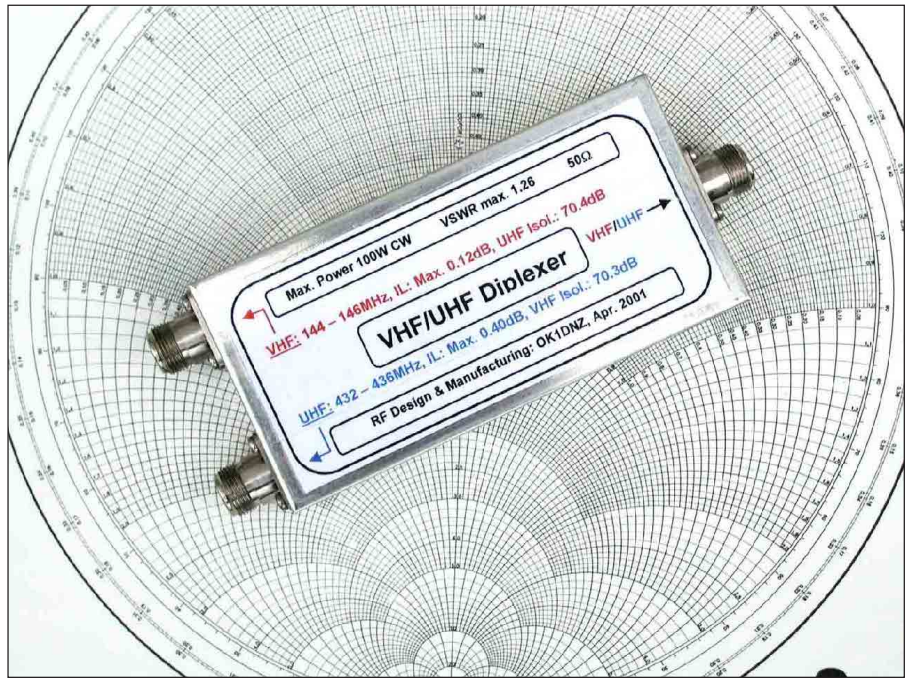

Fig 3—A photo of the VHF/UHF diplexer.

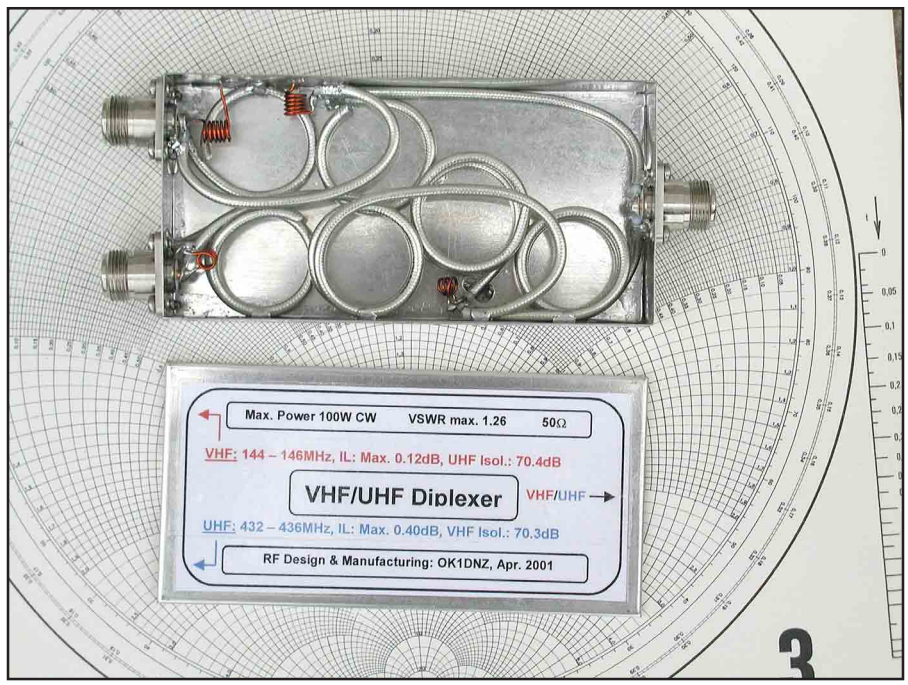

Fig 4—A photo of the VHF/UHF diplexer interior.

and CC7. The UHF signal is transported by CC6 and CC8 to the common VHF/UHF port.

Voltage Analysis

This analysis was made using *SUPER COMPACT* software and verified by using a high-impedance Rohde and Schwarz URV4 RF millivoltmeter. A complete-loss model of the diplexer was used. If either the VHF or common VHF/UHF port were driven by a 2-meter transmitter with an output RF power of P_{TxVHF} watts and the other ports were correctly terminated, then an RF voltage of amplitude V_{UHF} at the open ends of CC1, CC3 and CC7 would be approximately:

$$V_{\mathrm{VHF}} = 1.76\sqrt{50P_{TxVHF}} \qquad \text{(Eq 10)}$$

If either the UHF or common VHF/UHF port were driven by a 70-cm transmitter with an output RF power of P_{TxUHF} watts and the other ports were correctly terminated, then an RF voltage of amplitude V_{UHF} at the open ends of CC3, CC5 and CC7 would be approximately:

$$V_{\mathrm{UHF}} = 3.18\sqrt{50P_{\mathrm{TxUHF}}} \qquad \text{(Eq 11)}$$

Do not touch the open cable ends or live nodes when the diplexer is carrying RF power! Use the diplexer with both covers attached and use only a correctly adjusted diplexer!

Practical Construction

I have selected hand-formable semi-rigid coaxial cable, for it makes assembly of the diplexer very quick and easy. It holds its shape well after bending and the 100% cable shielding is soldered at several points to the grounded case of the diplexer. This 141-mil, 50-Ω cable[3] has these basic electrical characteristics: attenuation = 0.139 dB / meter at 150 MHz; 0.248 dB / meter at 450 MHz; power handling at +40°C is 1.8 kW at 150 MHz; 0.95 kW at 450 MHz; relative propagation velocity = 0.70. Keep in mind that its minimum bending radius for bending once is 11 mm. All physical lengths given in Table 1 are measured on the outer coaxial conductor. The physical lengths of CC*x* are 70% of the electrical lengths for the selected cable. Inner live coaxial conductors are isolated by about 2 mm of their own PTFE dielectric. Live connections must be as short as possible. Make CC1 and CC3 a little bit longer, approximately 130 mm! They will be correctly trimmed upon RF measurement. Coaxial-cable shields must be connected directly to the grounds of the N connectors to get the best SWR values. After cutting and stripping, be sure that each coaxial cable shield has a circular edge. That is especially important for the open ends.

The complete diplexer is shown in Fig 3. The internal mechanical arrangement of the diplexer is shown in Fig 4. The coaxial cables were wound 22 mm in diameter. The diplexer looks like a box full of silver snakes! The open ends are kept a little distance from ground areas.

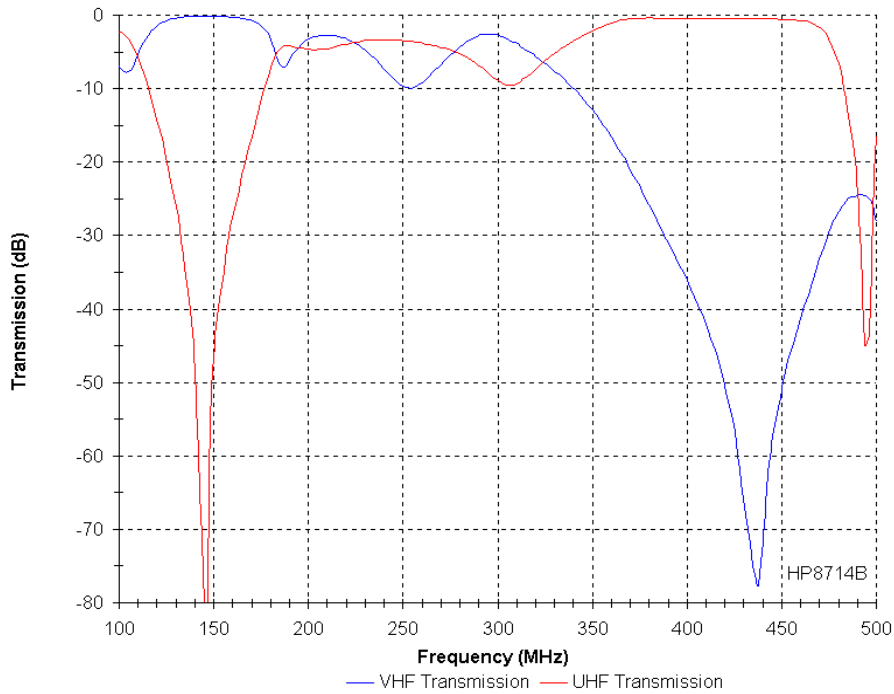

Fig 5—Measured transmission of the VHF and UHF paths.

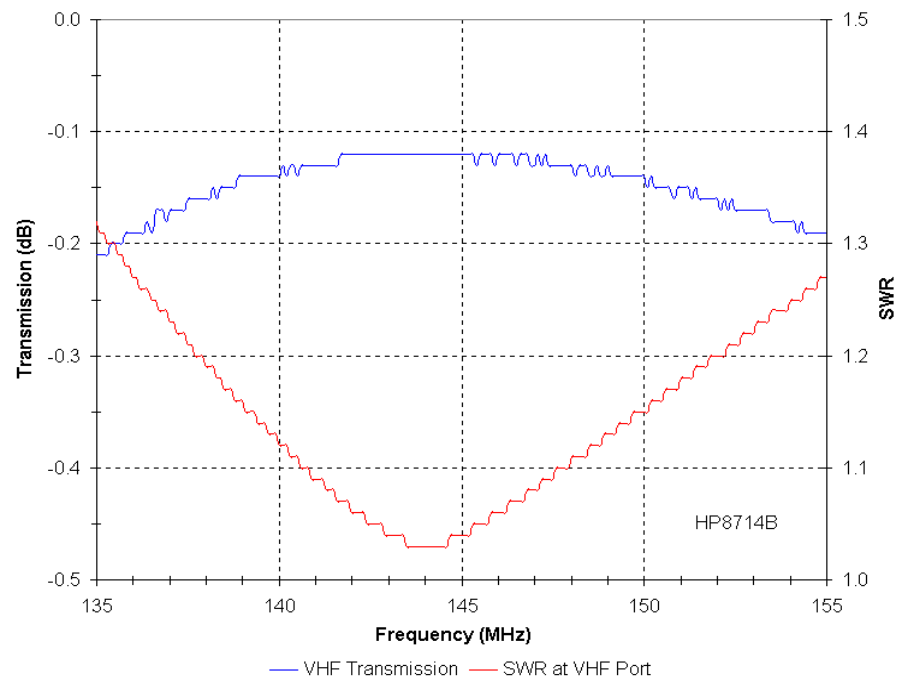

Fig 6—Measured transmission and SWR of the VHF path.

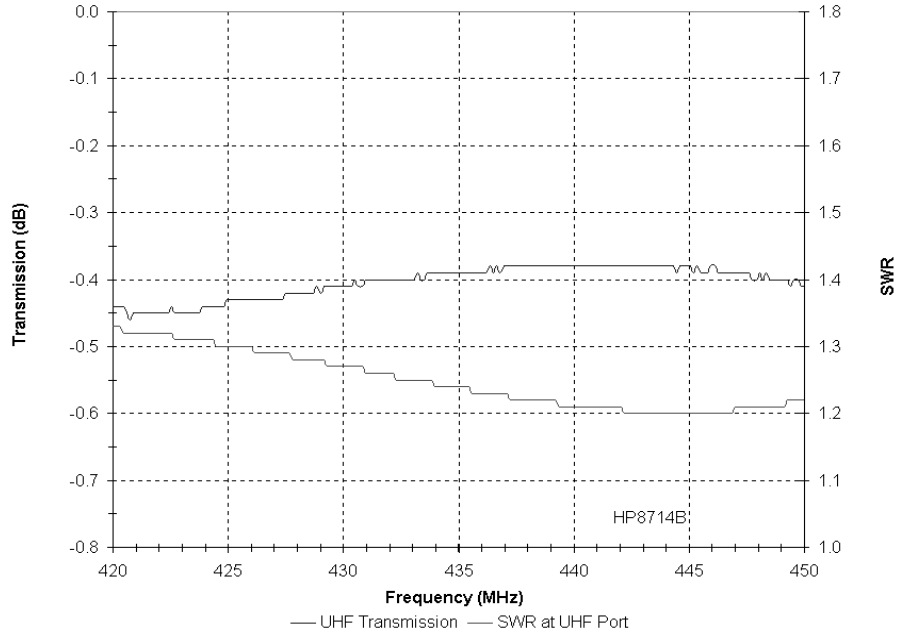

Fig 7—Measured transmission and SWR of the UHF path.

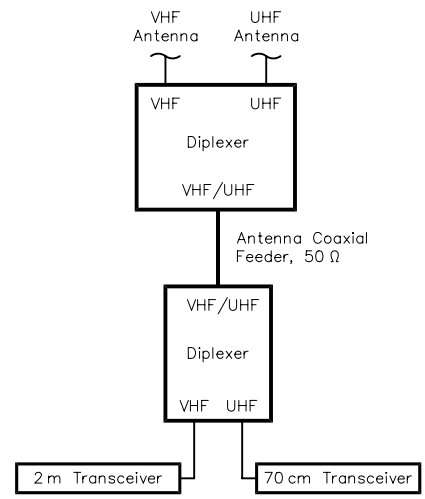

Fig 8—Full-duplex satellite communication using two transceivers.

RF Measurement and Adjustment

RF measurements and adjustments are necessary before using the diplexer. The high performance of the diplexer, which compares with similar professional products on the market, cannot be realized without sophisticated measurement equipment. When operating at higher power levels (up to 100 W for VHF or UHF input), perfect adjustment is especially necessary for good performance across the VHF and UHF bandwidths specified here.

Here are the basic steps of the adjustment procedure. A vector/scalar network analyzer is required for perfect adjustment. Set the swept frequency range to 100-500 MHz. Set the instrument to display both channels simultaneously (impedance and transmission traces). With this equipment, the adjustment procedures should take no more than 20 minutes.

VHF Adjustment

Connect a 50-Ω load to the UHF port. Drive the VHF port with a swept signal. The VHF/UHF port is connected to the input of the network analyzer. Shorten the open ends of CC1 and CC3 little by little to achieve maximum attenuation at 432–440 MHz. Do not deform the open ends of the cables during the adjustments. It is typical for the achieved attenuation to be about 70 dB (see Fig 5). Adjust coils L1 and L2 to minimize SWR at the VHF port for 144-146 MHz. It should be about 1.05:1 (see Fig 6).

UHF Adjustment

Reconnect the 50-Ω load to the VHF port. Now, drive the UHF port with a swept signal. Adjust coils L3 and L4 to achieve maximum attenuation at 144-146 MHz. It should adjust to about 70 dB (see Fig 7). Check the SWR at the UHF port for frequency range of 432-440 MHz. A typical achieved value is about 1.26:1 (see Fig 7). Close the upper cover and check all RF parameters again. If you can accept a narrower operating bandwidth, you may be able to achieve greater isolation.

RF Performance, Applications

The three graphs in Figs 5, 6 and 7 show the RF performance achieved with my unit. The VHF/UHF isolation is greater than 70 dB, and the power design permits use with VHF or UHF transceiver RF output levels up to 100 W.

The power lost will be 2.7 W for VHF transmitters and 8.8 W for UHF transmitters. Fig 8 shows a possible application for the diplexer. You can combine 2-meter and 70-cm equipment and split the VHF/UHF signals between two separate antennas. The big advantage of the configuration shown in Fig 8 is the use of only one coaxial antenna feeder. Also, two bias **T** connectors can be inserted into Fig 8 to feed receive preamplifiers using the coaxial-cable feeder. The tees must be inserted at both the source and load ends of the feeder.

Notes

[1]*Super Compact* is no longer available. It evolved into some of the current software offered by Ansoft; **www.ansoft.com**.

[2]David M. Pozar, *Microwave Engineering*, Second Edition (New York: John Wiley & Sons Inc, 1998) pp 56-73.

[3]Huber and Suhner, *Suhner Microwave Cable*, Type Sucoform 141 Cu, Item 22511635. For a datasheet, visit **products.hubersuhner.com/index_rfcoaxcable.html** and insert the order number: 22511635. □□

A picture is worth a thousand words...

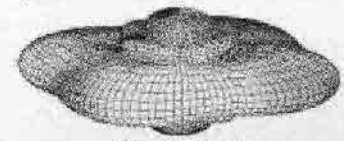

With the all-new

ANTENNA MODEL™

wire antenna analysis program for Windows you get true 3D far field patterns that are far more informative than conventional 2D patterns or wire-frame pseudo-3D patterns.

Describe the antenna to the program in an easy-to-use spreadsheet-style format, and then with one mouse-click the program shows you the antenna pattern, front/back ratio, front/rear ratio, input impedance, efficiency, SWR, and more.

An optional **Symbols** window with formula evaluation capability can do your computations for you. A **Match Wizard** designs Gamma, T, or Hairpin matches for Yagi antennas. A **Clamp Wizard** calculates the equivalent diameter of Yagi element clamps. A **Yagi Optimizer** finds Yagi dimensions that satisfy performance objectives you specify. Major antenna properties can be graphed as a function of frequency.

There is **no built-in segment limit**. Your models can be as large and complicated as your system permits.

ANTENNA MODEL is only $85US. This includes a Web site download **and** a permanent backup copy on CD-ROM. Visit our Web site for more information about **ANTENNA MODEL**.

Teri Software
P.O. Box 277
Lincoln, TX 78948

www.antennamodel.com

e-mail **sales@antennamodel.com**
phone **979-542-7952**

A Homebrew Shaft Encoder

Build a shaft encoder using parts you can salvage from dead computer mice.

By Doug Smith, KF6DX

Equipment designers often find that digital shaft encoders are more expensive than they would like. Encoders also may not be available in the angular resolutions they desire. Here is how I designed and built a tuning knob for my computer-controlled transceiver using readily available components and a little persistence.

Digital Rotation Sensors: Principles of Operation

When it comes to digital rotation sensors, the idea is to develop digital signals that indicate both direction and rate of rotation. The most common arrangement is a pair of digital signals in quadrature. That is, two digital signals having a 90° phase relationship (see Fig 1). When the shaft is rotating in one direction, signal A leads signal B; when rotating in the opposite direction, signal B leads signal A.

It is easy to determine the direction of rotation using an edge-clocked D flip-flop (see Fig 2). Applying signal A to the flip-flop's clock input and signal B to its data input, signal B is low at signal A's rising edge when rotation occurs in one direction; it is high when rotation is in the opposite direction. The flip-flop's output signal, Q, therefore indicates the direction of rotation. Such a direction signal, combined with the rate of one of the signals, A or B, yields the direction and speed of rotation.

Of Mice and Men

John Steinbeck is a better "read," but the method described above is exactly what happens inside your computer mouse or trackball. Movement of the

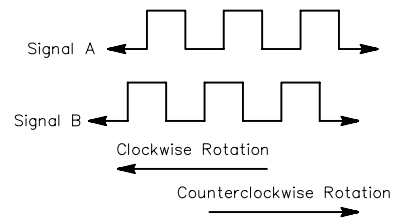

Fig 1—Desired shaft encoder output signals A and B.

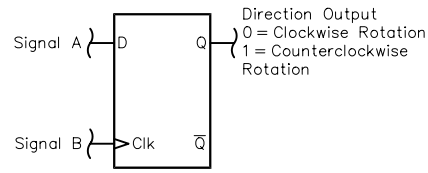

Fig 2—A rising-edge-clocked D flip-flop decodes rotation direction.

225 Main St
Newington, CT 06111-1494
kf6dx@arrl.org

pointing device causes two sets of direction and speed information to be conveyed to the computer. One set corresponds to movement left and right (X axis), the other to movement back and forth (Y axis). For radio tuning applications, only one set of information is needed, corresponding to clockwise or counterclockwise dial rotation.

It is possible to perform the function of the D flip-flop in software running on a microprocessor. Signals A and B are fed to two discrete inputs of the processor and code is written to compare their states. Problems usually arise, though, when the rotation rate exceeds the processor's ability to keep up. Backward steps and other strange things can occur when the processor is unable to read each and every transition of both signals. For that reason, mouse makers and embedded-control system designers have stayed away from decoding in software and have relied on hardware to do the job.

For a computer-controlled transceiver, a mouse chip seems an excellent choice. It does the decoding and delivers serial data commands that correspond to shaft rotation. Power consumption is so low that power may be derived from the host computer. I chose the HM8350A from Hualon Microelectronics.[1]

To get quadrature signals, a slotted wheel is generally used. Optical emitters and sensors are mounted on opposite sides of the wheel to generate signals A and B. A single infrared emitter is common, accompanied by a pair of phototransistors (see Fig 3). The distance between the phototransistors is chosen to be the product of an odd integer and one-quarter of the distance between transparent slots in the wheel so that light intensity varies in quadrature at the sensors. When the signals from the phototransistors are squared (hard-limited) inside the mouse chip, they resemble signals A and B as shown in Fig 1.

HM8350A chips, slotted wheels and photo-electronic devices may be salvaged from discarded mice that failed because of mechanical reasons. One alternate way of making a slotted wheel is described below.

The Slotted Wheel and Shaft Bearing

I wanted to use a 1/4-inch shaft for my tuning knob and the slotted wheels from mice were too small. I reasoned that with modern CAD software, it should not be too hard to create a pattern of radial segments that were alternately light and dark. Armed with a laser printer and some laser-compatible transparency film, I made my own photo-interrupter disk, shown in Fig 4.

I made the disk about 1 inch in diameter and with pairs of light and dark segments. I punched a hole through the center of the disk so that I could attach it to the end of the shaft using a regular fastener. At the last minute, however, I chose to secure it with cyanoacrylate adhesive (see Fig 5). A little touch-up with a fine permanent marker made the disk usable.

The shaft bearing is a critical part of tuning-knob design because any play, either back-and-forth or side-to-side, is quite undesirable. The shaft-to-bearing fit must be quite close and it was not easy finding the right shaft material. Fortunately, rod stock is available in very fine gradations of diameter. A generous blob of silicone grease helped eliminate any remaining play.

The shaft bearing I used has a 3/8-inch threaded bushing for panel mounting. A lever is used to provide variable friction on the shaft. The housing was made for this accessory from a track-lighting enclosure (see Fig 6). A heavy base was necessary to prevent the assembly from traveling across the desk when in use. The base is made from a roughly circular slug that was cut from thick steel plate at

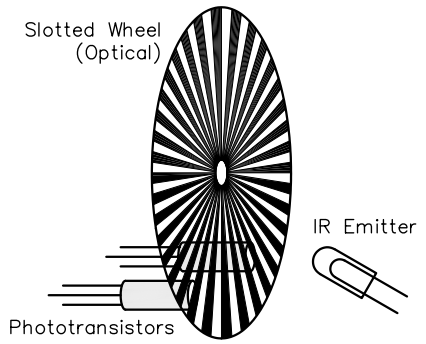

Fig 3—The general arrangement for generating signals A and B.

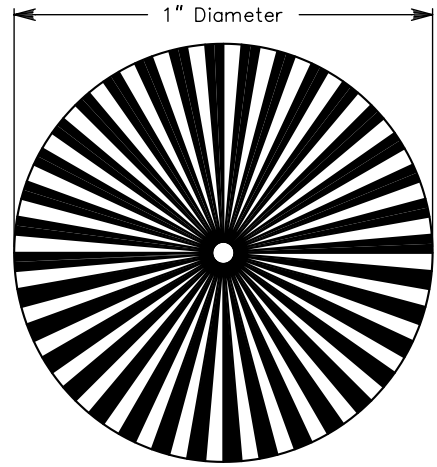

Fig 4—An opto-interrupter disk made from laser-printer transparency film.

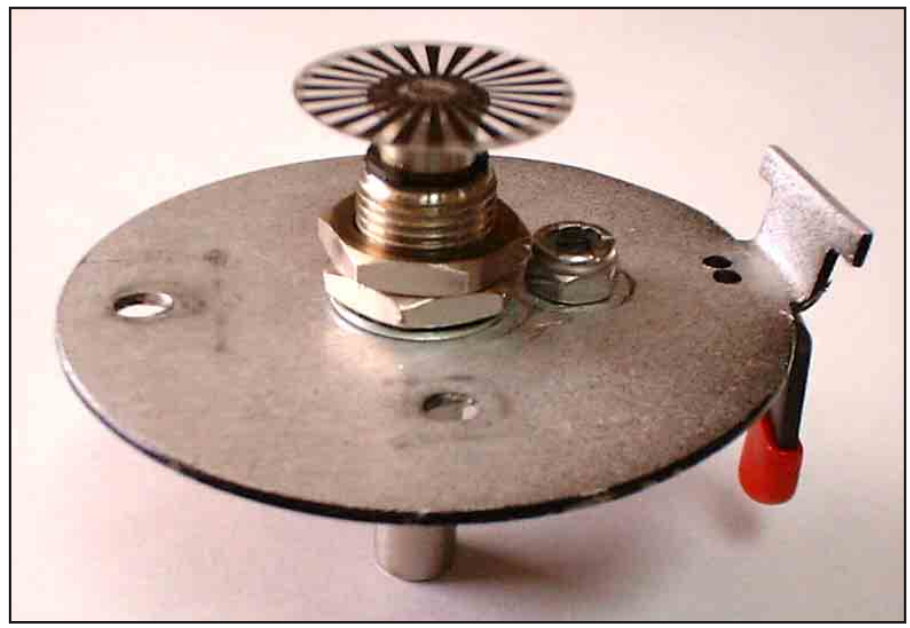

Fig 5—The disk attached to the shaft.

[1]Notes appear on page 54.

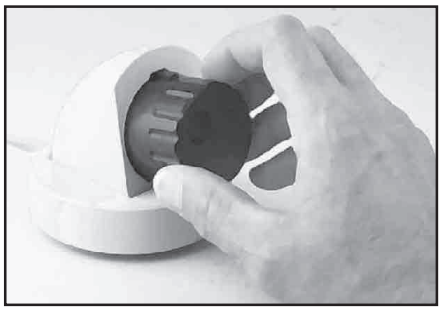

Fig 6—Completed tuning knob assembly.

a construction site and machined until presentable, then painted.

A Serial-Mouse Circuit

Refer to Fig 7, a schematic diagram. The mouse chip gets its power from the computer's EIA-232 TxD line, since that line is not doing anything else in this case. Only the RxD line carries data. D1 protects against reverse polarity in case the TxD line goes to the positive rail. D3 sets the supply voltage to the mouse chip at about 5 V dc. The power for the LED comes from the RTS line, which also does not toggle.

Phototransistors Q1 are tied directly to the chip. Tuning-fork resonator Y1 provides a clock for the chip. Transistor Q2 level-shifts the R×D output to EIA-232 levels. Output comes at 1200 baud and standard mouse driver software running on a PC may be used to detect knob rotation commands from either the X or Y detector. Pins L, M and R would normally be hooked to the three SPST switches on a mouse or trackball. Those could have been used to change the tuning rate or to implement some other function, but they were left unconnected here.

Fig 8 is a close-up of the circuit assembly. The encoder disk fits between the LED and the phototransistors when assembled. The LED is an LTE-302; the phototransistor pair is a single, three-pin unit: LTR-305D.[2]

Note: Modern PC operating systems tend to interrogate devices connected to serial ports at boot time. Since my knob circuit looks just like a mouse to the PC, it is wise to connect a serial PC mouse or trackball to a lower-numbered COM port than that of the knob. Otherwise, the PC will install the knob as the pointing device and you will find the icon traveling diagonally across the screen as you rotate the knob; your mouse will be tuning your radio!

The Knob Itself

In these days of push-button, menu-driven machinery, decent tuning knobs are becoming difficult to obtain "off the shelf." On the other hand, regular milling equipment makes it easy to make a custom knob from readily available rod stock.

Armed with some three-inch black Delrin stock[3] and a ball-end milling tool, I was able to produce the massive symmetrical tuning knob shown in Fig 7. I used Delrin because it is an easy-to-machine plastic that is already black in color. Aluminum may be used and subsequently anodized if you worry about marring the Delrin under heavy use. The ball-end milling tool made it easy to put a finger hole into the front surface of the knob and to make flutes that taper along the knob's length.

Zack Lau, W1VT, has more to say about making knobs. Watch for the topic in an upcoming RF column.

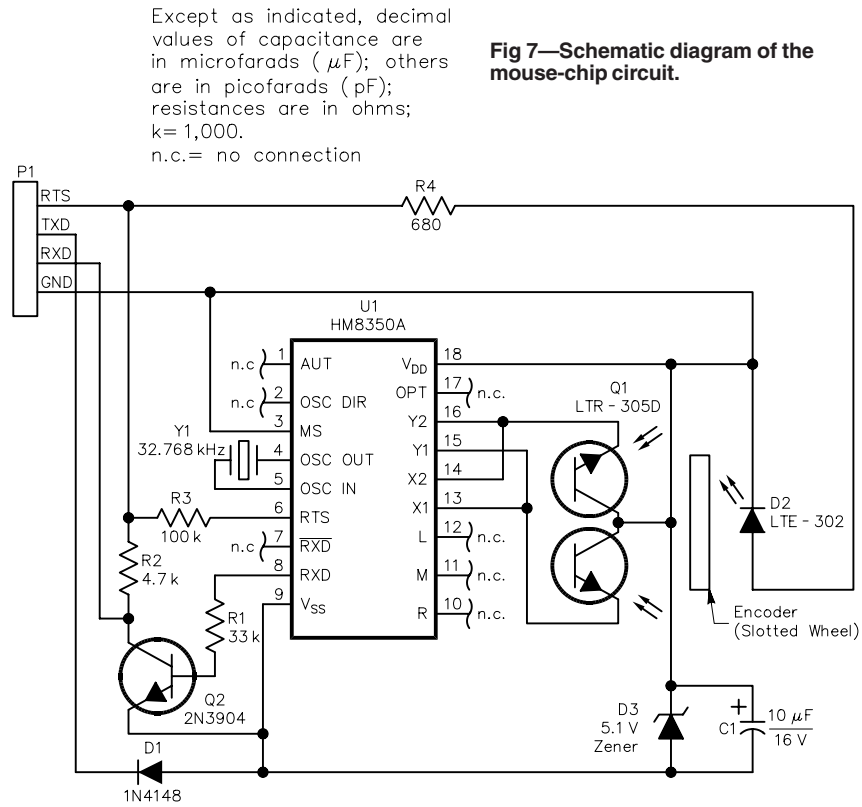

Fig 7—Schematic diagram of the mouse-chip circuit.

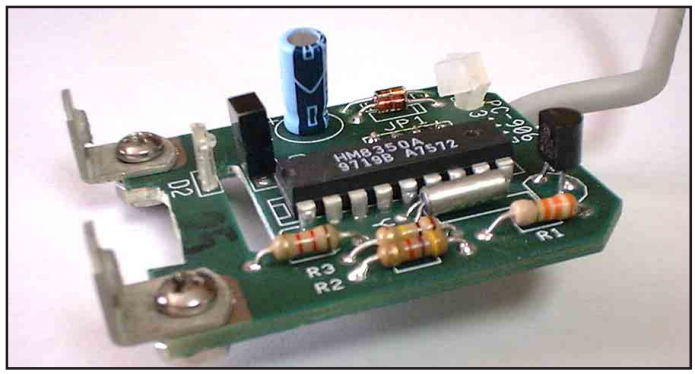

Fig 8—A close-up view of the PC assembly.

Notes

[1]Hualon Microelectronics (HMC), www.hualon.com.tw.

[2]LiteOn, www.liteon.com. These particular parts may no longer be available, but equivalents are. Scrounge them from dead mice!

[3]Delrin rod stock is available from McMaster-Carr Supply Co, www.mcmaster.com. □□

RF

By Zack Lau, W1VT

How to Work 10-GHz DX

(This discussion began in the previous issue, with consideration of station location and antenna-aiming techniques.—*Ed.*)

Part 2: Hardware

A conventional dish—a symmetrical parabola fed at the center—has several advantages for portable operations. Mounting the dish to a mast that supports a liaison antenna is usually quite easy. The symmetry makes it relatively easy to determine whether the dish has survived transport. Setting up a dish feed is straightforward; there is only one variable in adjusting the feed: the distance from the center. Visual aiming is often practical, in both azimuth and elevation. Cost is a disadvantage; they tend to be less common and more expensive. They also have worse receive performance—the symmetrical pattern typically picks up more ground noise than dishes optimized for satellite reception. Higher feedline loss also reduces receive performance.

Lightweight coax connecting a prime-focus feed to a transverter often has a loss of 1dB/ft, if not more. Reverse feeds fed with waveguide are typically too inefficient to merit much consideration. If you are lucky, you might be able to cut the loss in half or more with specialized cables, but these can be tough to obtain in the right lengths with the proper connectors. If you don't mind the bulk and weight, a good solution is to use circular waveguide, more commonly known as $^3/_4$-inch copper water pipe, to feed the dish.[7]

The most popular coaxial feedline is a short length of UT-141A semi-rigid coax. It is easy to find and relatively easy to work with.

UT-085 is thinner and even easier to work with, being easier to bend. However, the loss is significantly higher, and it is not recommended, unless nothing else is suitable. I often carry a spare flexible feedline that is longer than necessary—in case I need to improvise. I've used UT-250, which sells for about $5 an inch! It is tough to bend precisely. The rigidity might be useful

225 Main St
Newington, CT 06111-1494
zlau@arrl.org

[7]Notes appear on page 59.

for making sure the dish feed alignment doesn't change—holding it firmly in place. It could be a problem if you need to adjust the dish feed. You may have difficulty locating connectors. However, I have found them at hamfests, unlike the proper connectors for expensive expanded Teflon cables. Expanded Teflon cables can sometimes be found on eBay, but they are often bid up to rather high prices. The low loss and flexibility does make them interesting alternatives.

A possibility I've not fully investigated is Times Microwave LMR-400, with the properly installed EZ-400-NMH crimp connectors. The crimp connectors allow good electrical connections at the very end of the coax cable. Typical clamp connectors actually make electrical contact a short distance from the end of the cable, creating a long RF path that significantly degrades microwave performance. This is similar to choke flanges used with waveguide. Never mate a pair of choke flanges so that the annular ring is doubled in depth. The loss specification of LMR-400 is just 0.15 dB/foot. These are N connectors; SMA connectors are typically preferred at 10 GHz.

RG-213 is a nonstarter—it actually has more loss than RG-58! If the cable is too large, it also acts as a waveguide. This makes the cable somewhat unpredictable—you need to test your cable at the desired operating frequency for low loss. It is possible for a large cable to still be useful—1/2-inch heliax usually has a loss of just 0.1 dB/foot at 10.368 GHz. Its maximum operating frequency is specified as 8800 MHz.

An offset dish, a section of a parabola used for satellite work, is primarily used by amateurs because of its low cost. There is an abundant supply of surplus offset dishes, keeping the cost quite acceptable to amateurs. However, it is not obvious where to put the feed. Fortunately, Paul Wade has "done the math."[8] Neither is visual aiming as easy, at least in one plane. Receive performance is typically better, as the sidelobes are optimally pointed at the sky, reducing noise pickup. However, this does not apply if the dish is used on its side or upside down. The feedline is much shorter than with a conventional dish, further improving receive performance. This is a significant advantage to high-power stations (two or more watts) that want to hear stations running 10 dB less power. This advantage isn't as useful to low-power stations, which often have an extra 10 dB of signal-to-noise ratio on receive. While the dishes often come with mounts, mounting the dish to a mast may be a challenge.

I've had good luck with a homebrew scalar or *Chapparal* feed for conventional dishes. It is relatively easy to make the scalar rings out of brass sheet stock, as shown in Fig 1.[9] The VE4MA feed also looks to be a good choice, according to a study by Paul Wade, though it is a good thing commercial feeds are Chaparrals and not of the VE4MA design.[10] The VE4MA is a narrow-bandwidth design, so one would not expect good performance far from the design frequency. Conversely, hams have gotten good results out of 11-GHz Chaparrals at 10 GHz.[11] Unfortunately, the 11-GHz "Superfeeds" are no longer produced and are hard to find.

The simple DSS-dish horn-feed designed by Paul Wade is a good compromise between performance and complexity. It was my feed of choice for feeding an 18-inch DSS dish in the 2001 "10-GHz and Up" contest. While my effective radiated power was reduced slightly compared to the two-foot conventional dish it replaced, the improved receive performance and slightly wider beamwidth made up for it. I've been using a roof-rack-mounted rotator on my Saturn SL2 sedan. While the pointing isn't as precise as a tripod arrangement, the extra height and mounting stability are quite useful. I may replace it with a large W2IMU feed for improved performance. However, my experience with building smaller W2IMU feeds is that bending the transition section out of thick copper takes a bit of skill—I may try machining a section out of brass.

A Cheap Tripod Mount

I recommend using a RadioShack #15-516 three-foot tripod. It is rugged, cheap and easy to find! I don't recommend the five-foot version—it is much less stable. "Three feet" here refers to the length of each leg—the actual height is 32.6 inches. There is no adjustment for leveling the tripod, but I can usually find a rock or similar object to prop up one leg. Pieces of square tubing with holes that match your U-bolts can be very convenient if you do a lot of portable operation. The three-foot tripod can be reasonably stable if there is a lot of weight supported at the top of legs. If more stability is needed, I've attached a triangle of heavy angle iron to the bottom of the legs. Such a setup has even supported a small 6-meter Yagi. For even more stability, as when operating from Mt Washington, I recommend using a car to hold the tripod down. Fig 2 shows my Saturn SL2 holding down a 10-GHz two-foot dish and 2-meter liaison antennas. A similar setup by Terry Wilkinson, WA7LYI, appears on page 22-16 of the 2001 *ARRL Handbook*.

Fig 3 shows a 10×24-inch mounting plate for attaching a DSS dish to a RadioShack tripod. I made mine out of 3/8-inch plywood. I also rounded the corners. It is held in place with a two-foot piece of 1 1/4-inch mast and a 1/4-inch metal pin. I used the bottom half of a five-foot mast although the swaged top section would be easier to push through the plywood mounting plate. The mast runs through the center of the tripod and through the plate. Two 1/4-inch holes are drilled 15 inches apart for a pointer and metal pin. The top hole for the pin is about an inch from the end of the mast. The pointer should be just above the setting circle that sits on the horizontal support struts of the tripod. One end of a piece of brass tubing can be squashed flat to form the pointer. Alternately, you might use two pieces of steel rod, in case you need to improvise and use the

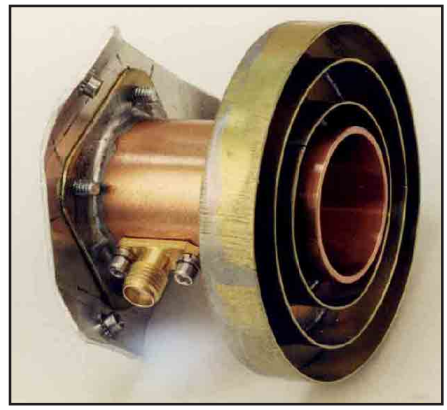

Fig 1—Homebrew Chaparral feed made out of a copper pipe coupling and brass sheet stock.

Fig 2—Saturn SL-2 holding down a RadioShack three-foot tripod loaded with antennas.

pointer as the holding pin. Ideally, the metal pin sits in a slot, so that the dish and pointer are always in alignment.

To form the slot, I've machined a piece of polycarbonate that is attached to the top of the plywood. The dimensions of the polycarbonate indexing plate are shown in Fig 4. I also attach a five-inch polycarbonate disk to the bottom. Often, I'll use a second five-inch disk between the tripod and the dish mounting plate as a large washer. The dimensions of the 1/4-inch-thick bottom mounting plate are shown in Fig 5. The 3/8-inch mounting holes are drilled to a depth of just 0.14 inches, to allow the heads of 1 1/4-inch-long #10 hex-head screws to lie below the surface of the plate. I used special drill bits with a small starting point and a second edge that cuts a flat countersink (sometimes known as "brad point" bits—*Ed.*). These are easy to find at big hardware stores. It takes a lot more work to mill out flat-bottomed holes with a milling machine. A milling machine is more useful for cutting the 1.27-inch holes. The standard 1.25-inch hole is too small—the mast will often get stuck in the hole. A half-round file is useful for enlarging the hole for a loose fit. In a dry climate, you might be able to use wood. I've discovered that wooden versions expand in the wet New England environment and become stuck to the mast. This was quite a problem in previous versions, which used a longer mast that barely fit in the car. It is a good idea to make sure that your DSS dish bracket matches the dimensions shown before drilling any holes. You may also want to mount an IF radio to the plywood plate with a mounting bracket. In windy weather, you don't want your radio to fall off the plate.

To use the tripod, the tripod is unfolded and placed in position. Next, the setting circle is placed on the horizontal support struts and the mast is placed in position. The support screws on the tripod are then adjusted to fit loosely against the mast. It may be desirable to temporarily lock the screws against the mast to hold it in place. The large polycarbonate washer is placed over the mast. The mounting plate can then be placed in position over the mast and against the top of the washer that sits on the tripod. The metal pin is inserted into the mast. The mast is now lowered into the slot on top of the mounting plate, and the pointer is inserted into the mast. With the aid of a magnetic compass, I rotate the setting circle to indicate the proper bearing of the dish.

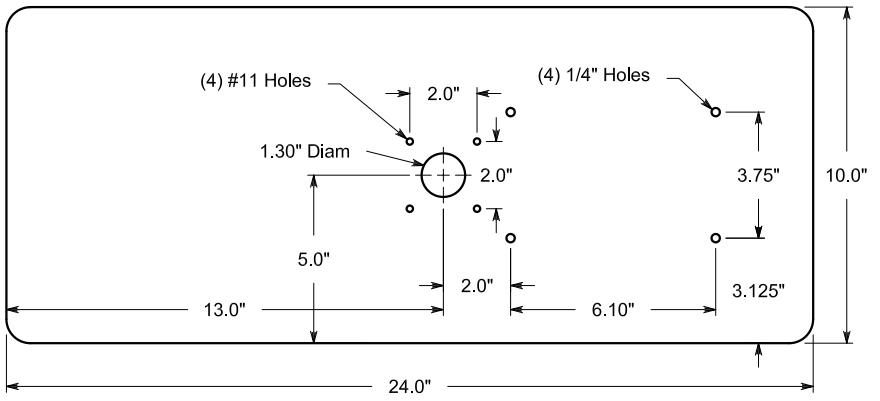

Fig 3—Plywood plate for attaching a DSS dish mount to a RadioShack tripod.

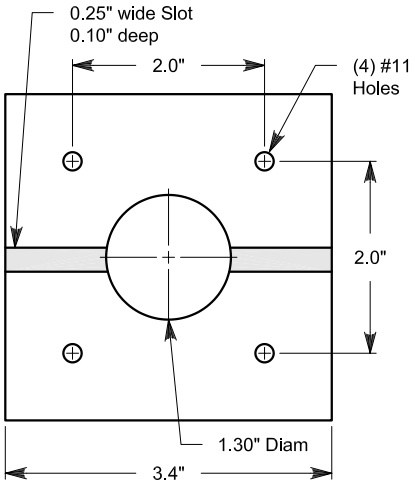

Fig 4—A top plate of 3/8-inch-thick polycarbonate for indexing the plywood plate to a pointer mounted on the tripod.

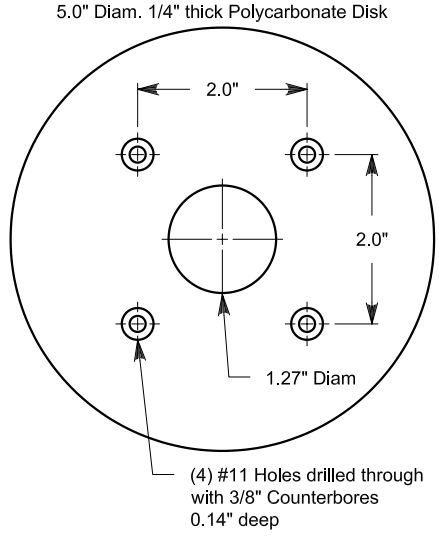

Fig 5—A 1/4-inch-thick polycarbonate bottom plate.

Mounting a 10-GHz Dish Feed on an RCA DSS Dish

I'll be describing a simple 10-GHz dish feed for 18-inch DSS dishes. These dishes are easy to find now that satellite TV has taken off. Since Paul Wade, W1GHZ, has done a great job on the electrical aspects of dish feed design, I'll concentrate on the mechanical aspects. Since even an error of one-quarter inch can result in a 1-dB reduction of gain, I think it is equally important to get the mechanical and electrical designs right.

Good mechanical design for reproduction by amateurs is an art—you want it to be as simple as possible, while sacrificing as little performance as possible. With a bit of thought, I decided that the optimum mounting scheme should allow adjustment in just one axis—along a line between the center of the dish and the focal point. This way, the feed always points in a near optimum direction while the feed is adjusted. Further, I decided that there should be a mounting surface perpendicular to the line. This makes it easy to fabricate a horn mounting.

I first marked the center of the dish. If you don't want the mark to be permanent, you could first cover the dish with removable Scotch tape. It has the same adhesive as Post-It notes. Next, I used the knotted string technique suggested by Paul to find the focal point. Some 3/16-inch aluminum rod between these two points gave a good indication of how the mounting plate should be aligned relative to the hollow-feed mounting arm. An angle of 120° seemed about right. Fig 6 shows the diagram for a wooden mounting block. I made mine out of hard maple. Polycarbonate or aluminum should work better if constantly exposed to

the weather, but I didn't have a large enough piece. Drilling the mounting holes may be difficult to do accurately. If you drill them from the flat side, the drill may wander quite a bit, even if you take care to remove the chips frequently. Alternatively, attempting to drill the angled side is difficult, though a center drill makes the task much easier. I drilled the block first, and then drilled matching holes in the plastic mounting plate.

Fig 7 shows a plastic mounting plate that forms a simple mounting for WR-90 waveguide. It has a 1/2-inch-wide slot for the waveguide. I find 3/8-inch polycarbonate thick enough to reduce the side-to-side movement of the feed. Thicker material might be useful if you have trouble cutting the slot accurately. Alternately, you can make a sandwich: a 1/2-inch spacer between the two mounting supports. The plastic mount is tightly closed around the waveguide with a 1 1/4-inch long #6-32 screw. To prevent marring the waveguide, I put a piece of brass tubing over the screw. Since I didn't have the right size in stock, I drilled out a piece of thick-wall tubing. This required a modified drill bit—standard drill bits bite into brass too fast and get stuck. Similarly, drilling deep holes in plastic requires special care. It is important to only drill a little at a time, and remove the plastic shavings regularly. Don't let the drill bit cool down inside the hole, as it can easily get stuck in melted plastic.

Other dish feeds can be mounted on similar mounting plates. A two-inch hole is useful for cylindrical feeds, such as the popular dual-mode feed invented by W2IMU. However, the standard IMU feed is too small for offset dishes. Dimensions for larger feeds suitable for 0.7- and 0.8-f/D dishes can be found in Paul Wade's Jan/Feb 2001 *QEX* article, "Understanding Circular Waveguide—Experimentally."

I made the feed horn out of copper sheet, using a design by Paul Wade, W1GHZ. The cutting guide is in *UHF/Microwave Projects* Vol 2 on page 1-34. I found the book image was 2% small, so I found a photocopier with a zoom function and scaled it back up to the right size. Copper is a good material if you intend to bend a horn. Brass also works well, though it doesn't bend quite so easily. The conductivity isn't terribly important—horns are very low-Q structures so losses are minimal. While excessive losses melting solder are possible with high-power radar work, amateurs don't run that much power. I solder mine together with a 100-W iron and ordinary solder—very little cleanup is required. A torch typically oxidizes the copper excessively and requires cleaning—an unnecessary complication in my opinion. However, I'd recommend double-sided circuit board if you intend to solder a bunch of little pieces into a horn with a soldering iron. Copper has excellent thermal conductivity, which means that as you solder one joint together the other joints will melt. Circuit board is much better for spot soldering—it is possible to tack solder pieces together without unsoldering everything else. After the horn is soldered together, the edges of the mouth can be wrapped with copper tape and soldered. The tape can then be sol-

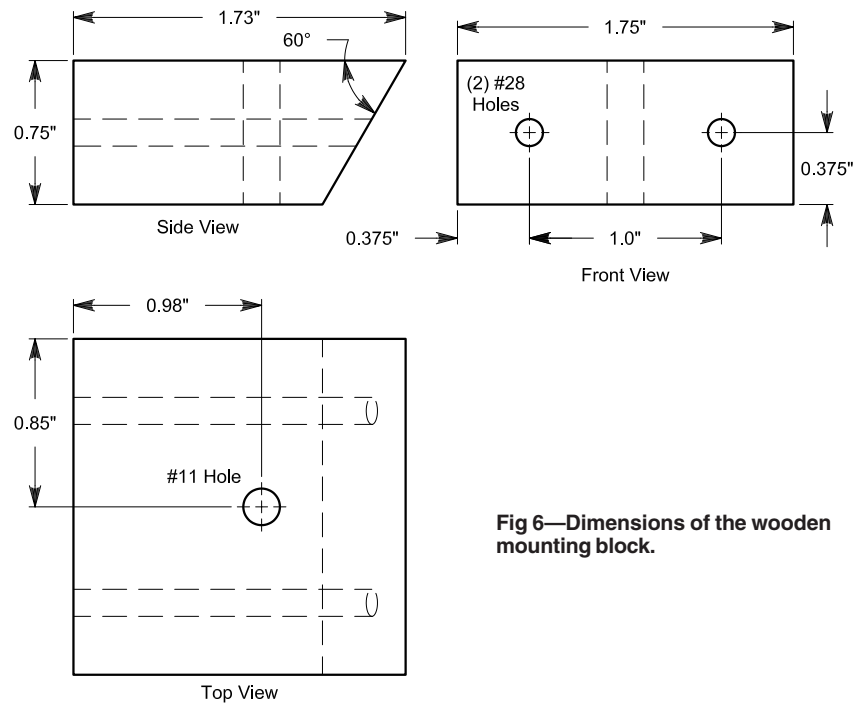

Fig 6—Dimensions of the wooden mounting block.

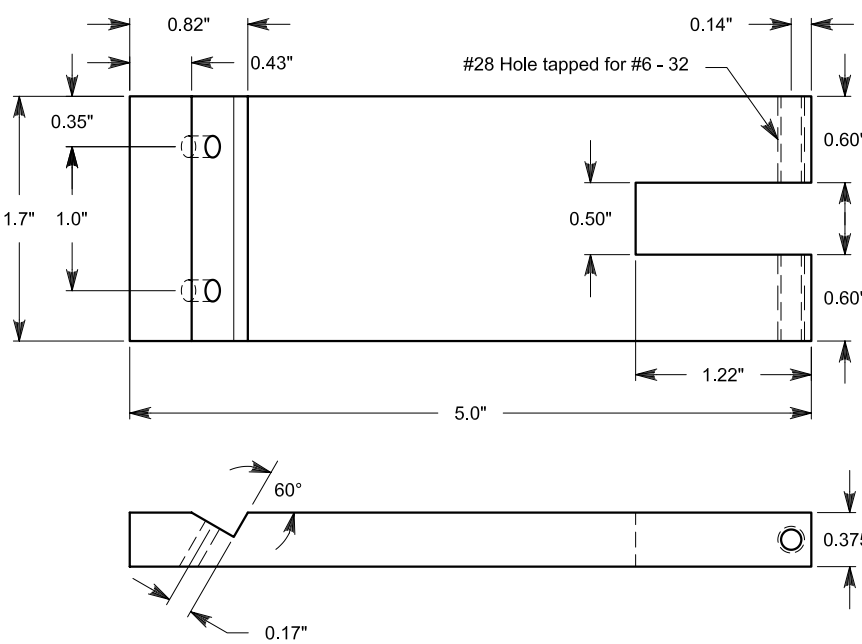

Fig 7—Dimensions of the polycarbonate feed mounting plate.

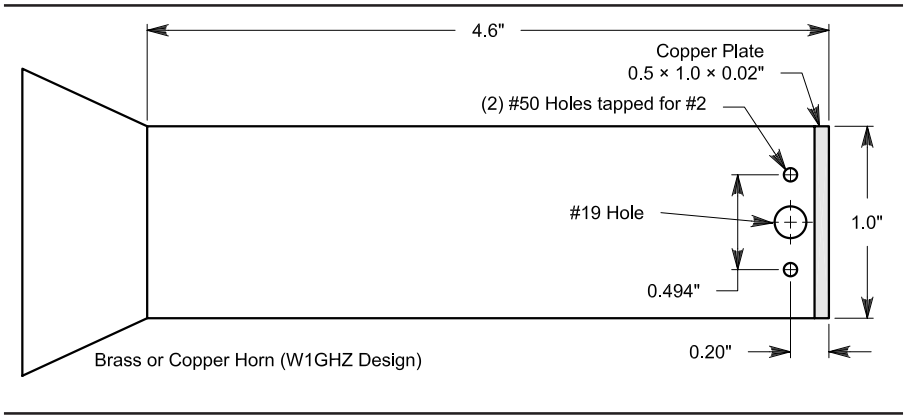

Fig 8—A simple waveguide horn feed using WR-90.

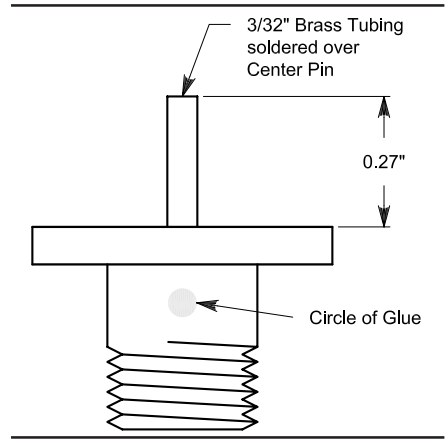

Fig 9—SMA connector and probe details.

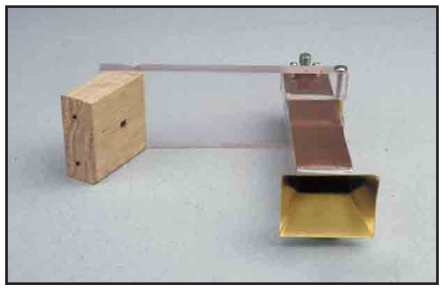

Fig 10—A simple 10-GHz DSS dish feed that attaches to the stock mounting bracket.

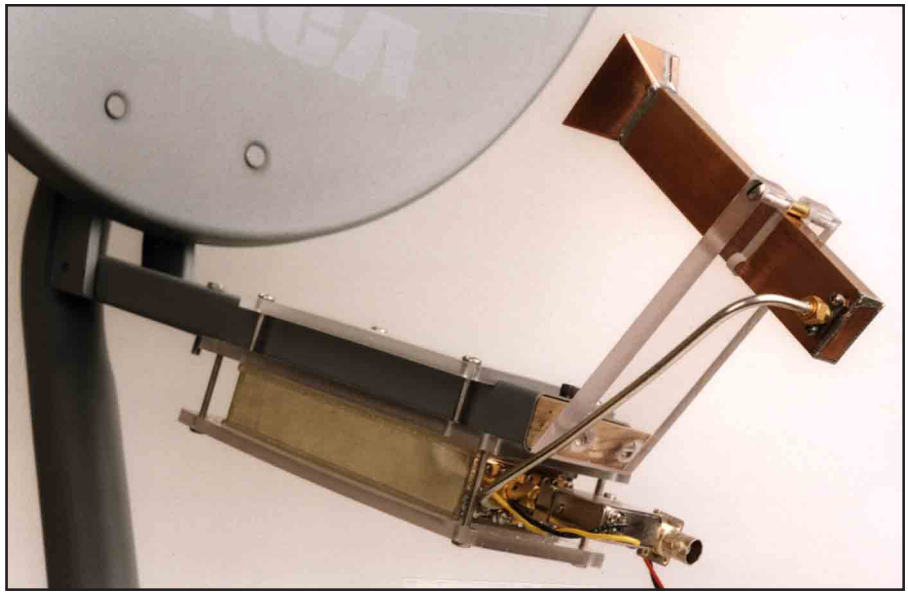

dered to the waveguide for a reasonably rugged feed. Electrically, it is only necessary to attach the inside foils of the printed circuit board to the waveguide. Brass sheet is also a good material for soldering a bunch of little pieces together, but it tends to be more expensive than surplus circuit board.

Fig 8 shows the machining dimensions for the WR-90 waveguide. To keep it simple, I soldered the horn on one end and made an SMA transition on the other. The length of the waveguide isn't critical, but it looks like the waveguide should be at least four inches long. Otherwise, the mounting bracket will interfere with easy access to the SMA connector. The transition is based on a design I published in my Nov 1995 "RF" column in *QEX*. Fig 9 shows the details of the probe constructed out of a captivated SMA connector. The connector needs a captivated center conductor, typically indicated with a dot of glue. I wouldn't rely on a friction fit to hold it in place—Teflon is quite slippery. The SMA connector is attached to the waveguide with #2-56 machine screws. I've found that 1/8-inch screws are too short and 3/16-inch screws are too long. I've been doubling up on lockwashers, using a pair under each screw head. Alternatively, I've also used Loctite and 1/8-inch-long screws. The completed dish feed is shown in Fig 10.

It is also a good idea to make a Styrofoam radome to cover the dish feed. This will keep water out. I've tested both the blue and pink foam sheets used for insulating homes—the loss seems negligible. I carved out a hole, so it fits over the horn. Slits cut into the feed on the sides to simplify the cutting are easily covered with electrical tape to keep the water out.

Notes

[7]B. Wood, N2LIV, "Application of Circular Waveguide with an 11-GHz TVRO Feed," *The ARRL UHF/Microwave Projects Manual*, Vol 2, (Newington: ARRL, 2001; ISBN: 0-87259-631-1; #6311, $15) pp 1-44 to 1-45. Also see "Understanding Circular Waveguide—Experimentally," (Paul Wade, W1GHZ, *QEX*, Jan 2001, pp 37-48) and "More Properties of Circular Waveguide (William Bridges, W6FA, *QEX*, Nov 2001, pp 51-54).

[8]P. Wade, W1GHZ, "More on Parabolic Dish Antennas," *The ARRL UHF/Microwave Projects Manual*, Vol 2, pp 1-30 to 1-38.

[9]Suggested dimensions appear on page 9-31 of *The ARRL UHF/Microwave Experimenter's Manual* (Newington: ARRL, 1997; ISBN: 0-87259-312-6; #3126, $20).

[10]P. Wade, W1GHZ, "Parabolic Dish Feeds—Phase and Phase Center," *Proceedings of Microwave Update, 1998* (Newington: ARRL, 1998; ISBN: 0-87259-703-2; #7032, $15), pp 50 to 73.

[11]P. Wade, W1GHZ, "Using the Chaparral 11-GHz Superfeed at 10.368 GHz," *Proceedings of the 30th Conference of the Central States VHF Society*, Bloomington, Minnesota, 1996, pp 135-136. □□

Letters to the Editor

A Noise/Gain Analyzer (Nov/Dec '99)

I have successfully tested the noise/gain analyzer described in the Nov/Dec '99 issue following a good idea from CT1DMK and I have a few comments. There is a very big mistake in the connection of the BC184 to the time sequencer: The base and associated resistor should be connected to pin 2 of U5A (Fig 2, p 7). Otherwise, the noise head is on when the rest of the system thinks it is off. The dc output of the AD8307 should be decoupled with 1 nF or less (this circuit was not described in the paper).

A reverse-biased base/emitter junction of an UHF transistor forms a very usable noise source up to 2 or 3 GHz. This is especially so if it is fed from a reasonably constant current source like an FET (I use an AT41511 from Agilent) and you permanently insert a 10- to 16-dB pad at the output. It is very important to pay attention to shielding, decoupling of the various dc sources and to have a good mains filter if you want stable and repeatable results. It is a very good description and works fine with these minor changes.—*Georges Ricaud, F6CER, Ste Modem ZA de l'orme-91750-Chevannes, France;* **gricaud@meteomodem.com**

Author's response:

I hate to admit it but Georges is quite right. I even opened my own unit and found that I swapped the functions of U3A and U3C. I also found in my project file an early and ugly, but correct, drawing. Then somehow the mistake was never corrected in subsequent drawings. I apologize for any inconveniences it may have caused. I wonder why nobody else has found this error before as I know more people have built this instrument. It simply does not work as published.

With respect to the circuit around the AD8307, I closely followed the datasheet as provided by Analog Devices (Rev. 0). I don't have access to the RF board so I don't know what capacitor was used at its output. The suggestion to use an RF transistor base-emitter junction in reverse bias is right. I also made one some time ago for different purposes.

I strongly support the final remark on shielding and decoupling. I touch this issue now and then in the article but, as it is no beginner's "weekender," I consider this point part of "expert's routine."—*Harke Smits, PA0HRK;* **harke.smits@hccnet.nl**

PTC: Perceptual Transform Coding...Part 2 (Mar/Apr 2000)

I've enjoyed reading your latest *QST* article [Jan 2002], which led me to your *QEX* article. After looking at Table 2, the frequency mapping in synthesis of a 4:1 PTC coder, I conclude that the frequencies below 488 Hz get expanded rather than reduced!

Would there be any advantage in just passing frequencies below 488 Hz straight through rather than expanding them? It seems that the encoded version might be more understandable that way.

I also enjoyed downloading the .wav files and listening to the results. Thanks for your good work.—*Roy Schaeffer, WB3AJH, 100 W Monument Ave, Hatboro, PA 19040;* **wb3ajh@erols.com**

Dear Roy:

Thanks very much for taking your time to write me. I'm glad you like the articles. You are right that those low frequencies could be quantized with a finer frequency resolution or just passed unmodified. It will be interesting for me to try your suggestion. I would like to increase the number of discrete frequencies across the entire range. The only thing preventing that is the processing "horsepower" available. I haven't had much chance to work on PTC since last year but I intend to get cracking on it again soon.—*Doug Smith, KF6DX;* **kf6dx@arrl.org**

Beyond Fractional-N, Part 2 (May/June 2001)

Hi Cornell,

I was just wondering if your *QEX* article from last summer was correct with regard to the two 0.68-µF bypass capacitors on the line between the OP27 output pin and the VCO varicap. If those capacitors really are that large, have you seen any signs of instability from the OP27? Some op amps don't seem to like capacitive loads, and that seems like a big one.

In addition, without some series resistance to roll off the gain/phase slope, isn't the pole formed by those capacitors (in combination with the OP27 output impedance) the lowest-frequency one in the loop? Seems that there would be stability problems [because of] the lack of phase margin. Is the 22-Ω series resistor at the OP27 output enough to keep the loop stable?

Thanks for a great pair of articles! I missed a couple of *QEX* issues after they came out, so I don't know if any errata were published later.—*John Miles, KE5FX, 10126 NE 63rd St, Kirkland, WA 98033-6820;* **jmiles@pop.net**

Dear OM,

Thank you for bringing this up. Nobody noticed it before. The printed material seems to be in error. C38 and C71 are a few hundred picofarads each at the most (nominally 680 pF for start, but they are tweaked for best performance in reality). The circuit acts as a series trap notch and that is customary in the output of op amps for such PLL loops. Additional tweaking was then used to optimize performance in the notch filter, but no instability resulted despite the fact that it was expected.

This arrangement is like any design: a good compromise that achieves outstanding close-in phase noise performance in the IF/AF band (better than –130 dBc at 1 kHz) while still maintaining a good performance farther out. It is not perfect, but superior to the alternative. This results in a better-sounding receiver than many of the best radios today.

As you probably know, it is much harder to achieve good phase-noise performance in a broadband, high-resolution synthesizer such as this one, compared to a brute-force, fixed-frequency synthesizer such as a multiplied-crystal-reference oscillator. The tradeoffs are great.—*Cornell Drentea, KW7CD, 757 N Carribean Ave, Tucson, AZ 85748-1815;* **cdrentea@aol.com**

Cornell,

You may be interested to hear that a similar loop on my workbench works fine with up to about 1.3 µF across the VCO tuning line. It certainly keeps any residual noise from the phase detector and op amp out of the VCO! Two 0.68-µF capacitors cause oscillation, but anything less than that seems to be stable.

Over the weekend, I was looking at my ICOM IC-R7000 schematic and noticed that they actually show a 4.7-µF capacitor between their VCO tuning lines and ground. I assumed there was a misprint in ICOM's schematic, but then I saw your article and started wondering if it actually did make sense to use a huge capacitor across the VCO tuning line. I'll probably take my R7000 apart tonight and see if that's what they're doing.

The problem I'm seeing is that with your 10-kHz loop filter, certain DDS settings either raise the noise pedestal by 10 or more decibels, or introduce several spurs for 10-30 kHz either side of the carrier. Since I don't really care about switching speed in my application, I'd really like to use a loop bandwidth of only a couple hundred hertz. The narrow-loop approach is very resistant to DDS artifacts, but unfortunately the VCO microphonics are literally out of control!

Of course, my observations have all been made with at least 0.1 µF directly across the VCO tuning line, so I should probably go back and get rid of that capacitor before drawing any final conclusions.

From what I've seen so far on my bench, it seems important to band-pass filter the output of the DDS chip, rather than just using a low-pass filter and hoping for the best. Especially in an octave-band implementation like mine (I'm driving a Mini-Circuits ROS-2150VW VCO at 1-2 GHz). If I decide to go with a fixed-modulus loop like yours, I think it'll be necessary to use a tracking filter of some type at the output of the DDS, or at least switch between two or three discrete low-pass filters. I think I'll try running the DDS output through an ordinary 10.7-MHz ceramic filter next, restricting its tuning range and changing the loop modulus for large frequency steps. —*John, KE5FX*

Hi John,

I agree with everything you say! Of course, a rather narrow band-pass filter such as a 10.7-MHz ceramic filter at the output of the DDS (if you can afford it) can go a long way, depending on how wide your coverage is, and of course, on how small the *N* is. You always want the smallest *N*, of course, for best phase-noise performance, since the PLL is simply a multiplier by the division number, *N* (something that not everybody sees).

It also helps to start at microwave frequencies and divide down as I did. That trick should be used more often in commercial equipment. It should be noted that wider PLL frequency coverage makes the spurious problem more critical (that was exactly your point, also) and makes it harder to combat the problem. However, if you treat the DDS as a mixer in your modeling, some optimum ratio guarantees best performance over the output frequency range. If the coverage is more limited (like in your example), you can sometimes get away with lesser multiples of the Nyquist rate—or even with under-sampling.—*Cornell, KW7CD*

Tech Notes: A Compact Six-Band, Off-Center Fed Vertical Dipole (Jan/Feb 2002)

Hi Rick,

I read with interest your article about off-center fed dipoles. You describe a very clever design to accommodate several bands on a common feed point and I congratulate you on a job well done. You make one statement near the end of the article [with which] I take issue: "Some added bandwidth may also be recovered by using the padding effect derived from normal feed-line losses." You then go on to recommend using RG-58 rather than LMR-400 on a 50-ft run to improve the bandwidth. I fear that many readers may mistakenly believe that high feed-line loss will improve the bandwidth of the antenna and be encouraged to use even longer runs of RG-58 to enhance coverage. I maintain that this is an undesirable approach and should be avoided. Low SWR at the transmitter is no indicator of the efficiency of the antenna system overall.

For example, if the antenna is fed with 150 ft of RG-58, the loss at six meters is over 5 dB. If the far end is opened, shorted or terminated in any impedance, the SWR at the transmitter will be always be less than 2:1 at all frequencies above 50 MHz. That doesn't mean that the antenna is working at these frequencies. In fact, most of the RF from the transmitter is simply being dissipated in the feed line rather than radiated by the antenna. At the 6-m resonant frequency, over two-thirds of the power is heating the line and less than one-third is being radiated by the antenna. As soon as you deviate from the center frequency on six, there will be a reflection loss due to the mismatch at the feed point and this loss increases rapidly as the antenna reactance swamps the resonant resistance. Worse yet, much of the reflected wave coming back to the transmitter is dissipated as heat because of the loss of the line, contributing still further effective loss. Therefore, the net effect is that you are radiating less than a third of the power at the center frequency and less than a fourth of the power as you approach the edges of the antenna bandwidth. All the while, the SWR at the transmitter is less than 2:1.

For this reason, I would recommend that you keep the feedline losses below 1 dB at the highest frequency of interest. On 6 m, 50 ft of RG-58 has about 1.8 dB of loss. I'd instead recommend going to a foam dielectric or something bigger like RG-213, even for this short run of 50 ft. For longer runs, lower-loss cables are even more important.

Please do not interpret these comments as criticism of your excellent article. I would simply feed your six-band antenna with low-loss coax and take my lumps with the resulting bandwidth. Adding 50 kHz of bandwidth will still not permit the antenna to cover the entire 20-, 15-, 10- or 6-m bands. The additional bandwidth is not necessary on the WARC bands because they are narrow enough to be covered fully by a properly adjusted antenna.—*Bob Buus, W2OD, 8 Donner Street, Holmdel, NJ 07733;* **w2od@arrl.net**

Dear Bob,

That is well stated, and I agree. My intended point was that someone using a typical ham rig with automatic 2:1 SWR protection might fare better by operating at the band edge with a decibel or so of attenuation loss than they would by attempting to communicate with a shut-down PA and no output at all! This suggestion was offered in the spirit of a down-and-dirty street solution rather than on a theoretical basis—probably not a good idea in an otherwise theoretical presentation. Thank you for your thoughtful reading and well-crafted response! —*Rick Littlefield, K1BQT, 109A McDaniel Shore Dr., Barrington, NH, 03825;* **k1bqt@aol.com**

Jan/Feb 2002 Issue

I have just received the latest issue of *QEX* and, while I have only scanned the articles, it appears to be one of the best issues ever! Congratulations to all!—*Jack Parker, W7PW, 5160 Deodar St, Silver Springs, NV 89429-7334;* **82ndairborne@prodigy.net**

On High-Speed Networking for Amateur Radio

To QEX readers:

Those of you who are networking professionals by day know all too well about the explosive growth business and industry has experienced in recent times. The increasing reliance on electronic data systems, e-commerce, TCP/IP (Internet protocol) based communications solutions and more continues to put enormous pres-

sure on data management and connectivity resources.

Non-networking operators will ask, "How does this affect Amateur Radio?" Simply put, the agencies and organizations that rely on Amateur Radio for emergency communications support have many of the same, exploding information needs, as was clearly demonstrated by the events of September 11th. It is incumbent on the Amateur Radio community to seek out 21st-century solutions to address this information avalanche.

One potential solution is 2.4-GHz spread-spectrum wireless networking. If you say "Whoa, wait a minute! That's Part-15 territory," you are only partially correct. Yes, 2.4-GHz wireless networking products are sold as Part-15 devices. Hundreds of thousands are currently in use supporting private networks in homes and businesses.

This same technology, with a twist, can also be Amateur Radio technology. You see, a significant portion of the spectrum used by these digital devices (2400-2450 MHz) is part of the Amateur Radio 13-cm allocation. Many of these devices can be easily adapted and enhanced to help modernize the Amateur Radio Service and enhance our communication capabilities.

The West Central Florida Section established a Task Force in May 2000 in an effort to bring high-speed digital networking to Amateur Radio in our part of the world. Here is some of what we have learned:

Both frequency-hopping (FHSS) and direct-sequence (DSSS) devices can be operated under Part 97. Both types of devices can be controlled through onboard firmware to limit operations to the 2400-2450 MHz in the 13-cm Amateur Radio band.

Part 97 allows these spread-spectrum devices to operate with transmitter power outputs up to 1 W without automatic power control and up to 100 W with automatic power control. This gives Amateur Radio operators a significant advantage when competing against unlicensed Part 15 operators for throughput.

A broad range of external 13-cm antennas is available at reasonable prices. These include omnidirectional, panel and parabolic-reflector types.

Power amplifiers with output up to 8 W and equipped with automatic-power-control circuitry are also readily available at a reasonable cost.

One of the challenges of operating a Part 97 spread-spectrum network is the 10-minute station-identification rule. Unlike voice repeaters and many other Amateur Radio operating modes, a spread-spectrum network is always on. The Task Force has studied this issue intensely. There are several options available for satisfying this requirement, ranging from including the station's call sign in each packet to a small utility program that automatically generates a packet containing the station's call sign every 9 minutes and 55 seconds.

A modern, spread-spectrum network is fast enough to support TCP/IP, the addressing protocol used on the Internet. How convenient (!) since this type of network is ideal for e-mail messaging, instant messaging, large file transfers, even digital voice over IP for repeater linking. Limited video conferencing is also an application you may wish to explore.

As mentioned earlier, the events of September 11th have added a new urgency to our project. Disaster-response organizations, including the Red Cross, Disaster Medical Assistance Teams (DMAT), local emergency management and others, need high-speed connectivity and modern tools to manage emergencies. These tools include digital messaging, high-speed data transfer and imaging. While conventional packet radio may be useful in the very short term, it does not provide the throughput to dent the information demands that will accumulate.

The biggest challenge our Task Force still faces is funding! We estimate the cost of a full featured 2.4-GHz node is about what a 2-m repeater costs. The dollars needed to finance a network of any size can add up quickly.

The Task Force is working closely with the West Central Florida Group Inc (WCFG), a nonprofit organization established to operate the K4WCF regional voice repeater system and provide support for other Amateur Radio technologies. The anticipated granting of 501(c)(3) status will enable WCFG to apply for private and public grants to help underwrite many of the construction and operating costs associated with this project.

Construction and operation of 2.4-GHz Amateur Radio networks, I believe, is just one aspect of the "modernization" the FCC pointed to in their 1999 Report and Order. They represent a productive use of the spectrum the Amateur Radio Service has been granted.—*Paul J. Toth, NA4AR, Chairman, WCF Wireless Network Task Force, 9231 120th St, Seminole, FL 33772-2643;* **na4ar@arrl.net**

Laser Transceiver Correction (Nov/Dec 2001)

We have learned of an error in Fig 6 (page 16) of Lilburn Smith, W5KQJ's "A Laser Transceiver for the ARRL 10-GHz-and-Up Contest." In that figure, the labels for the inverting and noninverting inputs of op amps U1 through U5 are transposed. The pin numbers and connections are shown correctly. To repair the error, simply relabel all pins 2 with minus signs and all pins 3 with plus signs.—*Bob Schetgen, KU7G,* **ku7g@arrl.org** □□

Next Issue in QEX/Communications Quarterly

Next time, Bill Young, WD5HO, combines two popular technologies in a regenerative superheterodyne receiver. Join us as another homebrew rig hits the ether!

In *Tech Notes*, Peter Bertini, K1ZJH, brings us a follow-on piece from ex-*QEX* Editor Rudy Severns, N6LF, about foil conductors for antennas. Rudy means to dispel a few common misconceptions about current distribution on flat conductors.

QEX staffer Zack Lau, W1VT, shows how to homebrew large knobs for your projects. □□

Out of the Box: New Products

EXTREMELY BROADBAND CAPACITORS

Two companies are producing broadband chip capacitors that provide performance from "dc to daylight." Dielectric Laboratories (DLI) and Presidio Components Inc have dc blocking capacitors that allow operation from 10 kHz to beyond 40 GHz. These parts allow much easier implementation of truly broadband operation for devices like the Mini Circuits ERA series MMICs. The parts provide high Q, low series inductance and high capacitance values. Although the manufacturers target the application at dc-blocking applications, they are also very well suited to broadband bypass applications.

Dielectric Laboratories calls their product Opti-Cap. It is a multilayer ceramic capacitor in parallel with a single-layer microwave ceramic

capacitor in a single package. The 0502 footprint is designed to match 50-Ω microstrip with only a 0.010-inch gap. Presidio Components calls their product a Buried Broadband Capacitor. Their product also combines a multilayer capacitor with a single-layer capacitor in parallel, but they provide parts in 0502, 0603 and 0805 sizes.

The most important difference between manufacturers is that the DLI parts are only specified for epoxy mounting, while the Presidio parts are available for epoxy, solder or gold wire bond.

Representative Capacitors

Presidio Components

Capacitance	Working Voltage	Dielectric/ Size
100 nF - 82 pF	16 V	X7R 0502
150 nF - 220 pF	16 V	X7R 0603
150 nF - 220 pF	16 V	X7R 0805
220 nF - 82 pF	16 V	Y5V 0502

Dielectric Laboratories

Capacitance	Working Voltage	Dielectric/ Size
150 nF - 82 pF	25 V	Z5U 0502
27 nF - 82 pF	25 V	Z5U 0502
27 nF - 30 pF	25 V	Z5U 0502

Sample quantities are available from both manufacturers. Presidio Components provides parts directly from the factory. Their minimum order is $125, but they consider sample quantities to be about 20 or less. The parts are about $1 each in large quantities and $2-$3 each in smaller quantities. Dielectric Laboratories parts are available through distribution.

Presidio Components Inc, PO Box 81576, San Diego, CA 92138; tel 858-578-9390; **www.presidio-components.com**.

Dielectric Laboratories, 2777 Route 20 East, Cazenovia, NY 13035; tel 315-655-8710; **www.dilabs.com**. □□

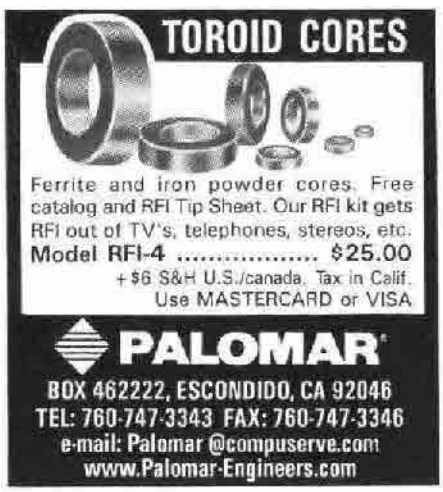

We Design And Manufacture To Meet Your Requirements

*Protoype or Production Quantites

800-522-2253

This Number May Not Save Your Life...

But it could make it a lot easier! Especially when it comes to ordering non-standard connectors.

RF/MICROWAVE CONNECTORS, CABLES AND ASSEMBLIES

- Specials our specialty. Virtually any SMA, N, TNC, HN, LC, RP, BNC, SMB, or SMC delivered in 2-4 weeks.
- Cross reference library to all major manufacturers.
- Experts in supplying "hard to get" RF connectors.
- Our adapters can satisfy virtually any combination of requirements between series.
- Extensive inventory of passive RF/Microwave components including attenuators, terminations and dividers.
- No minimum order.

NEMAL

Cable & Connectors for the Electronics Industry

NEMAL ELECTRONICS INTERNATIONAL, INC.
12240 N.E. 14TH AVENUE
NORTH MIAMI, FL 33161
TEL: 305-899-0900 • FAX: 305-895-8178
E-MAIL: INFO@NEMAL.COM
BRASIL: (011) 5535-2358

URL: WWW.NEMAL.COM

EZNEC 3.0

All New *Windows* Antenna Software by W7EL

EZNEC 3.0 is an all-new antenna analysis program for Windows 95/98/NT/2000. It incorporates all the features that have made ***EZNEC*** the standard program for antenna modeling, plus the power and convenience of a full Windows interface.

EZNEC 3.0 can analyze most types of antennas in a realistic operating environment. You describe the antenna to the program, and with the click of a mouse, ***EZNEC 3.0*** shows you the antenna pattern, front/back ratio, input impedance, SWR, and much more. Use ***EZNEC 3.0*** to analyze antenna interactions as well as any changes you want to try. ***EZNEC 3.0*** also includes near field analysis for FCC RF exposure analysis.

See for yourself

The ***EZNEC 3.0*** demo is the complete program, with on-line manual and all features, just limited in antenna complexity. It's free, and there's no time limit. Download it from the web site below.

Prices - Web site download only: $89. CD-ROM $99 (+ $3 outside U.S./Canada). VISA, MasterCard, and American Express accepted.

Roy Lewallen, W7EL *phone* **503-646-2885**
P.O. Box 6658 *fax* **503-671-9046**
Beaverton, OR 97007 *email* **w7el@eznec.com**

http://eznec.com

Down East Microwave Inc.

We are your #1 source for 50MHz to 10GHz components, kits and assemblies for all your amateur radio and Satellite projects.

Transverters & Down Converters, Linear power amplifiers, Low Noise preamps, Loop Yagi and other antennas, Power dividers, coaxial components, hybrid power modules, relays, GaAsFET, PHEMT's, & FET's, MMIC's, mixers, chip components, and other hard to find items for small signal and low noise applications.

We can interface our transverters with most radios.

Please call, write or see our web site ***www.downeastmicrowave.com*** for our Catalog, detailed Product descriptions and interfacing details.

Down East Microwave Inc.
954 Rt. 519
Frenchtown, NJ 08825 USA
Tel. (908) 996-3584
Fax. (908) 996-3702

QEX Subscription Order Card

American Radio Relay League
225 Main Street
Newington, CT 06111-1494 USA

QEX, the Forum for Communications Experimenters is available at the rates shown at left. Maximum terms for 6 issues, and because of the uncertainty of postal rates, prices are subject to change without notice.

For one year (6 bi-monthly issues) of QEX.
In the US:
☐☐ ARRL Member $22.00
☐☐ Non Member $34.00
In Canada, Mexico and US by First Class mail:
☐☐ ARRL Member $35.00
☐☐ Non-Member $47.00
Elsewhere by Surface Mail (4-6 weeks delivery):
☐☐ ARRL Member $27.00
☐☐ Non-Member $39.00
Elsewhere by Airmail:
☐☐ ARRL Member $55.00
☐☐ Non-Member $67.00

Subscribe toll-free with your credit card 1-888-277-5289

☐ Renewal ☐ New Subscription

Name _____ Call _____
Address _____
City _____ State or Province _____ Postal Code _____
Payment Enclosed ☐
Charge ☐ ☐ ☐ ☐
Account # _____ Good thru _____
Signature _____ Date _____

Remittance must be in US funds and checks must be drawn on a bank in the US.
Prices subject to change without notice.

11/98

SALE
Atomic Watch hard mineral lens, hi-tech polymer case black leather band $109.95

atomic radio with 2 alarms and tempature, day, date, LCD $39.95

NEW
Junghans atomic carbon, stainless bezel, sapphire lens LCD day, date - carbon/leather band • $279.00

ATOMIC TIME™

...self setting
...correct time
...atomic clock

World s most exact time... atomic clocks, atomic watches and weather stations

- for any time zone
- synchronized to the u.s. atomic clock in colorado
- accurate to 1sec. in 1 mil. years
- engineered in germany

complete line of atomic clocks

JUNGHANS MEGA CERAMIC Watch
JUNGHANS MEGA CARBON Watch
JUNGHANS MEGA CLOCKS
JUNGHANS SOLAR WATCHES
ATOMIC SPORTS WATCHES
ATOMIC SCHOOL/OFFICE CLOCKS
ATOMIC INDUSTRIAL CLOCKS
Oregon Scientific Weather Stations, Weather Forecast, World Time, NOAA Radios, Radio Controlled Clocks...

call for our FREE Brochure

or go to **WWW.atomictime.com**

credit card orders call toll free

1-800-985-8463

30 Day Money Back Guarantee
send checks incl. s&h $6.95 to

ATOMIC TIME, INC.
1010 JORIE BLVD.
OAK BROOK, IL 60523

atomic dual alarm clock w. temperature day and date, black 3.5x4.5x2 $29.95

jumbo digit atomic clock w. temperature & day and date,wall or desk 8.5 x8.5 x1 • $49.95

black arabic 12 wall clock for home or office • $59.95 (wood $69.95)

Name: ham radio, born January, 1968.

Why **ham radio** (magazine)? *The electronics and communications industry is moving forward at a tremendous clip, and so is amateur radio. Single sideband has largely replaced a-m, transistors are taking the place of vacuum tubes, and integrated circuits are finding their way into the ham workshop. The problem today, as it has always been, is to keep the amateur well informed.*— Editor Jim Fisk, W1DTY (SK), from the preview issue of *ham radio* magazine, February, 1968 (last issue published in June, 1990).

hr focus on communications technology . . .

Introducing Ham Radio CD-ROMs!

System Requirements: Pentium or equivalent IBM-compatible PC, and Microsoft Windows™ 95, 98, NT 4.0, Me, or 2000.

Now you can enjoy quick and easy access to back issues of this popular magazine! These CD-ROM sets include high quality black-and-white scanned pages, easily read on your computer screen or printed. All the articles, ads, columns and covers are included.

Readers will enjoy a wealth of material that spanned the gamut of Amateur Radio technical interests: construction projects, theory, antennas, transmitters, receivers, amplifiers, HF through microwaves, test equipment, accessories, FM, SSB, CW, visual and digital modes.

The complete set covers more than 30,000 pages!

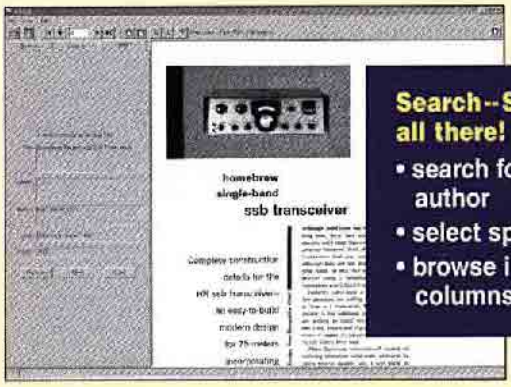

Search--Select--Browse—it's all there!

- search for articles by title and author
- select specific year and issue
- browse individual articles and columns

Only $59.95 per set:* **Each set includes four CDs!**

Ham Radio CD-ROM 1968-1976 ARRL Order No. 8381
Ham Radio CD-ROM 1977-1983 ARRL Order No. 8403
Ham Radio CD-ROM 1984-1990 ARRL Order No. 8411

SAVE $30! when you order the complete set:*
All 3 Ham Radio CD-ROM Sets (1968-1990)
ARRL Order No. HRCD **$149.85**

***Shipping/handling fee:** US orders add $5 for one set, plus $1 for each additional set ($10 max, via UPS). International orders add $2.00 to these rates ($12.00 max, via surface delivery). Sales tax is required for orders shipped to CA, CT, VA, and Canada.

ARRL *The national association for AMATEUR RADIO*

225 Main Street, Newington, CT 06111-1494
tel: 860-594-0355 fax: 860-594-0303

In the US call our toll-free number **1-888-277-5289** 8 AM-8 PM Eastern time Mon.-Fri.
Quick order **www.arrl.org/shop**

Ham Radio CD-ROM, © 2001, American Radio Relay League, Inc. Ham Radio Magazine © 1968-1990, CQ Communications, Inc.

ARRL Marketplace!

These publications have been added to the ARRL Library...
so you can add them to yours!

2002 Shortwave Frequency Guide

Schedules of clandestine, domestic, and international broadcast stations worldwide! Quickly find frequencies and a superb alphabetical list of stations. Includes another 10,078 entries for utility stations (Red Cross, United Nations and more).

ARRL Order No. 8663—$34.95

2002 Super Frequency List on CD-ROM

Includes all shortwave broadcast stations worldwide, plus all utility stations from 0 to 30 MHz. Nearly 40,000 entries! Find the latest schedules of clandestine, domestic and international broadcasting services compiled by top experts in this field.

ARRL Order No. 8671—$24.95

Passport to World Band Radio 2002 edition

There's a world of news, entertainment and exciting broadcasts you can tune into! Use this popular shortwave guide to find them all. Includes a 2002 channel-by-channel guide to World Band Schedules. Tips for new shortwave listeners, reviews of radios and accessories, and more.

ARRL Order No. 8468—$19.95

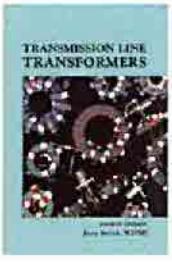

Transmission Line Transformers —NEW 4th Edition

Tremendous coverage of the subject of broadband transmission line transformers. Guanella and Ruthroff as well as hundreds of real transformers.

ARRL Order No. TLT4—$39

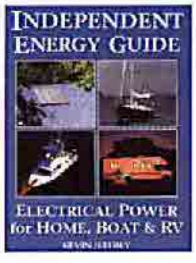

Independent Energy Guide —Electrical Power for Home, Boat & RV

Covers fixed, portable, and mobile energy systems; DC charging sources and AC power systems, solar, wind and water power, battery chargers, inverters, and more.

ARRL Order No. 8601—$19.95

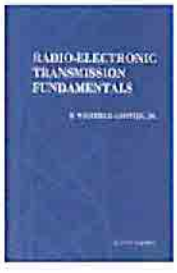

Radio-Electronic Transmission Fundamentals

Clear, concise explanations of antennas, transmission lines, and RF networks in the framework of electromagnetic field theory.

ARRL Order No. RETF—$75

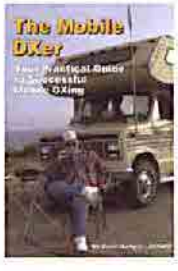

The Mobile DXer

A practical guide to successful mobile DXing. Learn how to select and install mobile gear and pick antennas. Understand propagation, mobile DX operating tips, and making the most of portable operating.

ARRL Order No. TMDX—$12.95

HF Radio Systems & Circuits

Includes Software! Comprehensive coverage of system definition and performance requirements down to the individual circuit elements that make up radio transmitters and receivers. Thorough attention is given to key circuits like oscillators, synthesizers, filters and amplifiers, speech processing, AGC systems, high linearity amplifiers, and solid state power amplifiers.

ARRL Order No. 7253—$75

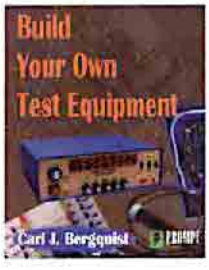

Build Your Own Test Equipment

Build practical devices with commonly-available components. Multi-output test bench power supply, signal generator and tester, IC tester, multimeter, frequency counter, and others.

ARRL Order No. 8604—$29.95

Electronic Applications of the Smith Chart

How the chart is used for designing lumped element (inductors and capacitors) and transmission line circuits (coaxial, waveguide, stripline or microstrip lines). Includes tutorial material on transmission line theory and behavior, circuit representation on the chart, matching networks, network transformations and broadband matching.

ARRL Order No. 7261—$59

***win*SMITH 2.0**

An easy-to-use, flexible computerized Smith Chart. Accelerate your RF and microwave designs! Unlock a greater understanding of transmission lines and simple matching problems. 3.5-inch installation diskette. Requires Microsoft *Windows*.

ARRL Order No. 7946—$80

The Hannibal Files*

by Bryan A. Bisley, VE7FH. A middle east adventure novel of political intrigue, espionage and international secrecy, with an interwoven theme of aviation, and Amateur Radio. *Some adult content.

ARRL Order No. 8635—$16.50

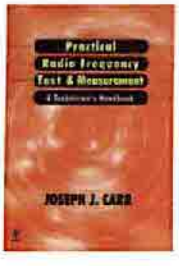

Practical Radio Frequency Test & Measurement

Learn the basics of performing tests and measurements used in radio-frequency systems installation, proof of performance, maintenance, and troubleshooting. Provides immediate applications, test set-ups, procedures, and interpretation of results.

ARRL Order No. 7954—$34.95

33 Simple Weekend Projects

A wide-ranging collection of do-it-yourself electronics projects. Useful accessories for VHF FMing, projects for satellite communications, CW, simple antennas, and a complete HF station you can build for around $100!

ARRL Order No. 7628—$15.95

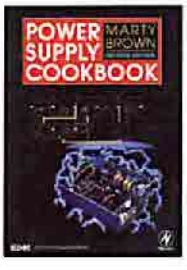

Power Supply Cookbook

A useful resource for amateurs interested in circuit design, and with a basic knowledge of electronics. A step-by-step design framework for power supplies, many of which can be designed in less than a day.

ARRL Order No. 8599—$39.99

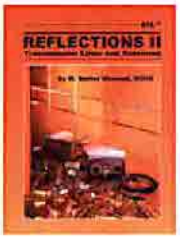

Reflections II —Transmission Lines and Antennas

by M. Walter Maxwell, W2DU. An in-depth treatment of transmission lines, standing waves, antenna matching, reflected power and antenna tuners. Second edition.

ARRL Order No. REF2—$19.95

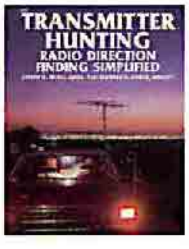

Transmitter Hunting —Radio Direction Finding Simplified

Covers equipment and techniques for HF and VHF radio direction finding. Locate jammers and other sources of malicious interference, engage in sport hunting, even help search-and-rescue groups!

ARRL Order No. 2701—$24.95

Order Toll Free

1-888-277-5289

www.arrl.org/shop

Shipping and Handling instructions: US orders add $5 for one item, plus $1 for each additional item ($10 max.). US orders are shipped via UPS. International orders add $2.00 to the US shipping rate ($12.00 max.). Orders are shipped via surface mail. Other shipping options are available. Please call or write for information.

Sales Tax is required for shipments to CT (including S/H), VA 4.5% (excluding S/H), CA (add applicable tax, excluding S/H) and Canada (excluding S/H).

ARRL *The national association for* ***AMATEUR RADIO***

225 Main Street, Newington, CT 06111-1494 USA tel: 860-594-0355
fax: 860-594-0303 e-mail: pubsales@arrl.org World Wide Web: http://www.arrl.org/shop